NASA CR-66383

SPACE PROBE RADAR ALTIMETER STUDY

Final Technical Report
Volume 1 of 3

Prepared under Contract No. NAS 1-5954 by
TEXAS INSTRUMENTS INCORPORATED
Apparatus Division
13500 North Central Expressway
Dallas, Texas 75222

for

NATIONAL AERONAUTICS AND SPACE ADMINISTRATION

NASA CR-66383

SPACE PROBE RADAR ALTIMETER STUDY

Final Technical Report
Volume 1 of 3

Distribution of this report is provided in the interest of information exchange. Responsibility for the contents resides in the author or organization that prepared it.

Prepared under Contract No. NAS 1-5954 by
TEXAS INSTRUMENTS INCORPORATED
Apparatus Division
13500 North Central Expressway
Dallas, Texas 75222

for

NATIONAL AERONAUTICS AND SPACE ADMINISTRATION

FOREWORD

This Volume One of a Three Volume set of documents comprising the final report of a study to define the design of a space probe altimeter. The documents of this series include the following:

1. Design
    a. Detailed Conceptual Design
    b. Drawings
    c. Growth Potential
2. Developmental Plan
    a. Project Planning Network
    b. Manufacturing Plan
    c. Environmental Tests Program Plan
    d. Flight Test Qualification Plan
    e. Facilities Plan
    f. Project Funding Plan
3. Reliability and Quality Assurance Plan
    a. Reliability and Quality Assurance
    b. Predicted Effects of Sterilization

This study was conducted by Texas Instruments Incorporated Apparatus Division for the National Aeronautics and Space Administration, Langley Research Center, Langley Station, Hampton, Virginia, under contract number NAS 1-5954, from March 1966 to November 1966.

TABLE OF CONTENTS

TABLE OF CONTENTS (Continued)

LIST OF ILLUSTRATIONS

LIST OF ILLUSTRATIONS (Continued)

LIST OF TABLES

SPACE PROBE RADAR ALTIMETER STUDY

Prepared by Texas Instruments Incorporated
Apparatus Division
13500 North Central Expressway
Dallas, Texas 75222

SUMMARY

The primary purpose of this study program is to define the design of a small, lightweight, minimum power consuming, sterilizable radar altimeter for use as a metric device to correlate atmospheric data obtained in a Martian lander. Secondary purposes are to define possible growth potential items and to establish sterilization procedures for the altimeter in line with present NASA specifications.

The primary operational guidelines under which the study was conducted were to design for satisfactory operation of an X-band radar altimeter over an altitude range of 300 m to 15.5 km, with an expected entry velocity of 3000 m/s, a flight vector to vertical angle of 60 deg (at 15.5 km), a measurement accuracy of 10 m or 2 percent of altitude (whichever is greater); the maximum input power consumption is not to exceed 15 W. Other restrictions relate to maximum size (300 $in.^3$), weight (6 lb), environmental extremes, mission life, data format and detection probability (along with false-alarm rate, specified as minimum signal-to-noise ratio).

This study gives arguments as to the best type of altimeter for use on the Mars mission including FM/CW, ICW, and short pulse modulation. In addition, methods of implementing the selected type are considered with attention given to fabricating, qualifying, and testing plans, including consideration of the need for a growth potential. A pulsed, steerable beam, all solid-state altimeter was recommended as the system best meeting the requirements of the work statement.

The proposed radar altimeter design has the following characteristics: Altitude range — 300 meters to 18 km; entry velocity of 3000 meters/second at a flight vector to vertical angle of 60 degrees; a measurement accuracy of 1.5 percent; maximum input power of 13.5 W; volume, 260 $in.^3$, weight, 7 lb; and it is capable of withstanding the chemical and thermal sterilization environments as well as the expected mission environments.

INTRODUCTION

Unmanned planetary probes are included in NASA's future exploration programs during the next ten years. Among the scheduled experiments is an attempt at a precise determination of the characteristics of the Martian atmosphere and surface conditions. An important parameter in the atmospheric measurements is altitude, and for this reason it is desirable to use a radar device to precisely determine the altitude at which the constituents of the atmosphere are identified and measured. A radar device for altitude measurements (radar altimeter) may also exhibit a capability for determining some characteristics of surface condition. Another desired feature of this altimeter is its capability to evolve into more elaborate systems without a system concept change and an associated extensive redevelopment program. Among the expected items of growth are extended maximum altitude range, low and zero altitude capability, attitude determination, and vertical and horizontal velocity determination.

Since the biological makeup of the planet Mars is unknown, it is imperative that any experimental landing on the surface, or even entering the near vicinity of the planet, be free from viable organisms with a high degree of certainty. Therefore, a sterile radar altimeter is required for this and future missions.

A study to define the design of a space probe radar altimeter has been performed by Texas Instruments Incorporated (TI) for the Langley Research Center (LRC) of the National Aeronautics and Space Administration (NASA) under contract number NAS 1-5954. This study, in accordance with the Statement of Work L-6050 dated 19 August 1965, was performed during the period March 1966 to November 1966, and was separated into two parts. Part I was a basic review of the mission requirements for the altimeter, with a thorough analysis of all applicable types of radar altimeters, including FM/CW, ICW, and short pulse modulation.

After concurrence with TI's recommendation, LRC directed TI to continue with Part II, which was a detailed design of the selected type, including plans for all phases of fabrication, testing, and prelaunch support. The proposed radar altimeter design has the following characteristics: Altitude range—300 meters to 18 kilometers; entry velocity of 3000 meters/second at a flight vector to vertical angle of 60 degrees; a measurement accuracy of 1.5 percent; maximum input power of 13.5 W; volume, 260 $in.^3$, weight, 7 pounds; and it is capable of withstanding the chemical and thermal sterilization environments as well as the expected mission environments.

Texas Instruments is developing a completely solid-state radar (refer to the appendix) that uses a phase scanning array of radio frequency building blocks (RFBB's). Solid-state microwave techniques developed in this

Molecular Electronics for Radar Applications (MERA) program are applicable to the space probe altimeter, and the altimeter would have the following features:

a. MERA is extension of well-known technologies

b. Present development fits time scale of intended missions

c. Inherent redundance in front end

d. 100 percent solid state

e. The analytical work preceding the hardware development has been proved valid by the test experience to date

f. Growth potential

1. Can add more RFBB's (directly expandable)
2. Pulse compression techniques are being developed
3. Adaptable to monopulse
4. Adaptable to coherent operation
5. Adaptable to shaped arrays

g. Maximum use of integrated circuitry.

Complete details of the results of this study are contained in the three documents listed in the Foreword.

LIST OF SYMBOLS AND ABBREVIATIONS

Symbol	Description	Units
A_T	Total illuminated terrain (target) area	m^2
A_e	Effective antenna aperature = $\frac{G\lambda^2}{4\pi}$	m^2
dA_T	Differential target area = $2\pi r dr$	m^2
A_u	Useable portion of A_T	m^2
$A(\theta)$	Target area as a function of $\theta = \pi H^2 \tan^2\theta$	m^2
A_s	Area of spherical segment	m^2
Ao	Area of sphere	m^2
AGC	Automatic Gain control	
B	IF Amplifier 3 dB bandwidth	Hz
b	Servo Amplifier 3 dB bandwidth	Hz

Symbol	Description	Units
c	Velocity of propagation of electromagnetic energy	m/sec
CW	Continuous wave	
C_1	Signal out of IF amp in ICW velocity channel	volts
C_{10}	Max. amplitude of C_1	volts
C_2	Signal out of VCO in ICW velocity channel	volts
C_3	Signal out of upper channel mixer	volts
C_4	Signal out of lower channel mixer	volts
C_5	Signal out of phase detector	volts
dB	Decibel	
D	Antenna directivity	
deg	Degree or degrees	
E_{S1}	Signal energy per pulse at output of IF	W-sec
E_{N1}	Noise intensity at output of IF	W-sec
E_{ND}	Noise intensity at detector output	W-sec
E_{SD}	Signal energy per pulse at detector output	W-sec
E_{RN}	Signal energy returned for narrow antenna	W-sec
E_{RB}	Signal energy returned for broad antenna	W-sec
F_N	Noise figure of receiver	dB
f_D	Doppler frequency shift	Hz
f_c	Carrier frequency	Hz
f_M	Modulation frequency	Hz
f_{IF}	IF frequency	Hz
f_ϕ	Phase measuring frequency	Hz

Symbol	Description	Units
f_p	PRF fundamental frequency	Hz
f_D max	Maximum doppler frequency shift	Hz
FM	Frequency modulation	
f_{VCO}	Frequency of VCO in ICW velocity circuitry	Hz
ft	Feet	
f_1	f_3 & f_4 are applied simultaneously to f_c as a modification of basic FM/CW system (See Table 1)	Hz
f_2		Hz
G	Antenna gain	dB
G(θ)	Antenna gain function (of θ)	dB
g(s)	Amplifier gain function	dB
G_o	Antenna boresite maximum gain response	dB
G_B	Gain of broad beam antenna	dB
G_N	Gain of narrow beam antenna	dB
G_L	Gain of servo loop circuitry	dB
h^1	Threshold slant range	meters
H	Altitude of altimeter normal to surface	meters
h	Slant Range	meters
ΔH	Increment of H	meters
Δh	h - H	meters
H_a max, min	Maximum and minimum acquisition altitudes	meters
H_{TH}	Threshold altitude = $\frac{c}{2}$ t_{TH}	meters
I_L	Argument of Bessel function for leakage signal	
ICW	Interrupted CW	
IF	Intermediate frequency	Hz

Symbol	Description	Units
in	Inch	
I	Argument of Bessel function	
I_3	Argument of Bessel function due to f_3	
I_4	Argument of Bessel function due to f_4	
J_{nB}	Bessel function of order nB	
$J_o(I_3)$	Bessel function (0 order) due to f_3	
$J_o(I_4)$	Bessel function (0 order) due to f_4	
$J_k(I_3)$	Bessel function (k^{th} order) due to f_3	
$J_m(I_3)$	Bessel function (m^{th} order) due to f_3	
$J_n(I_4)$	Bessel function (n^{th} order) due to f_4	
km	Kilometers	
K_L	Relative rise time of received signal	
K_B	Boltzmann constant (1.38×10^{-23})	W-sec/°C
K_2	$(\lambda\delta^2 \tan^2\theta) \div (64\pi^2 H^2)$	
kft	Kilofeet	
lb	pound	
Lc	Collapsing loss	dB
LO	Local oscillator	
m/s	Meters per second	M/Sec
M	Modulation index	
m	meters	Meters
mW	milliwatts (power)	$W \times 10^{-3}$

Symbol	Description	Units
M_H	Number of returns or bits	
ms	millisecond (time)	sec $\times 10^{-3}$
ns	nanosecond (time)	sec $\times 10^{-9}$
N_D	Noise power at detector output	Watts
N_i	Noise power at IF amplifier output	Watts
N_s	Noise power in Servo loop	Watts
n_B	Order of Bessel function	
n_H	Running integer (See eq. 7)	
n_W	Order of Bessel function (integer)	
N_A	Number of sectors	
NAGC	Noise AGC	
P_{RN}	P_R for narrow beam antenna	Watts
PRF	Pulse repetition frequency	Pulses/sec
P_{TB}	P_T for broad beam antenna	Watts
P_{TN}	P_T for narrow beam antenna	Watts
P_T	Peak transmitted power (per pulse)	Watts
$P_T(t)$	Time function of transmitted power	Watts
P_R	Peak received power (per pulse)	Watts
$P_R(t)$	Time function of P_R	Watts
P_{RD}	Signal power per pulse at detector output	Watts
$P_{R\,max}$	maximum value of $P_R(t)$	Watts
P_s	Signal power in servo loop (per pulse)	Watts
P_{RB}	P_R for broad antenna beam	Watts
r	Radius at A_T	meters

Symbol	Description	Units
dr	Differential radius of A_T	meters
S-Band	2-4 GHz	
t_1	Start of rise of received pulse	Sec
t_2	End of rise of received pulse	Sec
t_3	Start of fall of received pulse	Sec
t_4	End of fall of received pulse	Sec
t_r	Rise time of received pulse	Sec
t_T	Transmitted pulse length	Sec
t_R	Pulse length at receiver	Sec
t_W	PRF period	Sec
t_i	Servo integration time	Sec
t_a	Acquisition time	Sec
t_{gw}	Gate width	Sec
t_{rT}	Rise time of transmitted pulse	Sec
t_s	Integration time per second	Sec
t_L	Servo loop iteration time	Sec
T	Absolute temperature	^oC
u(t)	Time function of filtered output of mixer	Volts
V_F	Velocity along flight path	m/Sec
V_V	Vertical component of V_F	m/Sec
VCO	Voltage controlled oscillator	
v_{10}	Transmitted signal in FM/CW system	Volts

Symbol	Description		Units
v_{20}	Local oscillator signal in FM/CW system		Volts
v_{30}	Received signal in FM/CW system		Volts
V_1	Maximum amplitude of v_{10}		Volts
V_2	Maximum amplitude of v_{20}		Volts
V_3	Maximum amplitude of v_{30}		Volts
v_s	Output of phase detector		Volts
V_s	Maximum amplitude of v_s		Volts
$v_a(t)$	Time function of output of fϕ amplifier		Volts
V_A	Maximum amplitude of $v_a(t)$		Volts
V_{SL}	Peak voltage in Servo Loop		Volts
V_T	Track point voltage		Volts
W	Power		Watts
ω_p	$2\pi f_p$	PRF fundamental radian frequency	rad/sec
ω_ϕ	$2\pi f_\phi$	Phase measuring radian frequency	rad/sec
ω_M	$2\pi f_M$	Modulation radian frequency	rad/sec
ω_d	$2\pi f_D$	Doppler radian frequency	rad/sec
ω_{IF}	$2\pi f_{IF}$	IF radian frequency	rad/sec
ω_c	$2\pi f_c$	Carrier radian frequency	rad/sec
ω_{VCO}	$2\pi f_{VCO}$	VCO radian frequency	rad/sec
X-Band	8 - 12 GHz		
x, y, z	Coordinates of Cartesian system		

Symbol	Description	Units
α	Phase of f_ϕ oscillator	Deg.
β	Phase of VCO	Deg.
γ	Phase of f_ϕ amplifier	Deg.
α_1	Reference phase of IF signal	Deg.
β_1	Phase response of low pass filter	Deg.
α_A, θ_A, ψ_A, ϕ_A, d, P_A	See Figures 35, 36, 37, 38, 39 variables used to describe antenna look angle	
R_1, R_2, R_3, R_4	Radiators (See Figure 37)	
H_s, V_s	Horizontal (H_s) and vertical (Vs) bits required for particular phase shift in scan program	
δ	Surface backscattering coefficient	
ϵ_{HN}	Altitude error due to thermal noise	Meters
ϵ_{HB}	Altitude error due to antenna beam	Meters
ϵ_{HV}	Altitude error due to velocity	Meters
ϵ_{tN}	Time error due to thermal noise	Sec.
ϵ_{tB}	Time error due to antenna beam	Sec.
ϵ_{tV}	Time error due to velocity	Sec.
ϵ_ϕ	Phase error	Meters
ϵ_s	Specified max. time error	Sec.
$\epsilon_{t\phi}$	Time error due to ϕ	Sec.

Symbol	Description	Units
$\epsilon_{H\phi}$	Altitude error due to ϵ_{ϕ}	Meters
ϵ_o	Total error in pulse system	Meters
η	Duty cycle	
θ_B	1/2 Antenna 3 dB beamwidth	Deg.
θ	Antenna angle (variable)	Deg.
λ_M	Wavelength of modulation frequency f_M	Meters
λ_{M1}	Wavelengths of modulation frequencies	Meters
λ_{M2}	f_{M1} & f_{M2} used to eliminate altitude holes	Meters
μs	Microsecond (time)	Sec $\times 10^{-6}$
ρ	Antenna radiation efficiency	
σ	Radar cross section	Meter^2
τ	$\frac{2H}{c}$ round trip delay time	Sec.
τ_L	Delay time of leakage signal	Sec.
ϕ_x	Random phase angle associated with surface return	Deg.
X_{pi}	Power signal to noise ratio at output of IF Amp.	
X_{pD}	Power signal to noise ratio at output of detector	
X_{pL}	Power signal to noise ratio in Servo loop	
X_{pT}	Power signal to noise ratio of threshold in Servo loop	
ψ	Angle between antenna boresite and vertical	Deg.

PART I

RADAR ALTIMETER REQUIREMENTS

INTRODUCTION

This study involves the requirements of an altimeter used primarily to measure the altitude of a deep-space planetary lander above the planet's surface. Specifically, the altimeter will be a radar altimeter operating in the X-band of frequencies (8 to 10 GHz). Because the device is a radar altimeter, its principle of operation involves measuring the elapsed time required for electromagnetic energy to propagate to the surface and back again, assuming a constant velocity of propagation. This measurement must be made to a sufficient accuracy to be useful. It is therefore helpful to discuss fundamental limitations of the accuracy of measurements made by a radar altimeter.

Basic Considerations

Consider Figure 1 which outlines geometrically a basic radar range measurement to a target extensive enough to fill the antenna beam. As the wave front illuminates the target, the terrain will first reflect energy directly below the altimeter. As the wave front spreads out on the terrain, the additional reflected energy will be delayed in transit time from that first returned energy.

In order to ensure the measurement of altitude within a specified error, only a certain portion of the reflected energy will be useful in the measurement. That portion of energy will be represented by a limited area of the terrain or by a maximum antenna beamwidth. If, for example, the altitude measurement is required to be within 2 percent of the true altitude, the useful antenna beamwidth is about 22.7 deg by 22.7 deg. If the antenna beamwidth is any greater than that dictated by the accuracy requirements, the system is not optimized to efficiency, since some of the returned energy is arriving too late to be useful in the range measurement. Also, since antenna gain and beamwidth are inverse functions of each other, a narrow-beam antenna will result in a smaller required transmitter power than will a broad beam antenna, all other parameters being equal. Therefore, it is evident that an altimeter required to accurately measure height above terrain where the expected attitude variations (rather than the required accuracy) dictate

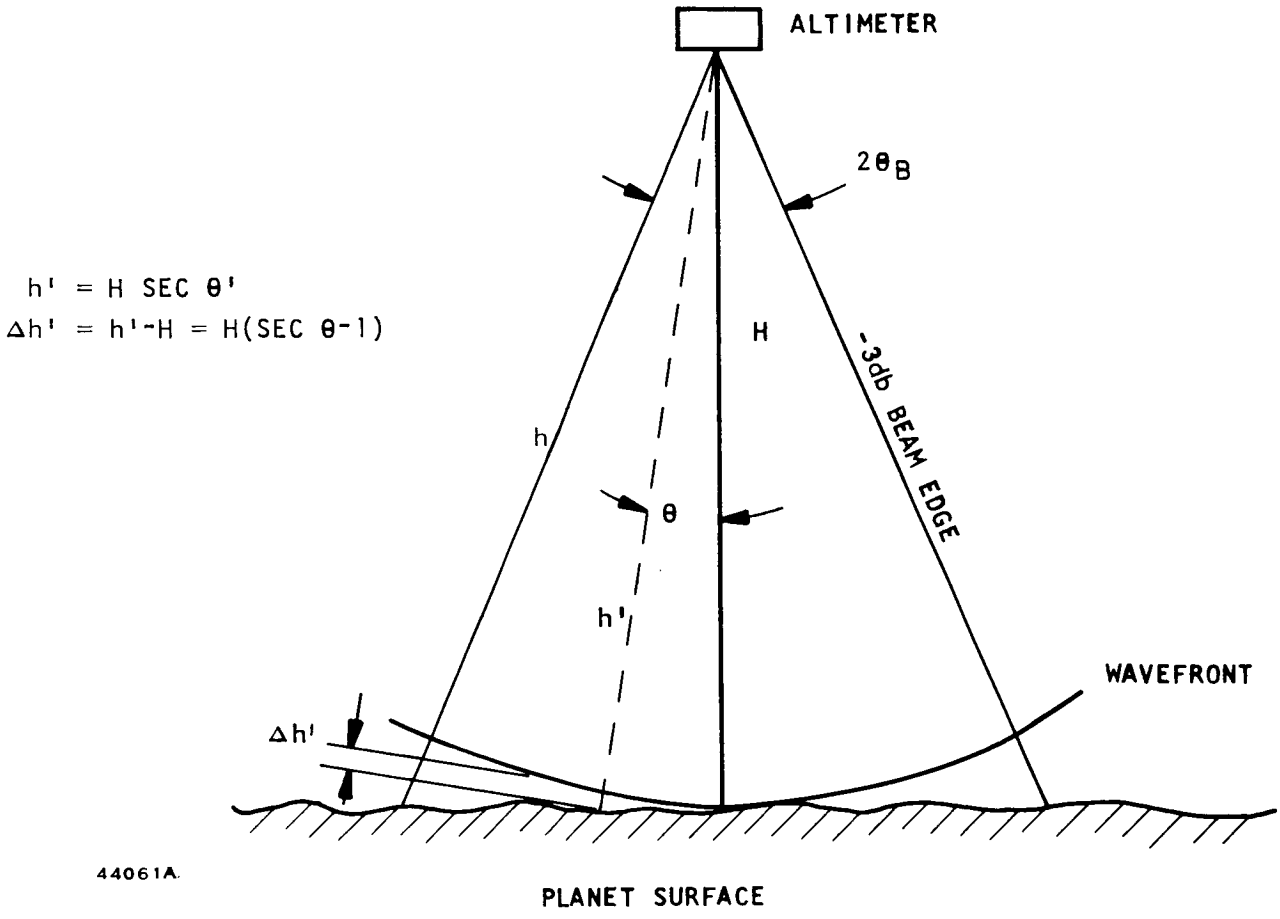

Figure 1. Geometric Representation of Radar Altitude Measurement

the minimum illumination coverage will not be the most efficient system, since much of the returned energy is not useful for the measurement.

Based on the required illumination and accuracy, calculations show for equal returned peak power, that a broad-beam system will require about 520 times more transmitted peak power than a scanned-beam system.

Accuracy also depends on the signal-to-noise ratio of the processed data. A high signal-to-noise ratio (clean signal) can be more accurately processed and will, therefore, produce fewer errors (due to noise) than a low signal-to-noise ratio. Since the target is beam filling, all the transmitted

power will be incident on the target. If the target (terrain) is assumed to be dispersive, with a mean reflectivity of δ, then the power reflected back to the altimeter is $P_T\delta$, where P_T is the transmitted power. Of course the characteristics of the Martian surface are unknown, so for the purposes of this study a value of −20 dB will be assumed for δ. In other words, the surface will absorb 99 percent of the incident power. This value is considered conservative for the Lunar surface (Figure 2), which probably is a good approximation of the Martian surface.

The parameters of the Mars probe altimeter that have a direct bearing on the selection of a modulation technique, as obtained from the Work Statement, are listed below:

Maximum altitude	~ 15.5 k/m
Minimum altitude	~ 300 meters
Accuracy	±2 percent, or ±10 meters
Antenna size	6 in.

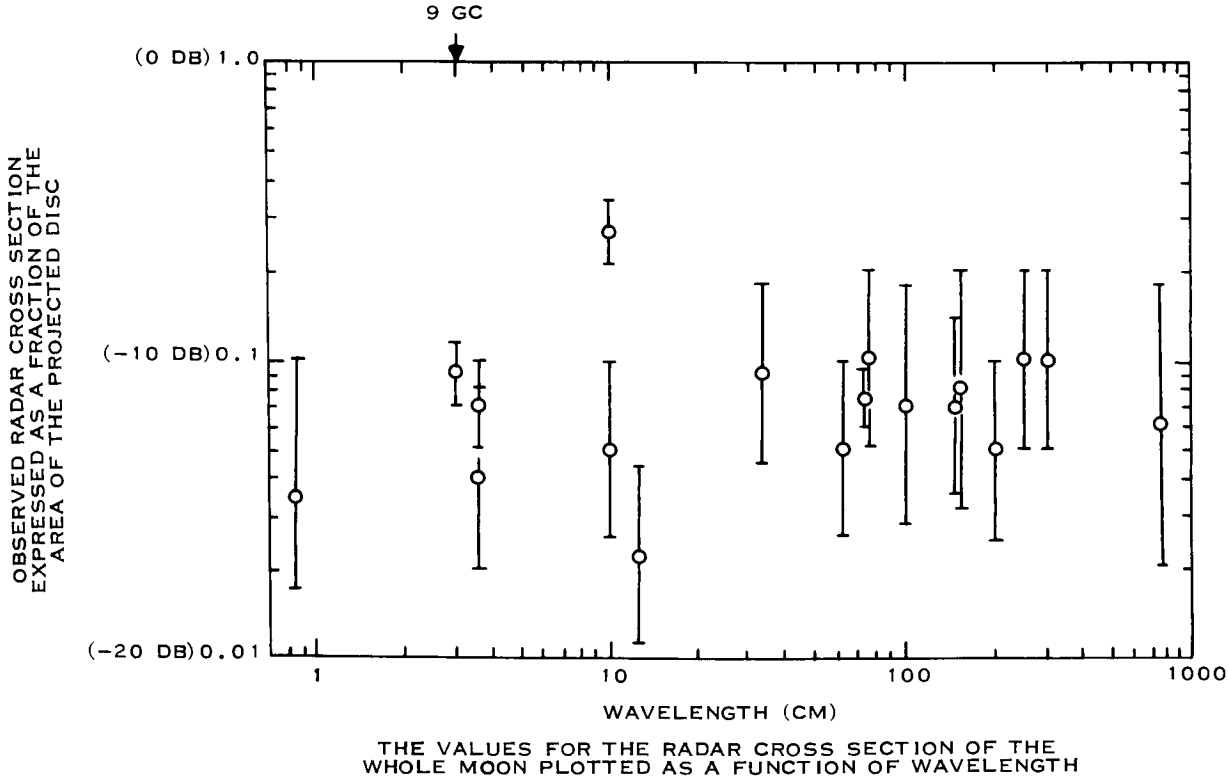

Figure 2. Radar Cross Section of the Moon (Reference 1)

Maximum Velocity

The maximum velocity listed in the Work Statement was 3.0 km/sec. Since the maximum doppler frequency is a critical parameter in the design of any of the systems considered, except the narrow pulse system, the velocity altitude profile given for a VM-8 atmosphere and an entry velocity of 20 k ft/sec has been used instead. The variation of doppler frequency with altitude is shown in Figure 3.

The major differences between the Mars probe altimeter and the usual aircraft application are the maximum operating altitude and the large doppler frequency produced by the high vehicle velocity during this phase of the entry.

In addition to these two characteristics, a third factor that must be considered is the effect on the antenna design produced by the change in vehicle attitude from maximum operating altitude to touch down. In a VM-8 atmosphere and at an entry velocity of 20 k ft/sec, the vehicle has an initial entry angle of approximately 60 degrees with respect to the vertical. This changes to 0 degrees at touch-down. This forces one to also consider the relative merits of a fixed versus a scannable antenna system.

EVALUATION OF MODULATION TECHNIQUES FOR THE MARS PROBE APPLICATION

Discussion of FM/CW System

A FM/CW system measures the amount of frequency change between the transmitted and received signal frequencies; thereby, determining propagation delay, assuming of course, apriori data concerning the modulation function. For a linearly modulated (frequency) transmitter, the IF frequency, developed by mixing the received signal with the sampled transmitted signal (with zero delay), is proportional to altitude.

FM/CW Modulation

An example of an FM/CW altimeter for standard aircraft application is shown in Figure 4. The transmitter, local oscillator, and received signal are given respectively by equations (1), (2), and (3).

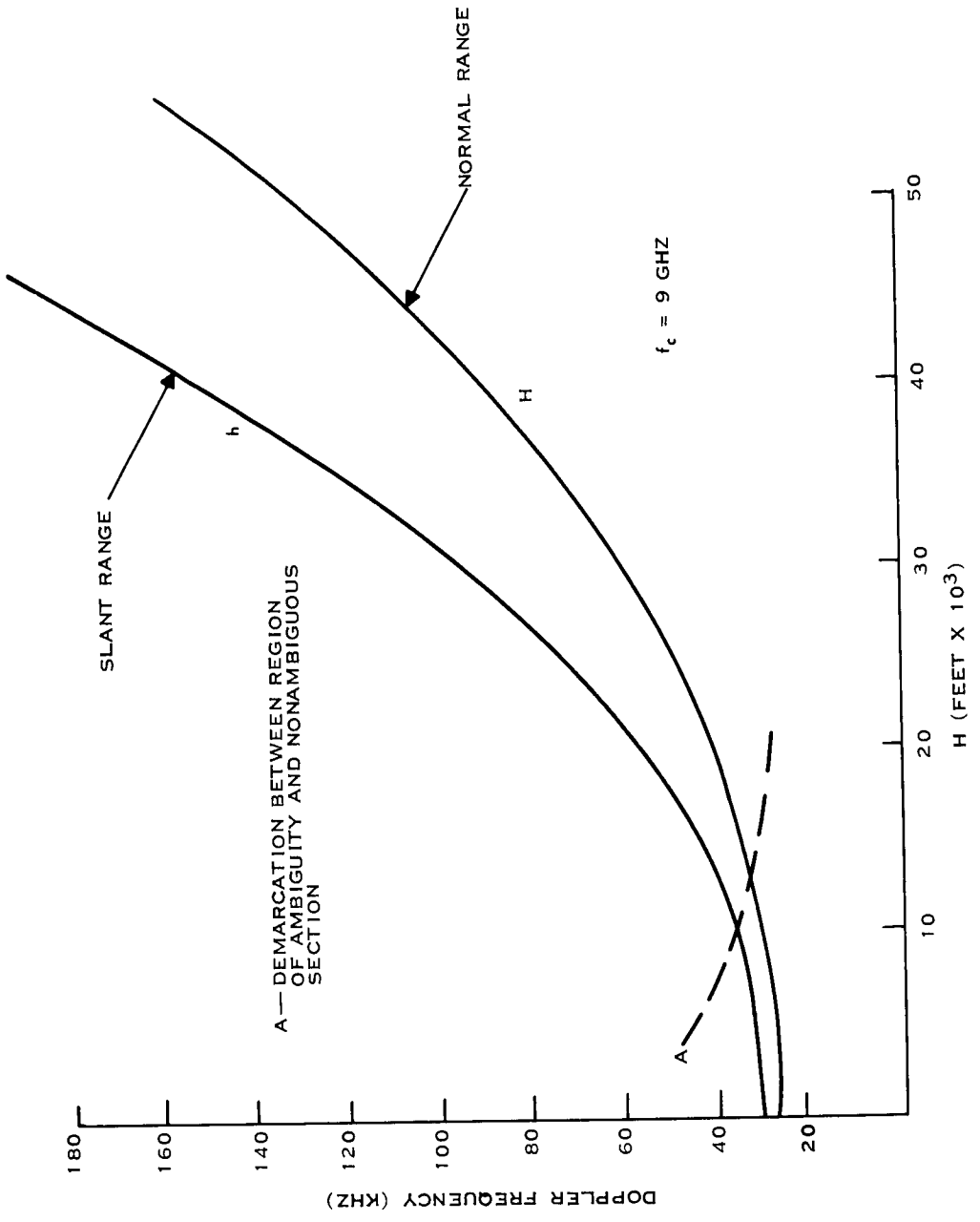

Figure 3. Doppler Frequency Versus Altitude

43501A

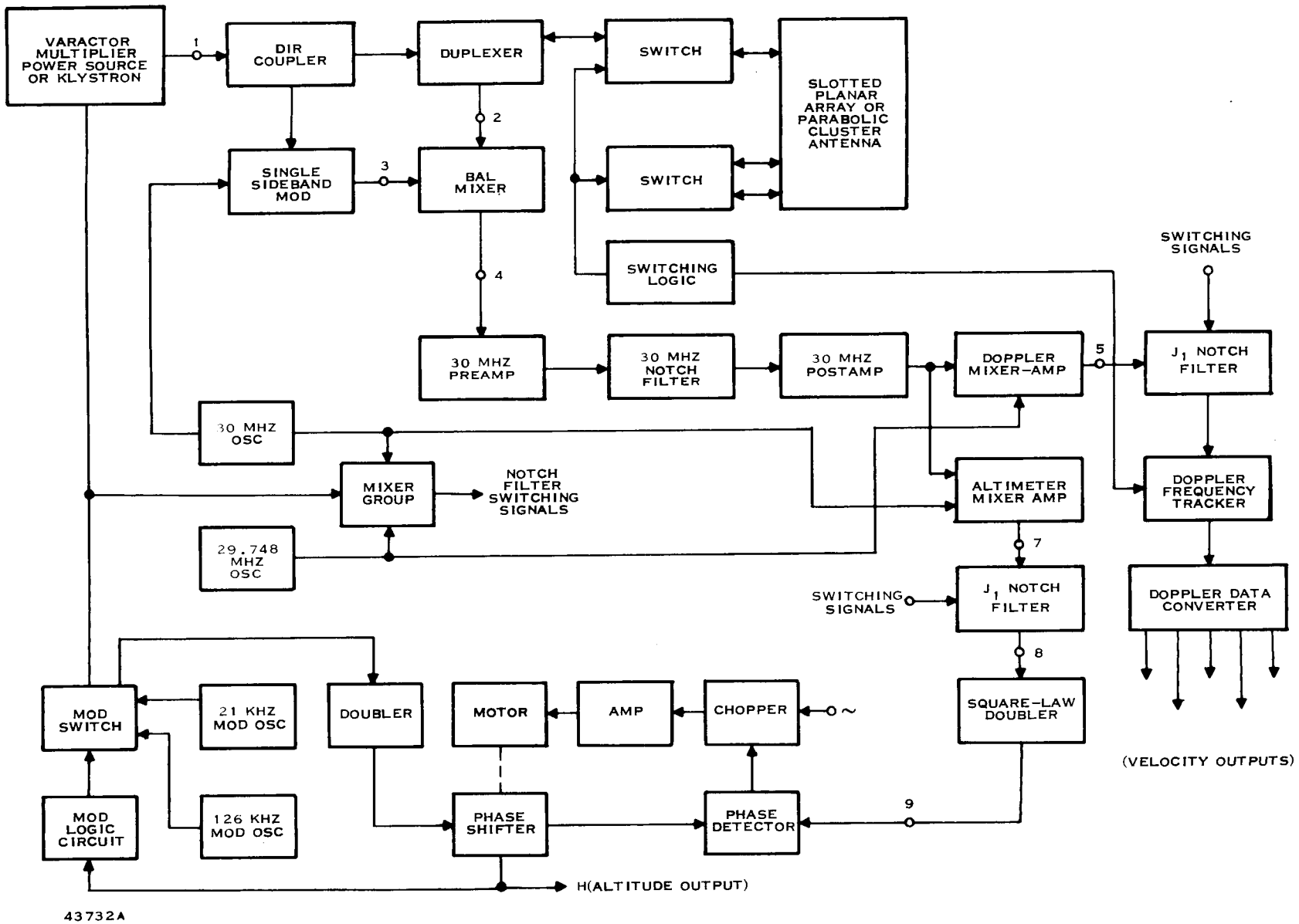

Figure 4. FM/CW Altimeter Block Diagram (Reference 2)

Transmitter Signal

$$v_{10} = V_1 \sin (\omega_c t + M \sin \omega_M t) \quad (1)$$

Local Oscillator Signal

$$v_{20} = V_2 \sin \left[(\omega_c + \omega_{if})t + M \sin \omega_M t \right] \quad (2)$$

Received Signal

$$v_{30} = V_3 \sin \left[(\omega_c + \omega_D)(t - \tau) + M \sin (\omega_M)(t - \tau) + \phi_x \right] \quad (3)$$

where ω_c is the carrier radian frequency

M is the modulation index

ω_M is the modulation radian frequency

ω_{IF} is the intermediate radian frequency

τ is the round trip delay time

ϕ_x is the random phase angle associated with the surface return.

The received spectrum, at IF, produced by mixing the received signal with the LO signal is shown in Figure 5. When the product of (2) and (3) is expanded in terms of Bessel functions, the argument of the Bessel function, I, is found to be

$$I = 2M \sin \frac{\omega_M \tau}{2} \quad (4)$$

From (4) it is seen that I is a function of delay time τ. This effect resulted from adding the f_M modulation to the LO signal as shown by (2) and serves to reduce the effects of transmitter leakage. Transmitter leakage, produced by the beating of the LO signal with the transmitter signal, will have a very short delay time, τ, so that the arguments of the Bessel functions are given by (5)

$$I_L = 2 M \sin \frac{\omega_M \tau_L}{2} \quad (5)$$

where I_L = argument of Bessel functions for leakage signal

τ_L = delay time, transmitter to receiver, for leakage signal.

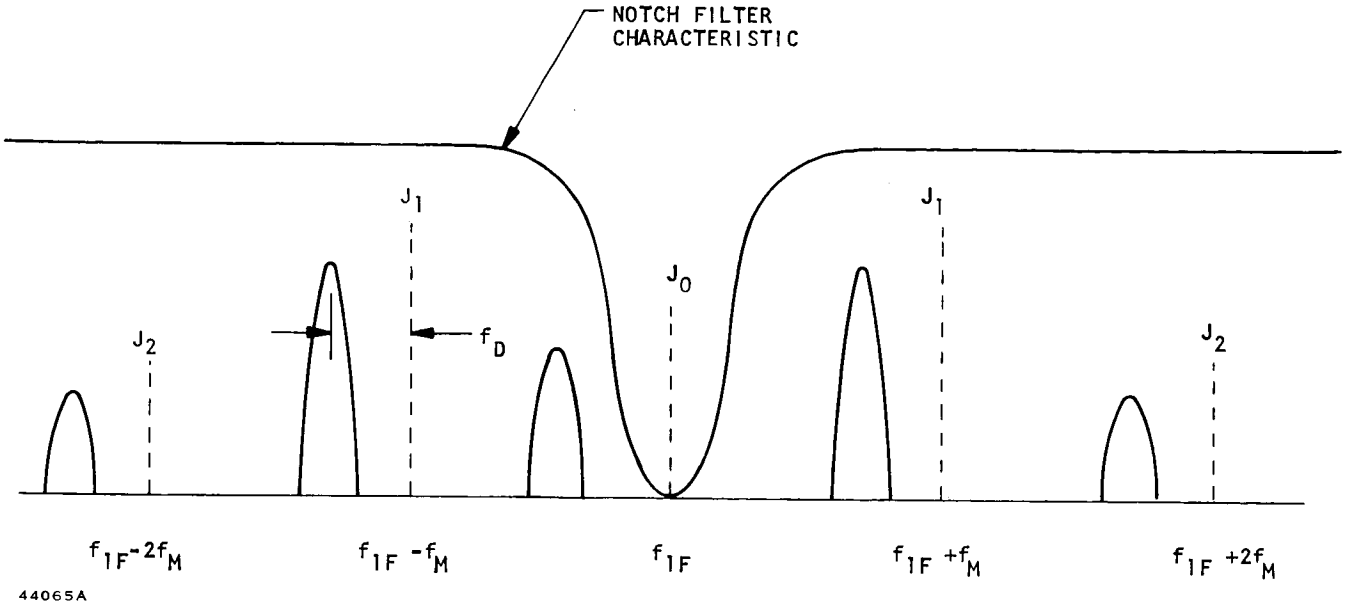

Figure 5. Received Signal IF Impression

A sketch of the first few orders of Bessel functions is shown as a function of I in Figure 6. From this sketch it is seen that the amplitude of the leakage signals, except J_0, will be very small for very small I. The leakage signal J_0 is eliminated by the 30-MHz notch filter shown in Figure 5. The transfer characteristics of this filter is also shown in Figure 5.

One of the Bessel sidebands is then selected for further processing. The first sideband, J_1, has been used for the system shown in Figure 3, but the second or third can be selected if a wider frequency spacing is required between the signal sideband and the spectrum about J_0 produced by unavoidable amplitude modulation on the transmitter signal.

The output of the IF amplifier is then mixed, in the altitude channel, with a signal at the IF frequency to produce a folded spectrum. The desired signal sideband pair is then isolated in the notch filter (Figure 4 as J_1) and doubled to produce a relatively clean signal at $(2n_BJn_B)$ from which phase measurements are made in the feed-back circuitry to provide a measurement of altitude. The n_B in $(2n_BJn_B)$ above is the order of the Bessel sideband selected for altitude determination.

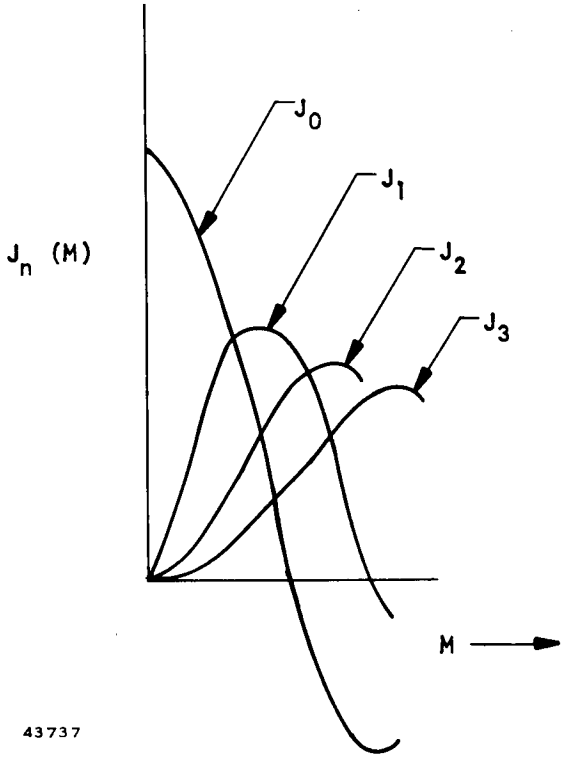

Figure 6. Bessel Functions for Small Arguments

Two factors are involved in the selection of a modulation frequency for this system. These are the elimination of altitude holes and the ability to make unambiguous altitude measurements.

Altitude holes are produced when the argument of the Bessel function goes to zero when the delay τ is not zero.

$$I = 2_M \sin(\pi f_M \tau) = 0 \quad \text{for} \quad \tau \neq 0 \tag{6}$$

This will occur when

$$f_M \tau = n_H \ . \tag{7}$$

Therefore, f_M must be selected to satisfy the following criterion

$$f_M \leq \frac{1}{\tau} \equiv f_M < \frac{c}{2H} \quad (\text{for } n_H = 1) \tag{8}$$

Or, in terms of wavelength, this becomes:

$$\lambda_M < 2H \ . \tag{9}$$

Unambiguous altitude measurements can be made only when twice the maximum altitude is less than a wavelength at the frequency from which phase measurements are obtained. If the first order sidebands are used, this will be, after doubling, equal to 2 f_M; therefore,

$$\frac{c}{2f_M} \geq 2H \quad , \qquad f_M \leq \frac{c}{4H} \ . \tag{10}$$

From (8), it is seen that if this frequency is chosen for unambiguous altitude measurement, then there will be no altitude holes.

For the Mars probe application, the maximum modulating frequency that can be used is:

$$\begin{aligned} f_M &= \frac{c}{4H} \\ &= 4.92 \text{ kHz} \end{aligned} \tag{11}$$

at 50,000 feet. Analysis of the system shown in Figure 4, and the spectrum shown in Figure 5, shows this system will work properly only when the doppler frequency is small enough to prevent the signal side bands from shifting into the 30-MHz notch filter. This requirement prevents the use of the FM/CW system as described since the doppler shift for the Mars probe application will far exceed 5 kHz at the maximum operating altitude.

Two modifications of the basic system were devised to overcome these difficulties. The first used two modulation frequencies which were applied in an alternating sequence to transmitter and LO signals in manner employed for the basic system. Each of these frequencies would be larger than the maximum doppler shift to overcome the difficulty noted above. Ambiguities would be eliminated by choosing the frequencies so that their wavelengths were relatively prime and the product met the requirement set by the inverse of equation (10).

$$f_M \leq \frac{c}{4H} \equiv \lambda_M \geq 4H \tag{12}$$

Therefore,

$$\lambda_{M1}\lambda_{M2} \geq 4H \quad . \tag{13}$$

This is completely equivalent to the method employed to eliminate range ambiguities in high PRF pulse doppler systems.

Altitude holes would occur for each frequency but not, mathematically at least, for both frequencies simultaneously.

This modification would not appear to be suitable for the Mars probe application because of the large number of times that the modulation frequencies would have to be switched (generates "holes" in data rate due to acquisition time) to eliminate altitude holes. This condition results from the wide discrepancy between the desired modulation frequency (about 5 kHz) and the modulation frequency required to exceed the maximum doppler shift (about 180 kHz for doppler along velocity vector).

The second modification uses two modulation frequencies applied simultaneously to the transmitter. One is greater than twice the doppler frequency and acts as a subcarrier for the other frequency at about 5 kHz as required by equation (12). Only the 5-kHz modulation frequency is applied to the local oscillator. This produces the sidebands as shown in Table 1.

Table 1. –Amplitude and Frequency for Subcarrier Modulation

Amplitude	Frequency
$Jo(I_1)Jo(I_2)$	$f_{If} - f_D$
$Jo(I_1)J_k(I_2)$	$f_{If} - f_D \pm Kf_2$
$Jo(I_2)J_k(I_1)$	$f_{If} - f_D \pm Kf_1$
$J_M(I_1)J_N(I_2)$	$f_{If} - f_D \pm Mf_1 \pm Nf_2$

The $J_1(I_1)Jo(I_2)$ is selected as the subcarrier and the $J_1(I_1)$ $J \pm 1(I_2)$ as the signal sidebands. Since only the frequency f_2 was applied to the LO, the Bessel function argument, I_2, is the same as that given for the basic system

$$I_2 = 2M_2 \sin\pi f_2\tau \quad , \tag{14}$$

but the Bessel function argument for I_1 is just

$$I_1 = M_1 \quad . \tag{15}$$

Thus, altitude holes are produced only by $J(I_2)$, while the desirable property of leakage signal suppression is still retained since leakage signal amplitude is also proportional to the product, $J_N(I_1)J_M(I_2)$. And one of these is small for small delays as discussed in the section on the basic system.

It is also necessary in this system to derive the doppler in the doppler system and use it to derive a second local oscillator signal at $(f_{IF} - f_D)$ to beat with the IF output in the altitude channel. This stabilizes the altitude spectrum and allows the desired sidebands to be isolated and doubled for phase measurement.

This system will then be applicable in situations where the doppler spectrum spread is less than the signal sideband separation or approximately 5 kHz. If the spread is greater than this, the doppler spectrum from adjacent sidebands will overlap the position of the sideband from which phase measurements are to be made and a valid phase measurement could not be obtained.

The doppler spectral spread is determined by the vehicle velocity, the antenna pointing angle (with respect to the velocity vector), and the antenna radiation pattern. A plot of spectrum spread for the antenna, pointing normal to the surface, and the flight profile of Figure 3 are shown in Figure 7 in terms of normalized doppler. From the figure, it is apparent that the greatest portion of received power contains frequency components near the maximum doppler frequency. Figure 8 shows the spectral distribution of doppler frequencies if the antenna boresight is normal to the surface with the same flight profile assumed in Figure 7. In this case, the received power is centered around the maximum doppler times the cosine of the boresight to flight vector angle (55 degrees). Both Figure 7 and Figure 8 were developed by numerically integrating the received power and doppler frequency over selected strip or annular ring isodops within the effective illuminated terrain, taking into account the antenna radiation pattern and modified space loss for different look angles within the pattern. If it is assumed that spectrum overlap at the -10-dB level can be tolerated, then from Figure 7 and Figure 8 it is seen that this system could be used to obtain altitude only below 10 kft. That is, from Figure 7:

$$(0.986 - 0.923)f_D \max = 5 \text{ kHz } (-10 \text{ dB level})$$

$$f_D \max = \frac{5 \times 10^3}{0.063} = 79.3 \text{ kHz} ; \tag{16}$$

from Figure 3 (along velocity vector)

$$\text{Slant Range} = 30.5 \text{ kft } (f_D \max = 79.3 \text{ kHz}) ;$$

from Figure 8, h would be well below 10 kft. It is concluded from this that the FM/CW technique is not applicable for the Mars probe application.

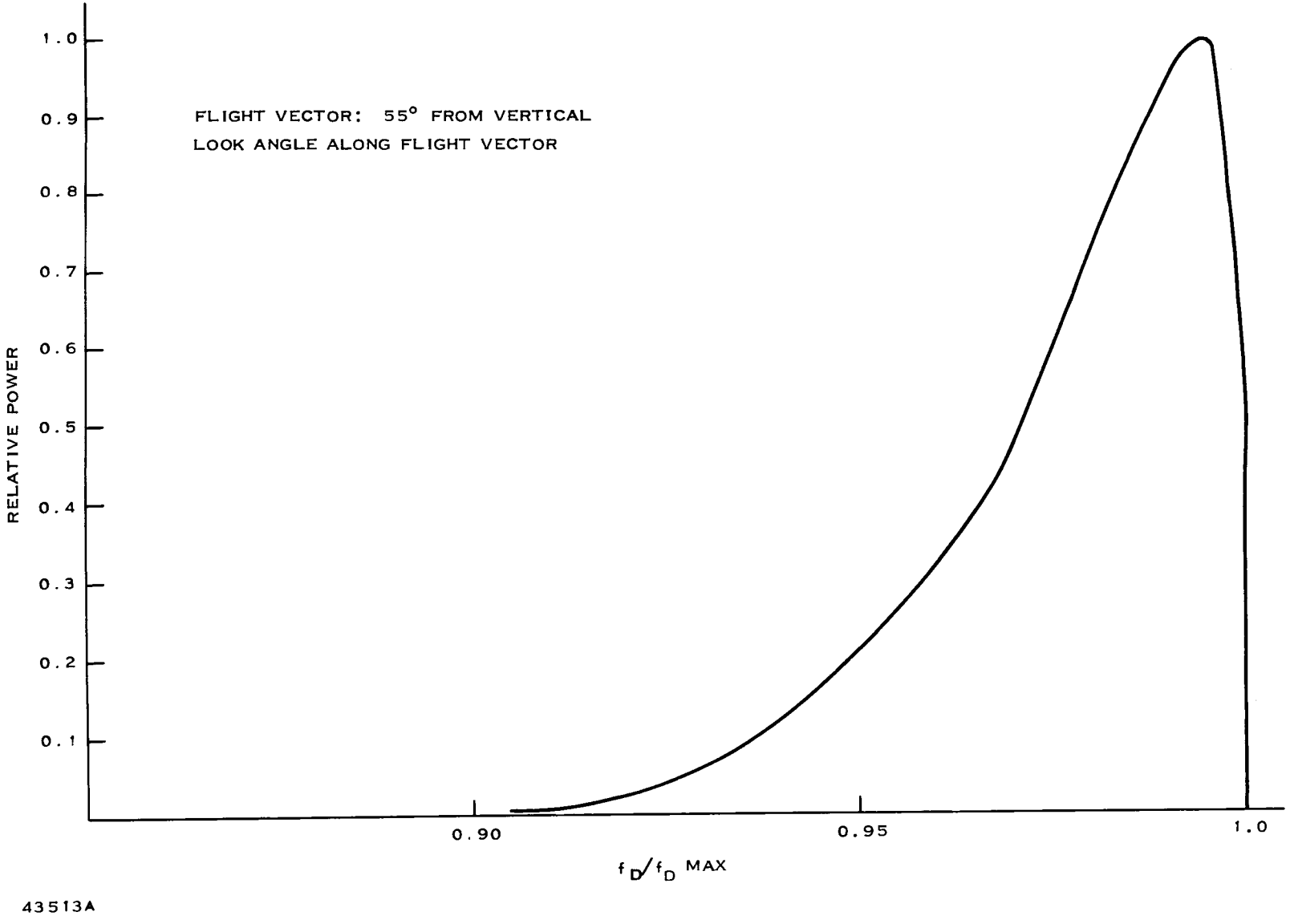

Figure 7. Doppler Spectrum, Look Angle Along Flight Vector

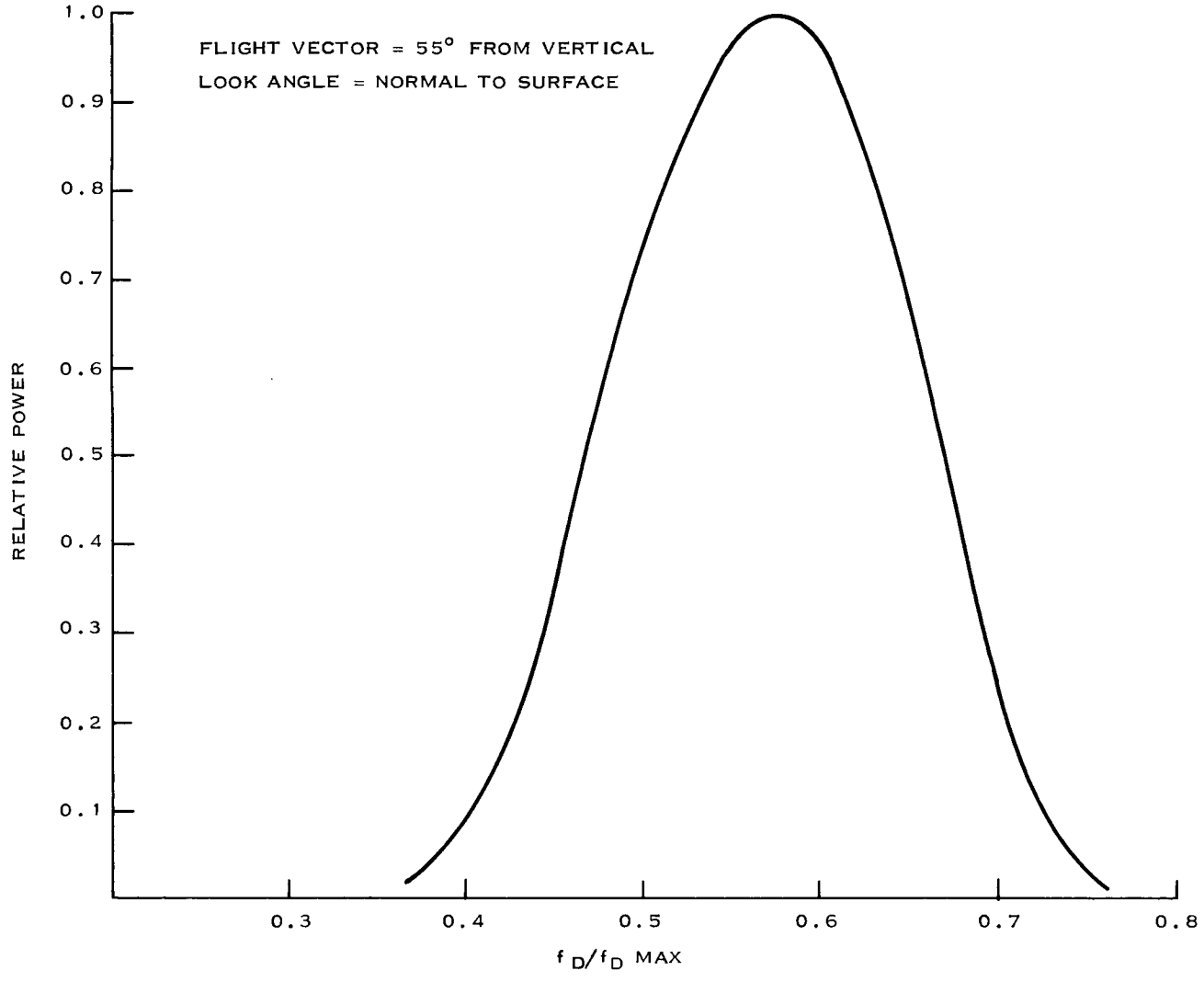

43502A

Figure 8. Doppler Spectrum, Look Angle Normal to Surface

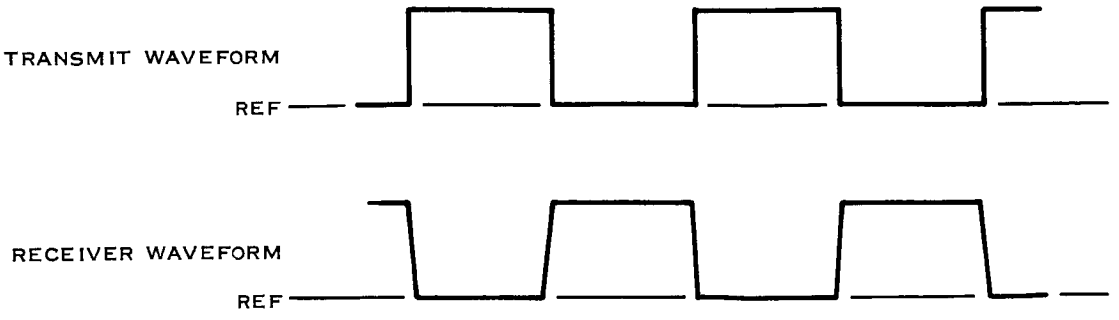

Figure 9. Transmit and Receive Waveform for a Point Target and a Properly Adjusted PRF, ICW System

DISCUSSION OF ICW SYSTEM

An ICW altimeter uses a form of pulse modulation where the duty cycle is 50 percent. The PRF is adjusted so that the transmitter is on for the length of time required for the leading edge of the pulse to reach the surface and return to the receiver. The transmitted and received waveforms, after detection for a point target and with a properly adjusted PRF, are shown in Figure 9.

When the PRF is adjusted so that the received pulse is exactly centered in the transmitter off period, the altitude can be found as a function of the PRF.

$$H = \frac{c}{4\ PRF} \quad . \tag{17}$$

The principal function of the altimeter circuitry is to detect changes in the relationship between the transmitter pulse train and the receiver pulse train and to automatically adjust the transmitter PRF to maintain the condition shown above. This is accomplished by monitoring the phase difference between the fundamental of the transmit waveform and the fundamental of the receiver waveform. The phase detector output is then used as a control voltage in a servo loop which is designed to maintain this phase difference at exactly 180 degrees.

The idealized waveform will not be achieved completely in practice because the actual target is not a point target but is a distributed target which completely fills the antenna beamwidth. This causes the leading edge of the pulse to rise more slowly than the inherent rise time of the transmitter pulse

and stretches the pulse on the trailing edge because of the path length difference at the edges of the antenna beam. The magnitude of these effects will vary with the altitude, antenna beamwidth, and angle between the antenna boresight and the vertical, Figures 10a and 11.

The received pulsewidth can be derived as follows (Figure 10):

$$t_1 = \frac{2H}{c} \tag{18}$$

$$t_2 = t_1 + \frac{2\Delta h}{c} = \frac{2H}{c} + \frac{2H}{c}(\sec\theta_B - 1) \tag{19}$$

$$t_3 = t_1 + t_T = \frac{2H}{c} + t_T \tag{20}$$

$$t_4 = t_1 + t_T + \frac{2\Delta h}{c} = t_T + \frac{2H}{c}\sec\theta_B\,, \tag{21}$$

where t_T is the transmitter pulse length. The overall pulse length at the receiver is then given by

$$t_R = t_4 - t_1 = t_T + \frac{2H}{c}(\sec\theta_B - 1)\,. \tag{22}$$

Equivalent relationships for the antenna boresight off the vertical can also be derived.

$$t_1 = \frac{2H}{c}\sec(\psi - \theta_B) \qquad t_T \geq \frac{2\Delta h}{c} \tag{23}$$

$$t_2 = \frac{2H}{c}\sec(\psi + \theta_B) \tag{24}$$

$$t_3 = t_1 + t_T \tag{25}$$

$$t_4 = t_1 + t_T + \frac{2\Delta h}{c} \tag{26}$$

Threshold pulse length in this case will be

$$t_4 - t_1 = t_T + \frac{2\Delta h}{c} = t_T + \frac{2H}{c}\left[\sec(\psi + \theta_B) - \sec(\psi - \theta_B)\right]\,. \tag{27}$$

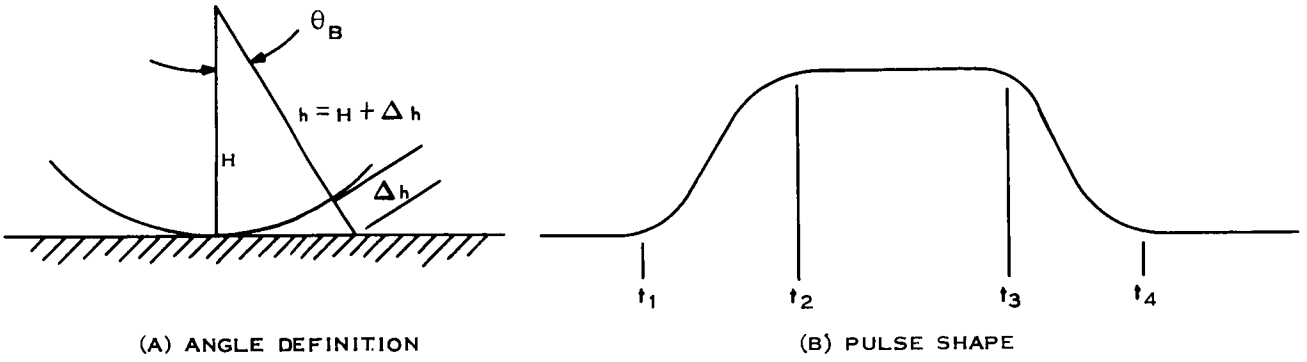

43512A

Figure 10. Received Pulse Stretching for Vertical Incidence

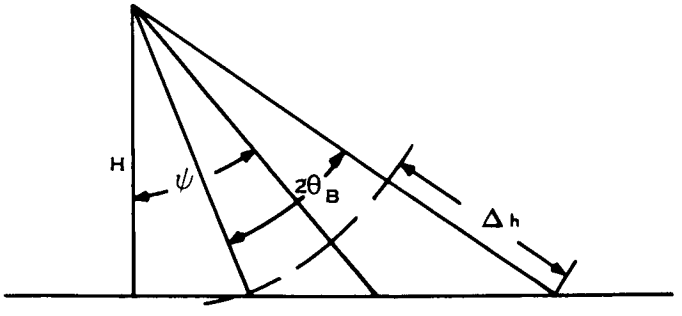

43506A

Figure 11. Angle Definition for Off Vertical Incidence

This stretching at maximum altitude for a 24-degree antenna beamwidth and vertical incidence will be approximately 2.23 percent overall or about 2 percent at the 10-percent points. It will increase to 13 percent under the same conditions for an incidence angle of 30 degrees off the vertical. This would indicate that the ICW modulation technique would not be applicable for a non-steerable antenna aligned in the direction of the velocity vector.

This brief analysis would indicate that ICW modulation would be applicable on a theoretical basis for altitude measurements on the Mars probe if a steerable antenna is provided.

ICW modulation will not provide doppler information until an altitude and velocity are reached where the Nyquist sampling criterion is met. Since the PRF is set by the altitude,

$$PRF = \frac{c}{4H} \quad . \tag{28}$$

Frequency folding and, therefore (unless special design techniques are employed), ambiguous doppler frequency measurement will be obtained wherever the doppler frequency is greater than one-half the PRF. The curve labeled A in Figure 3 separates the regions of ambiguous and unambiguous doppler. This indicates that unambiguous doppler can be obtained, when the antenna is aligned with the vertical, below 15,000 feet.

ICW Block Diagram Using Phase Measurement to Obtain Altitude

A simplified block diagram of the altitude channel for an ICW altimeter is shown in Figure 12. The reference signal for the phase detector is obtained by mixing the PRF reference signal from the transmitter modulator with the PRF plus the phase measuring frequency f_ϕ. This yields a continuous signal out of the upper amplifier at f_ϕ of cos $(2\pi f_\phi t + \alpha + \beta + \gamma)$ where α is the phase of the f_ϕ oscillator, β is the phase of the VCO, and γ is the phase of the f_ϕ amplifier.

The signal input to the phase detector is obtained as follows. The 50-percent duty cycle signal from the IF preamplifier, which is at the IF plus doppler, is mixed with the continuous signal at the PRF derived from the VCO plus the phase measurement frequency. The output is then demodulated in the amplitude detector. The output of the detector is a 50-percent duty cycle pulse which is amplitude modulated at the PRF plus f_ϕ. This signal can be represented as shown by Equation 29.

$$e_s(n_W t_W) = V_s(n_W t_W - \tau) \cos \left[(\omega_p + \omega_\phi)(n_W t_W - \tau) + \alpha + \beta\right] \tag{29}$$

where $V_S(n_W t_W - \tau)$ is the received pulse envelope as modified by the receiver gating function

t_W is the PRF period

$\omega_p = 2\pi$ PRF

$\omega_\phi = 2\pi f_\phi$

α = the phase angle of the f_ϕ oscillator

β = the phase angle of the VCO

τ = the time delay of the received pulse with respect to the transmitted pulse.

The pulse input out of the amplifier will drive the f_ϕ amplifier to produce a continuous signal which can be represented by Equation 30.

$$v_A(t) = V_A(t)\cos(\omega_\phi t - \omega_p t + \alpha + \beta + \gamma) \tag{30}$$

V_A is the amplitude of the signal which is nearly constant since the f_ϕ amplifier is a limiting amplifier. γ is the phase response of the f_ϕ amplifier. The other terms in (30) were defined in (29). It should also be noted that the term, $\omega_p n_W t_W = 2\pi n_W$ disappears because t_W was the period of the PRF and the addition of an integral number of 2π radians does not offset the value of (29),

When (30) is mixed with the reference signal in the phase detector, the output will be after filtering

$$\mu(t) = K_1 \cos(\omega_p \delta + \gamma_1 - \gamma_2) \tag{31}$$

where K_1 is a constant. If the phase response of the two f_ϕ amplifiers are the same, then the output will be only a function of the PRF as desired.

The accuracy required of the phase detector can be evaluated as follows: Since the servo is designed to null for a phase difference of π radians,

$$\epsilon_\phi = 2\pi f_p \frac{t_W}{2} - \left(2\pi f_p \frac{t_W}{2} - 2\pi f_p \epsilon_s\right)$$

$$= 2\pi \frac{\epsilon_s T}{t_W} = \frac{2\pi\, 0.02H/c}{4H/c} = 3.6^\circ \tag{32}$$

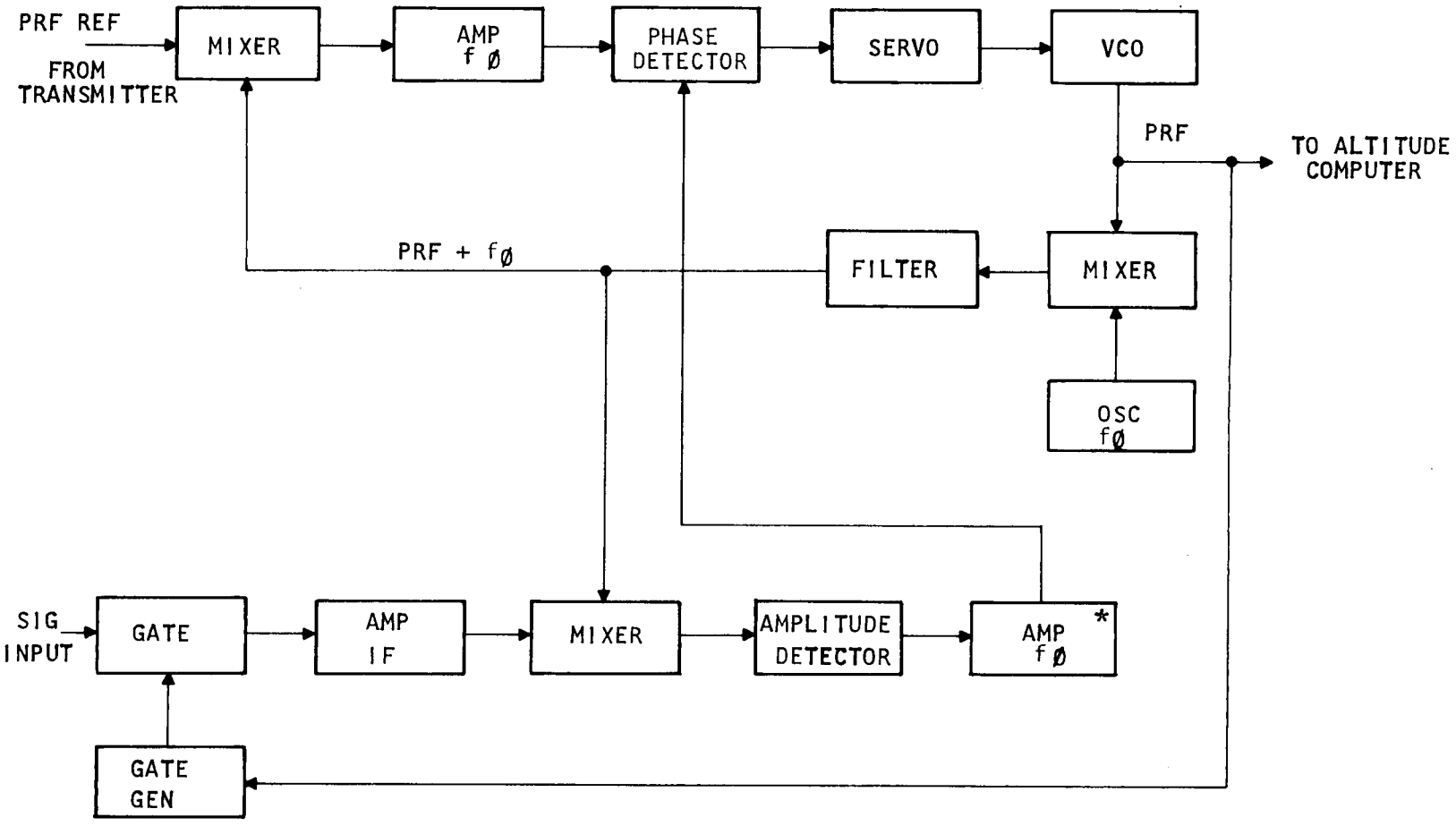

* THIS fØ AMPLIFIER IS A LIMITING AMPLIFIER

Figure 12. ICW Altitude Channel Phase Measurement Technique

This indicates a reasonable accuracy requirement and it will be a constant percentage of the altitude at all altitudes.

It would appear that crisper control could be obtained, at the expense of some loss in signal energy, by making the duty cycle somewhat less than 50 percent and thus prevent clipping so much of the leading and/or trailing edge of the received pulse in the receiver gate.

ICW Modulation with Early/Late Gate Tracking

It is also possible to design the receiver so that the received pulse is maintained in the center of the off period by an error signal obtained from an early/late gate tracker. A simple means of implementing this system is shown in Figure 13.

The received pulse position is monitored in the early/late gate detectors and an error voltage is derived in the difference amplifier to drive the servo amplifier that controls the VCO. The VCO output sine wave is coupled and fed to the early/late gate generators. The sine wave at twice the PRF is clipped and amplified to form a square wave. The leading edge of a positive pulse opens the early gate. The trailing edge then turns the early gate off and opens the late gate. The trailing edge of the negative square wave turns off the late gate and activates an inhibit circuit which prevents the early gate opening for one cycle. This causes the early/late gates to operate on alternate cycles of the doubled PRF.

The PRF sine wave is shifted by 180 degrees and fed to the trigger generator. This circuit generates a turn-on pulse for the transmitter when the positive going part of the PRF sine wave exceeds a threshold and a negative pulse to turn the transmitter off when the sine wave falls below the threshold. The threshold level is set for the desired duty cycle. If the threshold is at the zero level, a 50-percent duty cycle is produced. If it is set above this, the duty cycle is reduced. A sketch of the waveforms are shown in Figure 14. From Figures 12 and 13 it is seen that this is a particularly simple means of implementing an ICW altimeter.

The feed-back loop in this system adjusts the PRF to make

$$\frac{3}{4} t_W + \tau = \frac{5}{4} t_W \tag{33}$$

$$\tau = \frac{t_W}{2}$$

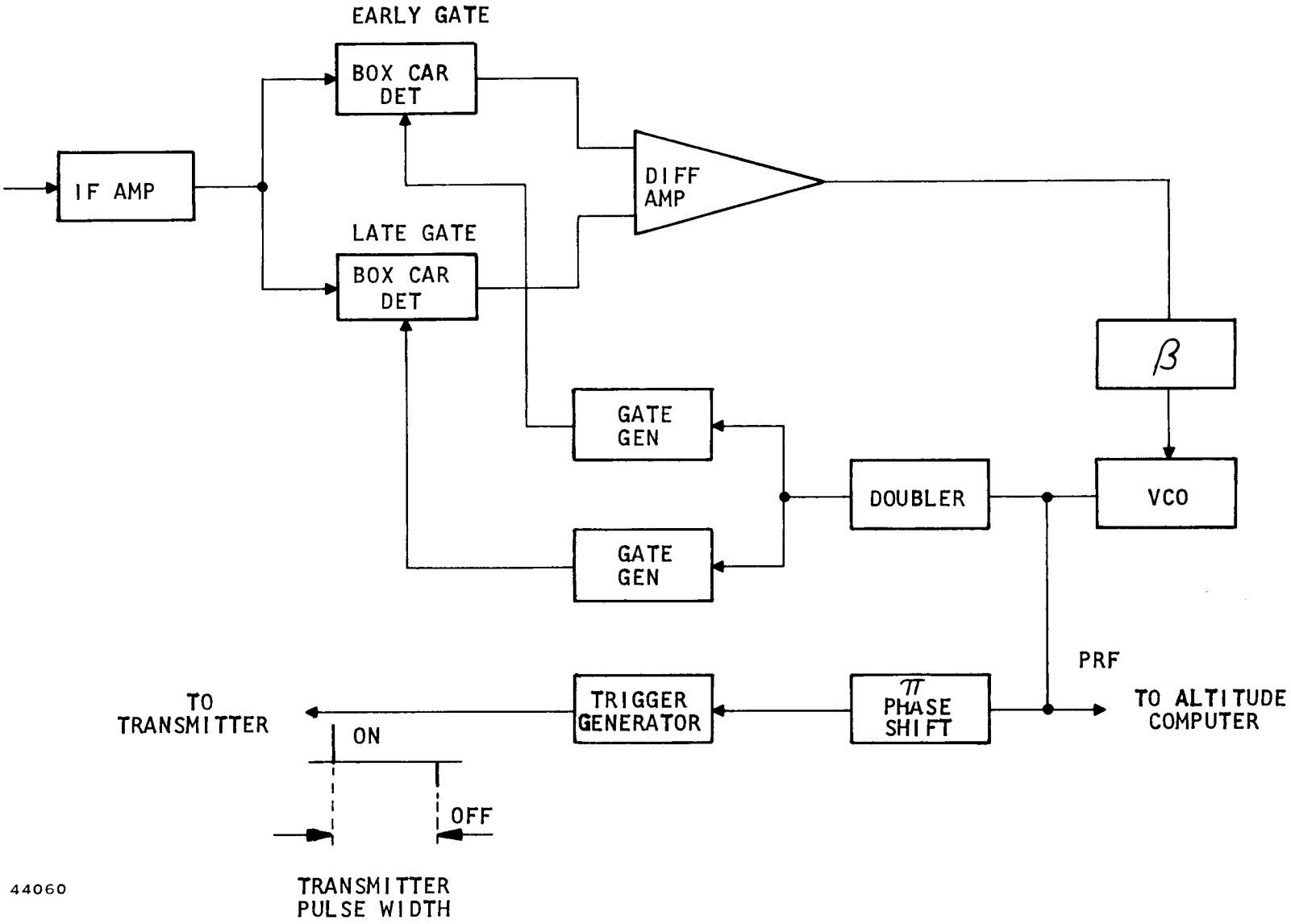

Figure 13. ICW Altitude Channel Early/Late Tracker

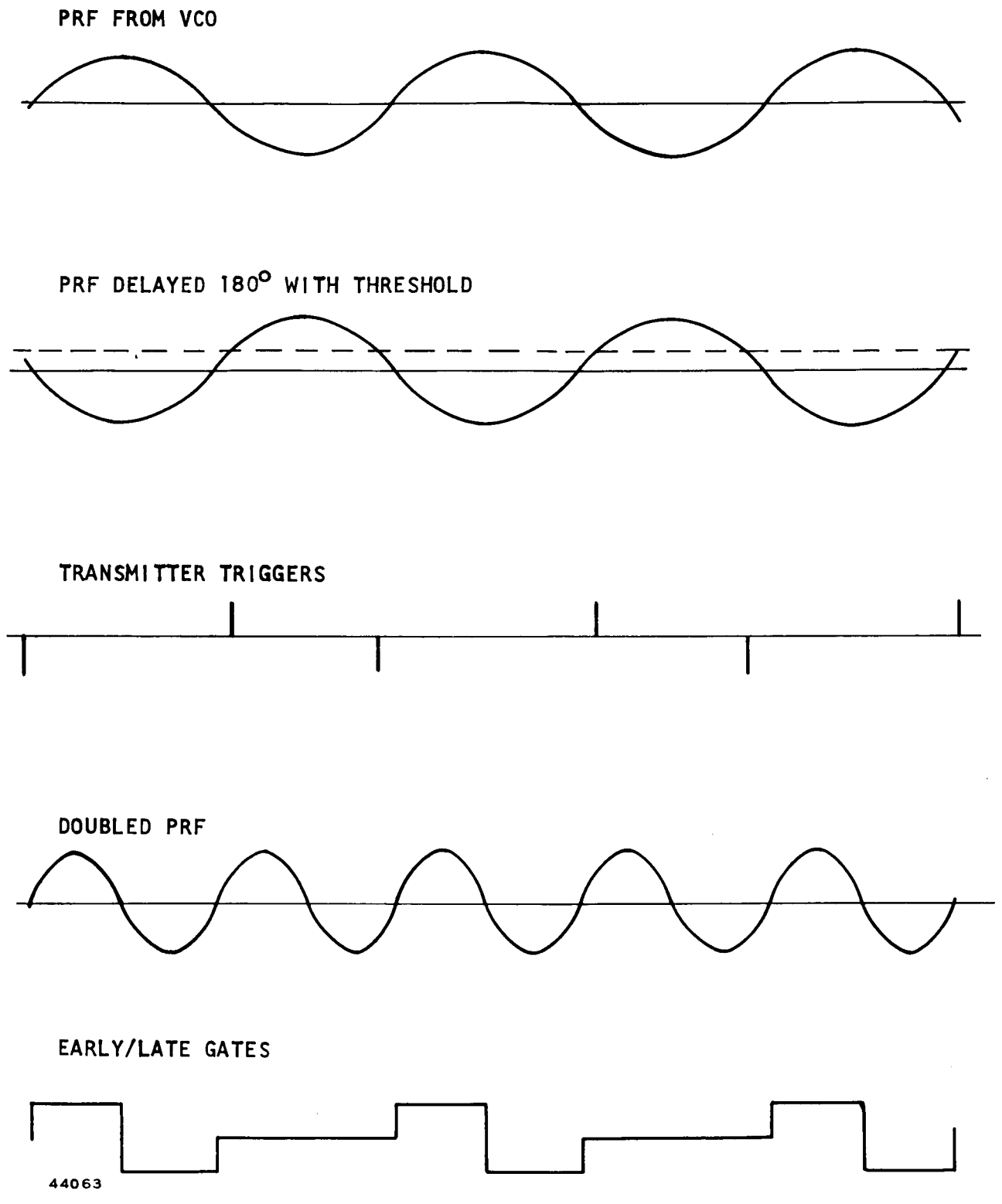

Figure 14. Waveforms for ICW with Early/Late Gate

or

$$\frac{1}{t_W} = PRF = 2\tau = \frac{4H}{c} \tag{34}$$

as was the case for phase difference processing. The time delay, τ, is measured from the center of the transmitter pulse to the centroid of the received pulse which was also the reference point for the phase at the transmitted and received waveforms in phase detection processing.

Accuracy Comparison

From an information content point of view, phase detection processing and early/late gate tracking should provide the same accuracy in the measurement of altitude. The basic accuracy equation for measuring the time of arrival of bandlimited pulse signals is given by (35).[3]

$$\epsilon_{tN} = \left[\frac{t_T}{4B\,\frac{E_{SD}}{E_{ND}}}\right]^{1/2} \tag{35}$$

where ϵ_{t_N} = the error in time measurement

t_T = the pulsewidth

B = the IF bandwidth

E_{SD} = the signal energy at the detector output in W-sec

E_{ND} = the noise intensity at the detector output in W/cycle.

This equation can be modified for later comparison with the accuracy equation for phase detection as follows:

$$E_{SD} = P_{RD}t_T R = \frac{P_{RD}t_T\, t_i}{t_W} \tag{36}$$

where P_{RD} = the signal power in each pulse at the detector output

t_W = the PRF period

t_i = the servo integration time

t_T = the pulsewidth.

$R = t_i/t_W$

And if a square law detector is assumed in both cases

$$P_{RD} = P_R^{\,2} \tag{37}$$

$$E_{ND} = B\,E_{Ni}^{\,2} \tag{38}$$

where P_R is the signalpower at the IF output
E_{Ni} is the noise intensity at the IF output

substituting (36), (37) and (38) into (35) gives:

$$\epsilon_{tN} = \frac{t_W}{\left[4B^2 t_i t_W \left[\frac{P_R}{BE_{Ni}}\right]^2\right]^{1/2}} \tag{39}$$

also

$$t_i = \frac{1}{2b} \tag{40}$$

$$\epsilon_{tN} = \frac{2}{c}\,\epsilon_{HN} \tag{41}$$

$$t_W = \frac{4H}{c} \tag{42}$$

$$\eta = \frac{t_T}{tW} \tag{43}$$

Substituting (40), (41), (42) and (43) into (39) gives, finally:

$$\frac{\epsilon_{HN}}{H} = \left(\sqrt{\frac{2b}{t_T B^2}}\right)\left(\frac{1}{(S/N)_{IF}}\right) \tag{44}$$

This analysis assumes that the full value of the pulse amplitude is available. This requires that $Bt_T \geq 1$. It may also be noted that (44), as it stands, is independent of the IF bandwidth, since the B^2 under the square root would cancel the B associated with the IF signal-to-noise ratio. It has been shown in practice, however, that the proper value for (44) is

$$\frac{\epsilon_{HN}}{H} = \left(\sqrt{\frac{2b\eta}{Bt_T/t_{gw}}}\right)\left(\frac{1}{(S/N)_{IF}}\right), \tag{45}^4$$

where t_{gw} is the full width of the early/late gate. This agrees with the optimum (44) only when $Bt_T = 1$.

The accuracy equation for the phase detection system is given by (46).[5]

$$\epsilon_\phi = \frac{1}{(2\,P_R/N_i)^{1/2}} = \frac{1}{\left[\frac{2P_{RD}}{2b\eta E_{ND}}\right]^{1/2}} \quad . \tag{46}$$

A square-law detector has again been assumed. Therefore,

$$P_{RD} = \frac{2}{\pi^2}\eta^2 P_R{}^2 \tag{47}$$

$$E_{ND} = BE_{Ni}{}^2 \tag{48}$$

where η = the duty cycle

P_{RD} = the signal power in each pulse after square-law detection and is proportional to the square of the signal power at the IF output

B = the IF bandwidth

E_{Ni} = the noise intensity at the IF output

b = the servo bandwidth

(assuming unity dimensional coefficients)

The signal power (49) is the power in the fundamental of a train of square pulses, each of which has a peak power $P_R{}^2$. When (47) and (48) are substituted into (46), equation (49) is obtained.

$$\epsilon_\phi = 2\pi\,\frac{\epsilon_{t\phi}}{\tau} = 2\pi\,\frac{2\epsilon_{H\phi}/c}{4_H/c} = \frac{1}{\left[\frac{B2\eta^2}{b\eta\pi^2}\,\frac{P_R{}^2}{BE_{Ni}}\right]^{1/2}} \tag{49}$$

or

$$\frac{\epsilon_{H\phi}}{H} = \frac{1}{\pi}\,\frac{\pi}{P_R/N_i\sqrt{\frac{2B\eta}{b}}} \quad . \tag{50}$$

A comparison of (45) and (50) shows that the results are identical if $\tau/t_{gw} = 1$ and $\eta = 1/2$, i.e.,

$$\frac{\epsilon_{H\phi}}{H} = \frac{1}{(P_R/N)_i}\,\sqrt{\frac{b}{B}} \quad . \tag{51}$$

Acquisition for Early/Late Gate Processor

The volume to be searched has been divided into 16 sectors and it is desired to search each of the 16 sectors in the time required for the lander to descend 0.5 percent of the maximum altitude.

If the PRF for acquisition is adjusted so that the leading half of the full pulse is received in the interval between pulses when the range is equal to the maximum altitude, then the period for acquisition will be

$$\frac{3}{4}\, t_a = \frac{2H\,max}{c}$$

$$t_a = \frac{8h\ max}{3c} = \frac{8 \times 1.55 \times 10^4}{9 \times 10^8} = 1.38 \times 10^{-4}\ \text{sec.} \tag{52}$$

Then a conservative measure of the minimum altitude that could be acquired with this PRF is one where the last half of the pulse falls in the interval between pulses or

$$\frac{1}{4}\, t_a = \frac{2H_{min}}{c}$$

$$H_{min} = \frac{Ct_a}{8} = \frac{C}{8} \times \frac{8H\,max}{3c} = \frac{H\,max}{3} \quad . \tag{53}$$

Thus, acquisition could be obtained with one PRF from H max to 1/3 H max. Acquisition would then be indicated by putting a threshold at the output of both the early and late gate integrators.

The number of pulses that would be integrated for each sector during acquisition can be found by solving (54).

$$16\, t_i = \frac{0.005\, H\ max}{V_V(max)} \tag{54}$$

where 16 = the number of sectors that must be searched

t_i = the integration time per sector

$V_V(max)$ = the vertical velocity at maximum altitude = 1660 m/sec.

$$t_i = \frac{5 \times 10^{-3} \times 1.55 \times 10^4}{1.6 \times 1.66 \times 10^4} = 2.91 \times 10^{-3}\ \text{sec} \tag{55}$$

Then the number of hits, M_H, will be, using t_a from (52),

$$M_H = \frac{t_i}{t_a} = \frac{2.91 \times 10^{-3}}{1.38 \times 10^{-4}} = 21 \ . \tag{56}$$

The signal-to-noise ratio, at the IF output, is then found from page 36 and page 37, Skolnik[3], to be 2.6 dB for a probability of detection of 90 percent; a false alarm of 10^{-6}, and 21 pulses integrated.

The next step is to select an IF bandwidth. If the LO is fixed, then the IF bandwidth must be large enough to accept the maximum doppler shift. This is found to be

$$f_D(\max) = \frac{2\ V_V(\max) f_c}{c} = \frac{2 \times 1.66 \times 10^3 \times 9 \times 10^9}{3 \times 10^8} = 100 \text{ kHz} \ . \tag{57}$$

The noise power for acquisition will then be

$$N_i = K_B T B F_N = -204 + 10 + 50 = -144 \text{ dB W} \tag{58}$$

where F_N = the noise figure (10 dB)

B = the IF bandwidth 100 kHz from (57)

$K_B T$ = −204 dB W/cycle.

The transmitter power required is then found by solving the range equation

$$P_T = \frac{(P_R/N_i) K_B T B F_N}{\dfrac{G^2 \lambda^2 [\delta \pi \tan \theta]^2}{(4\pi)^3 H^2}} L_c \tag{59}$$

where the P_R/N_i required = 2.5 dB as discussed above

L_c = the collapsing loss = 1.4 dB [7]
(A collapsing loss will occur because the pulsewidth is not matched to the IF bandwidth. The product will be equal to $1/4\ t_a B = 1/4 \times 1.3 \times 10^{-4} \times 10^5 = 3.45$.)

$K_B T B F_N$ = the noise power, Equation (58)

G = the antenna gain, 18.2 dB

λ = the wavelength = 3.3 cm

δ = the reflection coefficient = 0.01

H = the max altitude = 15.5 km

2θ = the antenna beamwidth = 24 deg.

	+dB	−dB
P_R/N_i	2.5	
$K_B T B F_N$		144
$1/G^2$		36.4
$1/\lambda^2$	29.6	
$(4\pi)^3$	33.0	
$1/\delta$	20.0	
$1/\pi$		5.0
$1/\tan^2 12°$	13.4	
H^2	83.8	
$1/L_c$	1.4	
	183.7	185.4
		183.7
		−1.7

$$P_T = -1.7, \text{ or } \approx 0.675 \text{ W}. \tag{60}$$

A check can now be made for the tracking accuracy expected using the S/N required for acquisition. From (45)

$$\frac{\epsilon_{HN}}{H} = \sqrt{\frac{2b\eta}{Bt_T/t_{gw}}} \quad \frac{1}{(P_R/N_i)} \tag{61}$$

for the following values:

t_T/t_{gw} = ratio of pulse to full gate width = 1

η = duty cycle = 1/2

B = 100 kHz from (57)

$$2b = \frac{1}{t_i} = \frac{1}{2.91 \times 10^{-3}} \quad \text{from (55)}$$

required for acquisition

$$\sqrt{\frac{2b\eta}{Bt_T/t_{gw}}} = \sqrt{\frac{1}{2 \times 10^5 \times 2.91 \times 10^{-3}}} = 0.414 \times 10^{-1} = -13.8 \text{ dB} \tag{62}$$

$$10 \log \frac{\epsilon_H}{H} = -13.8 - 2.5 = 16.3 \quad \frac{\epsilon_H}{H} = 0.0234. \tag{63}$$

This is slightly more than the 2 percent required. By increasing the signal noise at the IF output to 32 dB, Equation (63) would become $\epsilon_H/H = 0.02$. This would increase the power required in Equation (60) from 0.67 W to 0.8 W.

The effective S/N after the servo can be found from (64).

$$P_s/N_s = \frac{P_R^2}{2E_{Ni}^2} = \frac{B}{2b}(P_R/N_i)^2 \qquad (64)$$

$$= 10 \log B - 10 \log 2b + 2 \times 3.2$$

$$= 50 - (-10 \log t_i) + 64$$

$$= 56.4 + 10 \log (2.91 \times 10^{-3})$$

$$= 56.4 - 25.4 = 31 \text{ dB.}$$

(again using unity dimensional coefficient)

This exceeds the 20 dB required in the Work Statement by 11 dB.

Phase Detection Processing for the ICW Altimeter

It is not clear how an acquisition procedure for phase detection processing could be devised that would be as simple and efficient as that described for early/late gate processing. It has been shown, however, that the same accuracy would be obtained during tracking for the same IF signal-to-noise ratio, Equation (51).

Velocity Channel

It was shown earlier that no pulse system would provide doppler measurement above 15,000 ft. along the velocity vector or above 17,500 ft. normal to surface. Below this altitude doppler can be measured. Suitable circuitry for the doppler channel is shown in Figure 15.

The signal out of the IF amplifier can be represented as shown by (65).

$$C_1 = C_{10} \sin\left[(\omega_{IF} \pm \omega_D) + \alpha_1\right] \quad . \qquad (65)$$

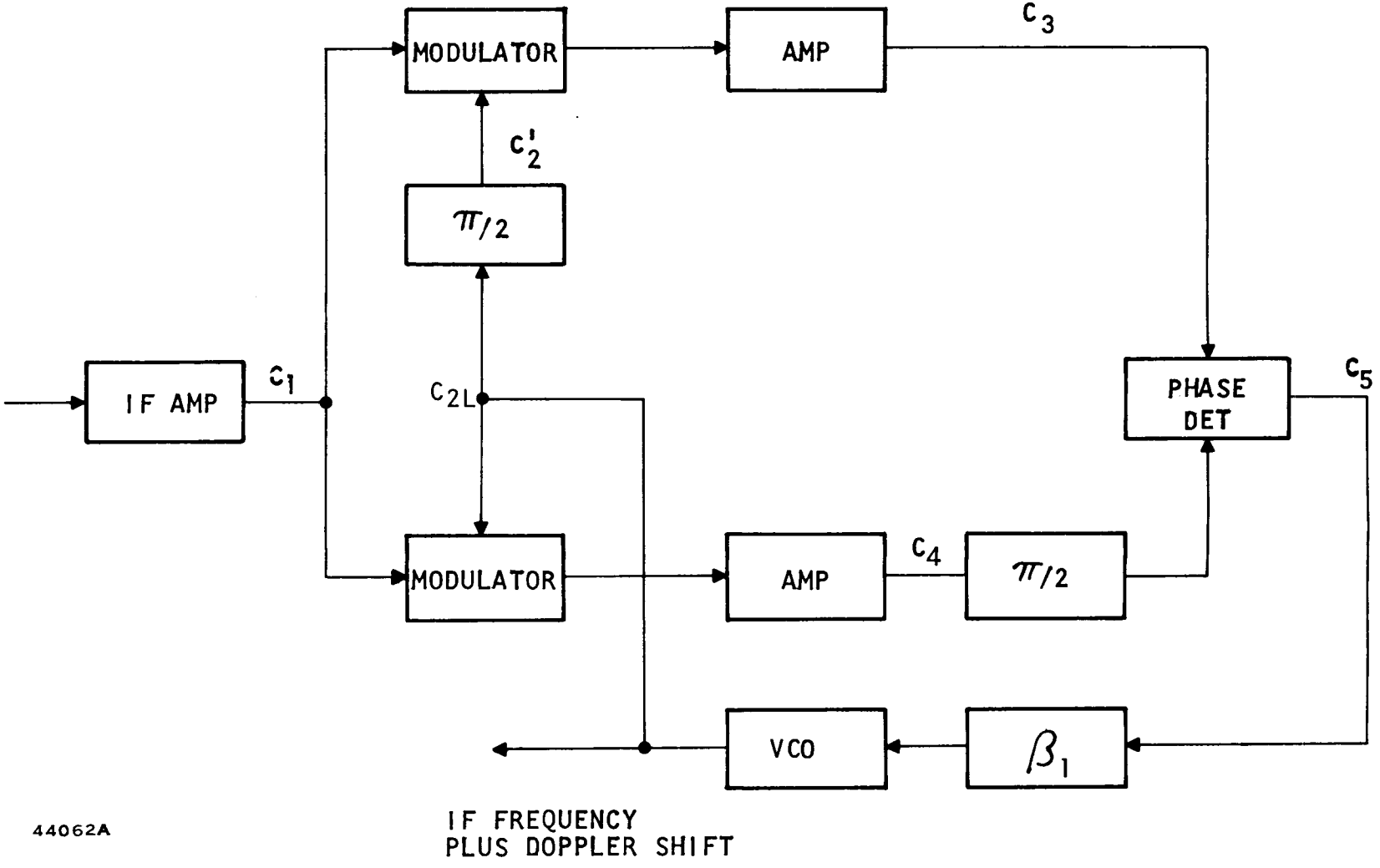

Figure 15. Doppler Channel, ICW Altimeter

This is mixed in the upper channel with $C_2 = \sin(\omega_{VCO}t + \beta_1)$, and in the lower channel with $C_2 = \cos(\omega_{VCO}t + \beta_1)$. The output of upper channel amplifier will then be

$$C_3 = \begin{cases} \frac{C_{10}}{2} \cos\left[(\omega_{IF} \pm \omega_D - \omega_{VCO})t + \alpha_1 - \beta_1\right]; (\omega_{IF} \pm \omega_D) > \omega_{VCO} \\ \frac{C_{10}}{2} \cos\left[\omega_{VCO}t - (\omega_{IF} \pm \omega_D)t + \beta_1 - \alpha_1\right]; (\omega_{IF} \pm \omega_D) < \omega_{VCO} \end{cases} \quad (66)$$

The output of the lower channel is given by (64).

$$C_4 = \begin{cases} \frac{C_{10}}{2} \sin\left[(\omega_{IF} \pm \omega_D - \omega_{VCO})t + \alpha_1 - \beta_1\right]: (\omega_{IF} \pm \omega_D) > \omega_{VCO} \\ \frac{C_{10}}{2} \sin\left[\omega_{VCO}t - (\omega_{IF} \pm \omega_D)t + \beta_1 - \alpha_1\right]: (\omega_{IF} \pm \omega_D) < \omega_{VCO} \end{cases} \quad (67)$$

After the $\pi/2$ phase shifter in the lower channel, the sine terms become cosine terms so that the dc output of the phase detector will be as shown by (68).

$$C_5 = \begin{cases} \frac{C_{10}^2}{4} \cos^2\left[(\omega_{IF} \pm \omega_D - \omega_{VCO})t + \alpha_1 - \beta_1\right] = C_{10}^2/8\ (\omega_{IF} \pm \omega_D) > \omega_{VCO} \\ \frac{C_{10}^2}{4} \cos^2\left[\omega_{VCO}t - (\omega_{IF} \pm \omega_D)t + \beta_1 - \alpha_1\right] = C_{10}^2/8\ (\omega_{IF} \pm \omega_D) < \omega_{VCO} \end{cases} \quad (68)$$

This analysis of the doppler channel assumed that the input was a pure sine wave. The time input will actually be a distributed signal due to the doppler spread. However, the β_1 circuit in the servo loop is essentially a low-pass filter so that the actual signal, C_5, will tend to make the VCO track the centroid of the doppler spectrum. The output of the VCO will then be a clean signal equal to the IF plus or minus the centroid of the doppler spectrum.

DISCUSSION OF PULSE SYSTEM

Introduction

Another type of modulation is that using a low duty cycle, short pulse. The major difference between this type of modulation and the FM/CW or ICW is that the pulsed system utilizes a higher frequency spectrum than the others, and is therefore least affected by large doppler frequency shifts.

Characteristics of Received Pulse

Measuring range with a pulsed altimeter is a direct measurement of two-way transit time between the transmitted and received pulse. It is important to analyze the characteristics of the received pulse, and to select the type of measurement technique that yields the most accurate results. Consider Figure 16.

where

2θ = antenna beamwidth

H = absolute altitude

r = illuminated target radius

$dA = 2\pi r dr$ = differential target area

$h = H \sec$ = slant range

$P_R(t)$ = the time function of received power

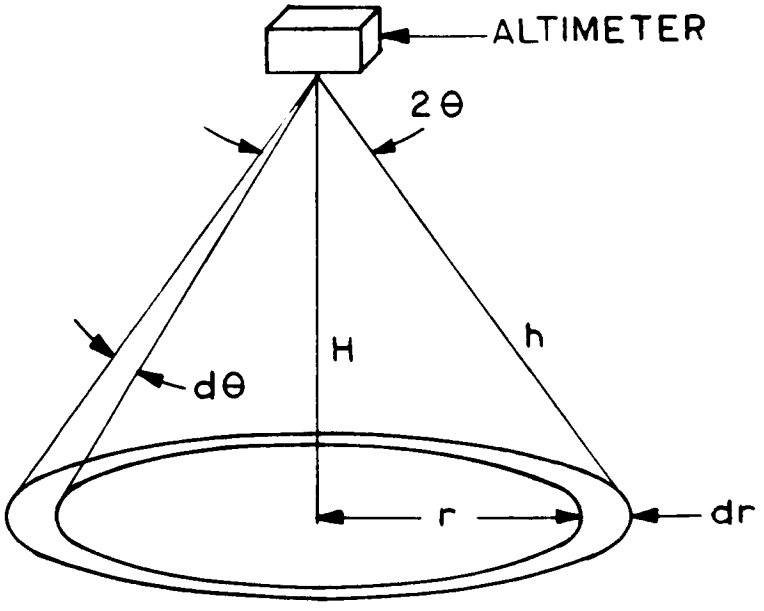

Figure 16. Radiation Pattern Definition

Since the two-way transmission time of a wavefront from the altimeter to the differential target area is a function of θ, $\tau = (2H \sec \theta)/c$, it is obvious that a delay will be encountered by the energy incident upon the outer extremities of the target when compared to that incident on the target directly below the altimeter. To determine risetime of the returned pulse, this pulse-stretching factor will be evaluated as a function of altitude.

The basic radar range equation can be stated as follows:

$$P_R = \frac{P_T G^2 \lambda^2 \sigma}{4\pi (4\pi h^2)^2} \tag{69}$$

where P_T, G, σ, and h are variables in either time or θ. For purposes of pulse-shape evaluation, the equation is reduced to the following.

$$P_R(t) = K \frac{P_T(t) G^2(\theta) A(\theta)}{h(\theta)^4} \tag{70}$$

where

$$P_T = \frac{1}{t_1} \qquad 0 \le t \le t_1 \qquad \text{(rise time, } t_{rT}\text{)}$$

$$= 1 \qquad t_1 \le t \le t_2$$

$$= 1 - \frac{t - t_2}{t_3 - t_2} \qquad t_2 \le t \le t_3 \qquad \text{(fall time)}$$

$$= 0 \qquad 0 > t > t_3$$

when the transmitted pulse form of Figures 17, 18, and 19 is assumed.

$$G = G_o \cos^2 3\theta$$

$$G^2 = G_o^2 \left[4 \left(\frac{H}{\sqrt{H^2 + r^2}} \right)^3 - \frac{3H}{\sqrt{H^2 + r^2}} \right]^4$$

(first approximation for 30-degree beamwidth, this angle was chosen for ease of calculation)

also,

$$A_T = \pi H^2 \tan^2 \theta = \pi r^2$$

and

$$h = H \sec \theta = \sqrt{H^2 + r^2} \quad .$$

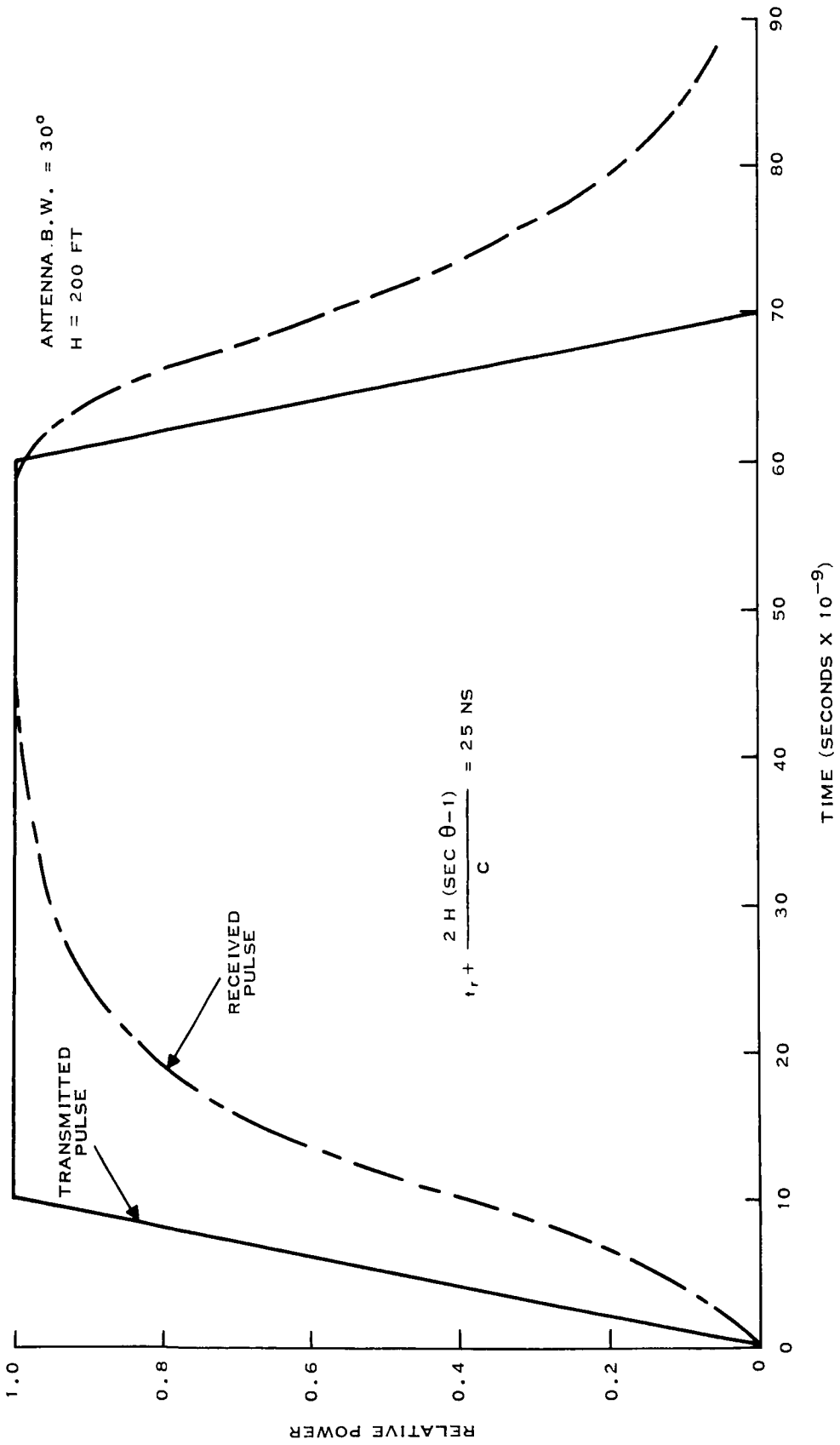

Figure 17. Comparison of Leading Edge of Transmitted Pulse with Received Pulse, H = 200 Ft.

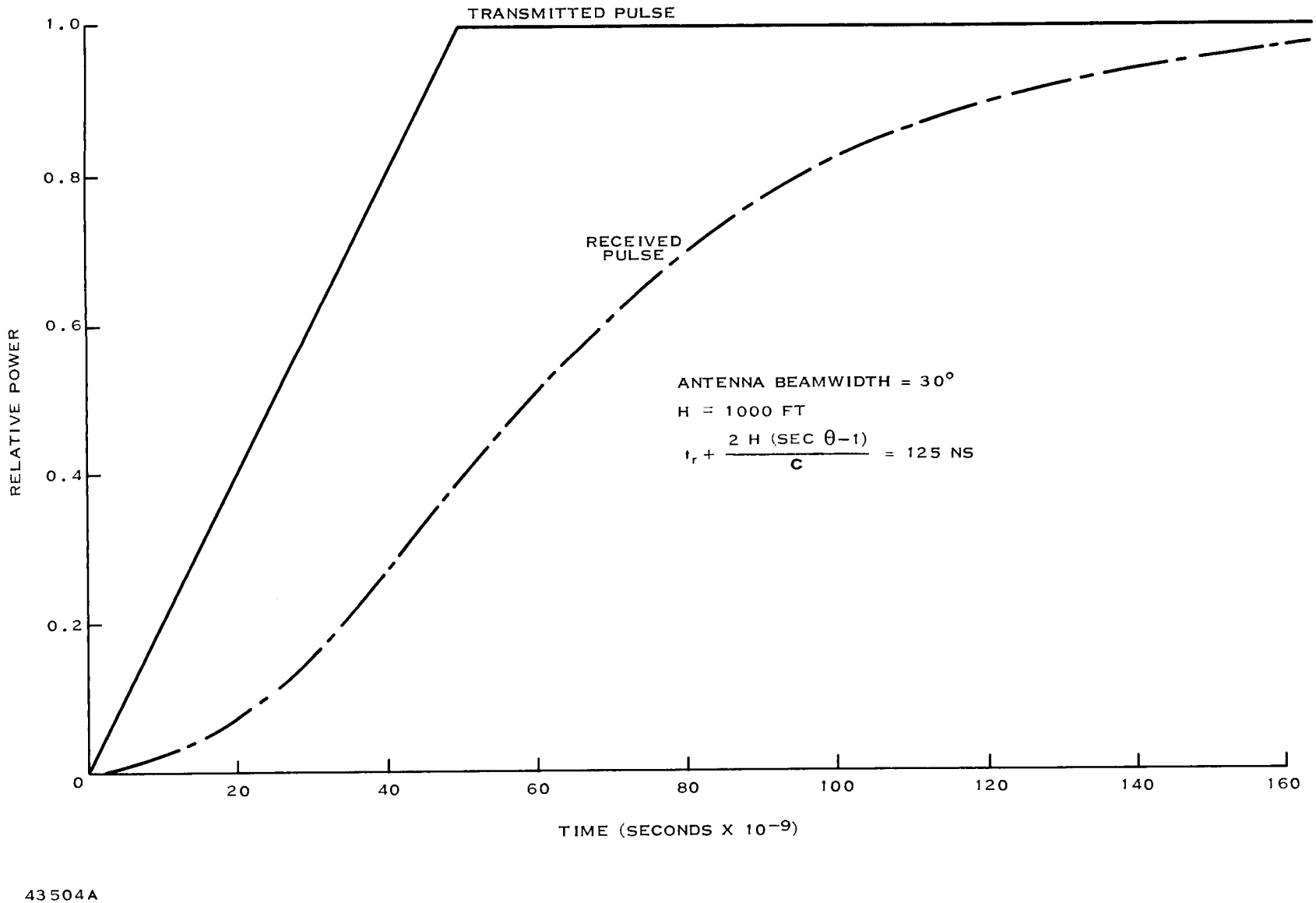

Figure 18. Comparison of Leading Edge of Transmitted Pulse with Received Pulse, H = 1000 Ft.

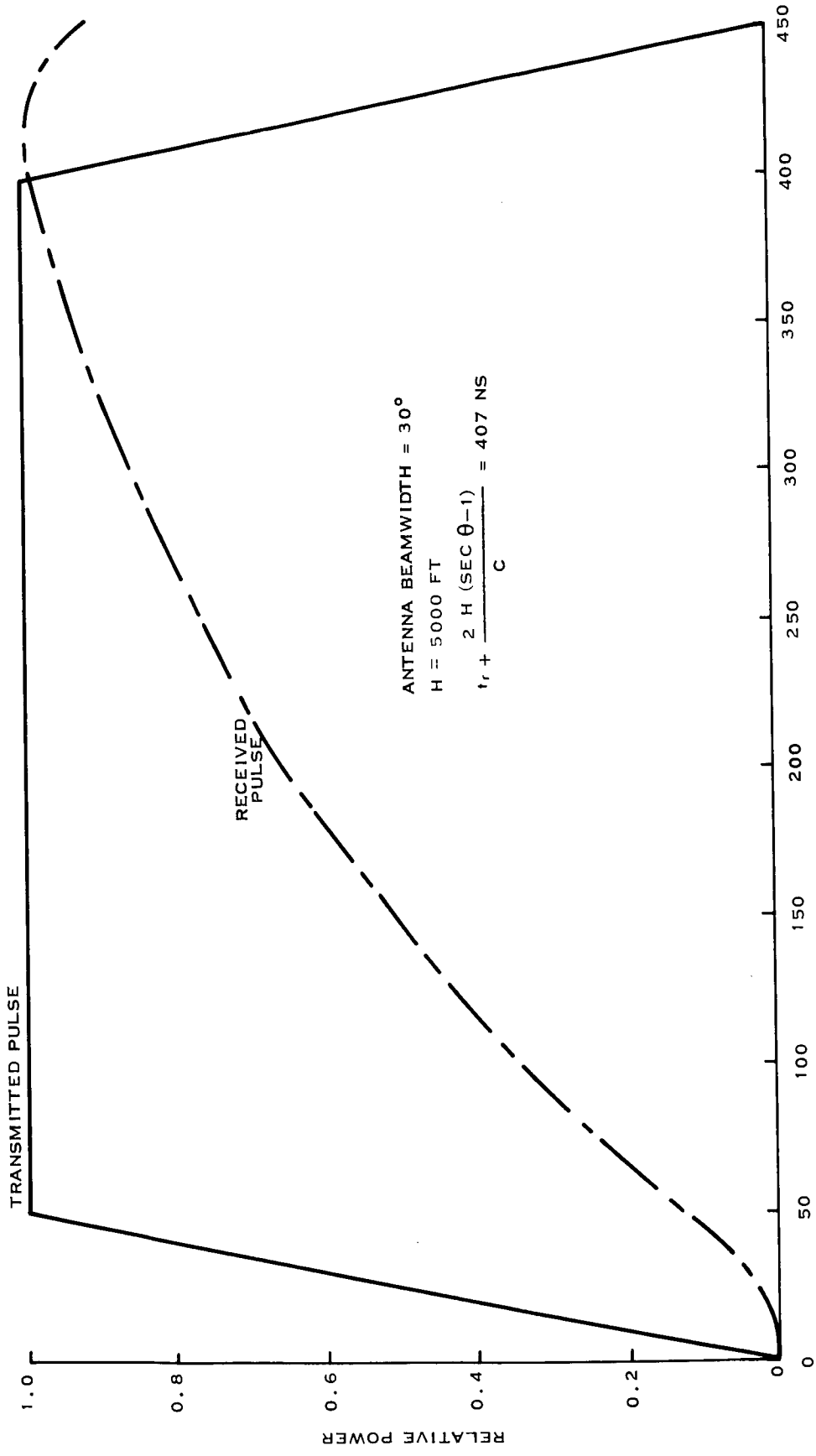

Figure 19. Comparison of Leading Edge of Transmitted Pulse with Received Pulse, H = 5000 Ft.

Now the relation for $P_R(t)$ can be rewritten in the following form

$$P_R(t) = K' \int \frac{P_T(t)\left(t - \frac{2}{c}\sqrt{H^2 + r^2}\right)\left[4\left(\frac{H}{\sqrt{H^2 + r^2}}\right)^3 - 3\left(\frac{H}{\sqrt{H^2 + r^2}}\right)\right]^4 2\pi \, r\,dr}{\left(H^2 + r^2\right)^2} \quad (71)$$

where transmission time is written as

$$\frac{2}{c}\sqrt{H^2 + r^2} \; .$$

Limits were assigned and a computer program was generated to evaluate Equation (71) as a function of time.

The results shown in Figures 17, 18, and 19 were obtained. It is interesting to note that in Figures 17 and 18, where the pulse is long, the approximation,

$$t_r = t_{r_T} + \frac{2H\ (\sec\theta - 1)}{c} \quad (72)$$

corresponds to the time required to achieve 90 percent of P_{max}. In Figure 19, the pulselength is approximately the same as the risetime approximation (from Figure 20) and is the maximum altitude at which a peak returned signal will be developed. Therefore, the approximation:

$$t_r = \frac{2H}{c}\ (\sec\theta - 1) \quad (73)$$

is valid if:

1. The transmitted pulse length is at least as long at t_r
2. $t_r \gg t_{r_T}$
3. The terrain is mostly dispersive, and the reflection is independent of incident angle.

These conditions will be assumed realistic for this application.

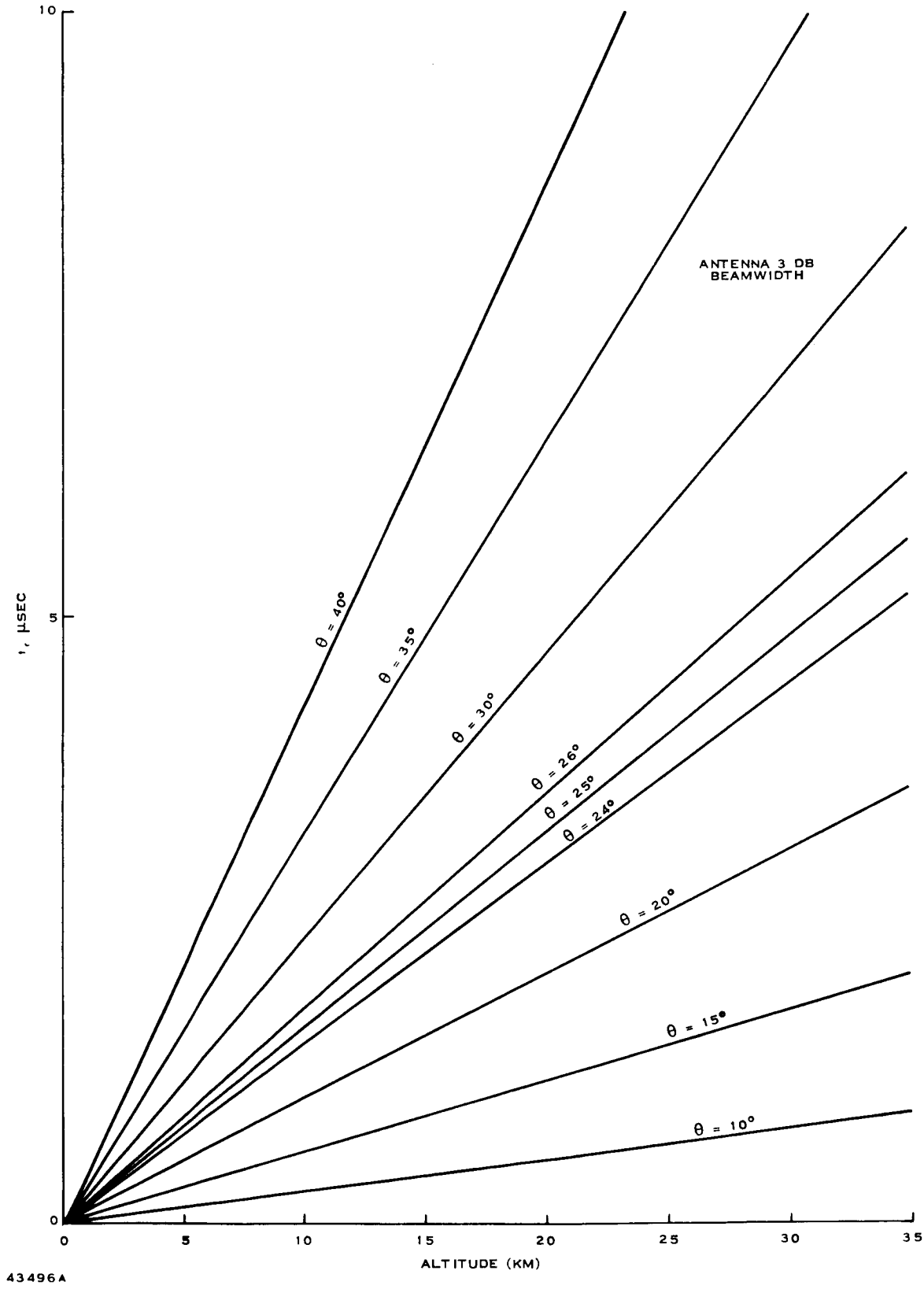

Figure 20. Increase in Rise Time Due to Extensive Target

Error Analysis

Now that the beamwidth degraded risetime can be approximated, consider the shape of the received pulse present in the servo loop, Figure 21.

Where

$$\tau = \frac{2H}{c} \tag{74}$$

$t_2 - \tau = t_r$ = rise time of leading edge

$t_3 - t_2$ = pulsewidth, since these times very closely represent the leading and trailing edges of a transmitted pulse packet

$t_4 - t_3$ = fall time, also degraded by the beam.

At the maximum altitude of 15.5 km, and an antenna beamwidth of 24 deg, the risetime degradation is:

$$t_r = \frac{2 \times 15.5 \times 10^3}{3 \times 10^8} \text{ (sec } 12° - 1) = 2.3 \text{ usec}$$

Assuming a transmitted pulse risetime of about 50 nanoseconds, then

$$t_r >> t_{r_T}$$

The maximum allowable error is 2 percent, or

$$\epsilon_H = 310 \text{ meters, which represents:} \tag{75}$$

$$\epsilon_t = \frac{2\epsilon_H}{c} = 2.07 \text{ usec.}$$

Therefore, the risetime is greater than the allowable time error. It is evident that the range measurement must be made when the received signal exceeds a certain threshold, and that threshold, when related to the risetime, must represent a smaller error than the total risetime represents. A servo loop which tracks a threshold crossing of the leading edge is indicated. Figure 22 is a block diagram which represents such a leading-edge tracker. The loop gain of this servo is $K_L G_L$, where G_L is the circuit gain and K_L is relative slope of the received pulse risetime, normalized to the minimum value.

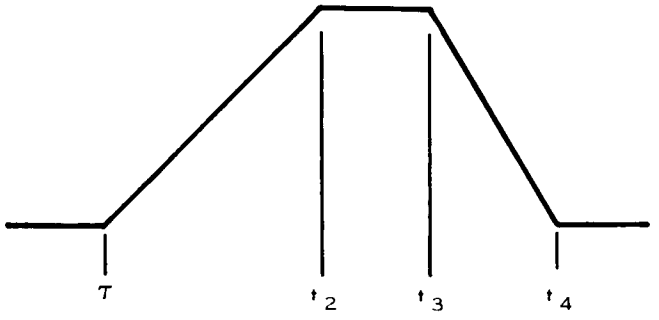

43508A

Figure 21. Received Pulse Definition in Servo Loop

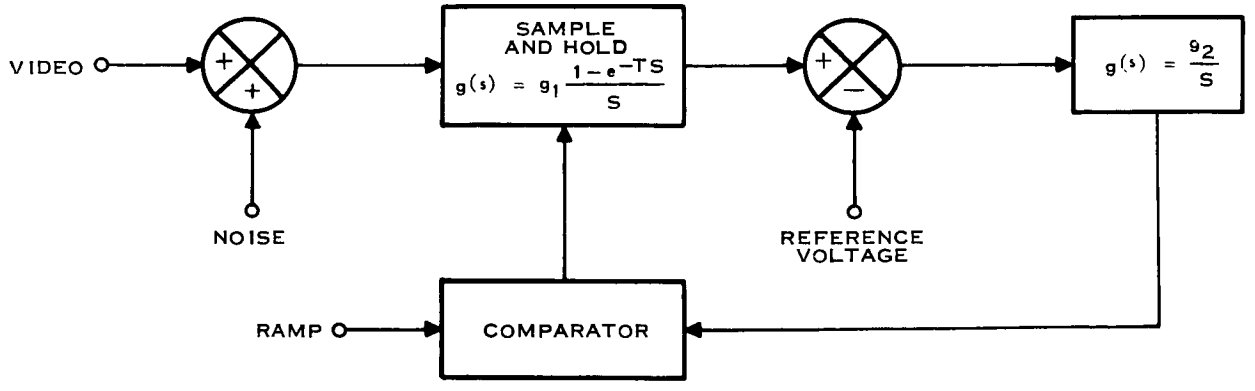

43511

Figure 22. Servo Loop Block Diagram

The velocity error, ϵ_{HV}, is:

$$\epsilon_{HV} = \frac{V_v}{K_L G_L} \text{ meters.} \tag{76}$$

This error is caused by a finite lag of the servo amplifier and is always positive, since the altitude is always decreasing. There are two other primary sources of error, which are, referring to Figure 23:

For large signal-to-noise ratios:

$$\epsilon_{tN} = t_r \frac{V_{NL}}{V_{SL}} = t_r \left[X_{pL}\right]^{-1/2} \tag{77}$$

$$\epsilon_{tB} = t_r \frac{V_T}{V_{SL}} = t_r \left[\frac{X_{pT}}{X_{pL}}\right]^{1/2} \tag{78}$$

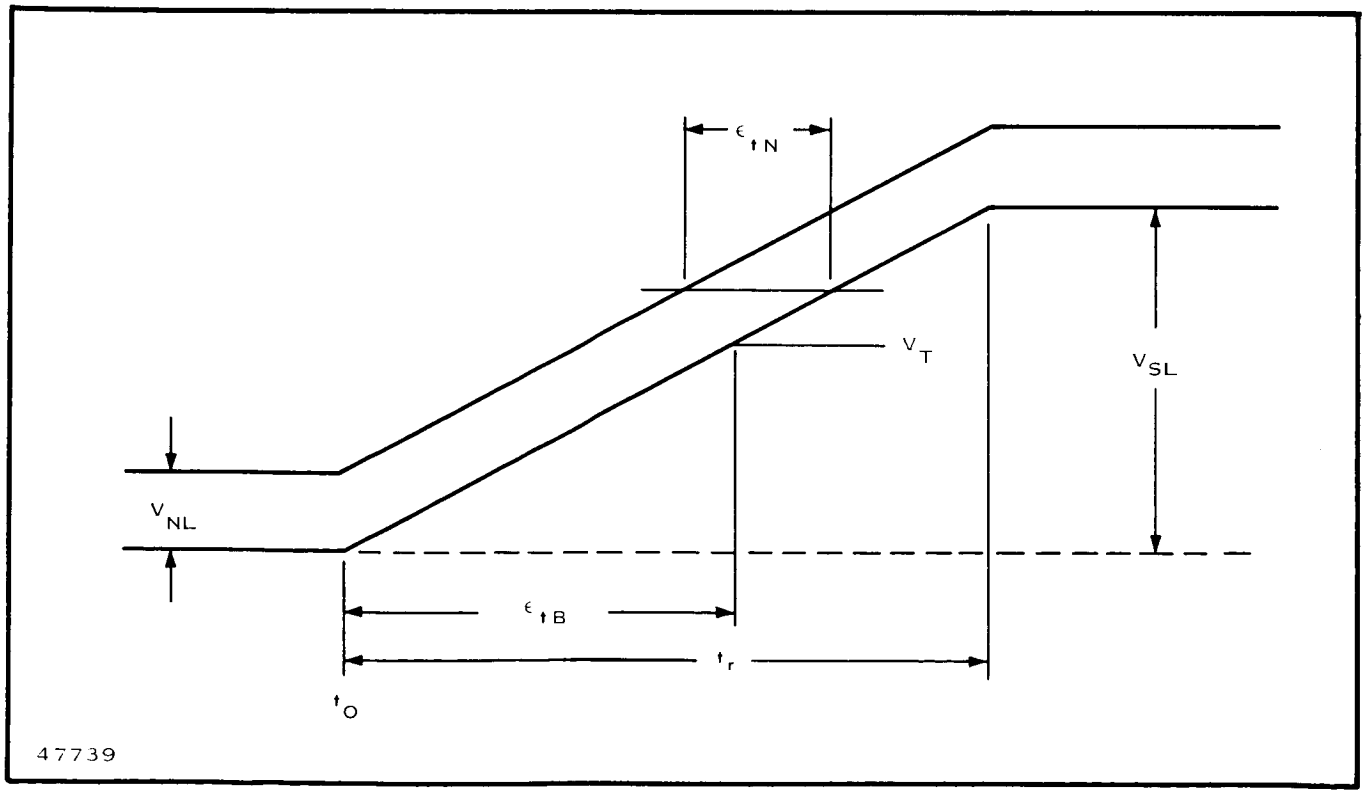

Figure 23. Video Signal in Servo Loop

since these errors are uncorrelated and positive, and the velocity error is always positive because the altitude is always decreasing:

$$\epsilon_o = \frac{c}{2}\left[\left(\epsilon_{tB}\right)^2 + \left(\epsilon_{tN}\right)^2\right]^{1/2} + \epsilon_{HV} \tag{79}$$

or

$$\epsilon_o = \frac{c}{2}\, t_r \left[\frac{X_{pT}}{X_{pL}} + \frac{1}{X_{pL}}\right]^{1/2} + \frac{V_V}{K_L G_L} \tag{79a}$$

$$\epsilon_o = \frac{ct_r}{2}\left[\frac{X_{pT}+1}{X_{pL}}\right]^{1/2} + \frac{V_V}{K_L G_L} \tag{80}$$

The value of $K_L G_L$ is found from the servo loop stability requirements:

$$K_{LM} G_L t_L < 1 \tag{81}$$

where K_{LM} is the maximum value of K_L, occurring at minimum altitude, or limited by the bandwidth of the IF amplifier. It is desireable to use a single IF bandwidth over the entire altitude range. Bandwidth switching does improve performance but is unnecessary for this particular mission. A 3-MHz bandwidth allows sufficient noise filtering at high altitudes and also permits a fast enough risetime at low altitudes to allow measurements within the required accuracy.

Let $B = 3$ MHz (82)

then $t_{r\,min} \simeq 0.33\ \mu s$

and $K_{LM} = \frac{2.3}{0.33} = 6.9$

$K_{LO} = 1$ (minimum value of K_L)

therefore $K_{LO} G_L\, t_L < \frac{1}{6.9}$

t_L is found by considering the type of sector scan, where four pulses are transmitted in each sector. For a pulse period of 0.5 ms, then 61 pulse periods elapse between pulse inputs for each of the 16 sectors.

Therefore $t_L = 0.0305$ sec

and $K_{LO} G_L = \frac{1}{0.0305 \times 6.9} = 4.75$ rad/sec max.

so $$\epsilon_V = \frac{V_V}{K_{LO}G_L} = \frac{1600}{4.75} = 337 \text{ meters at H = 15.5 km}$$

This is greater than the allowed error. By designing the ramp generator so that an exponential ramp, rather than a linear ramp is developed, G_L varies with altitude. It is then possible to hold $K_L G_L$ very nearly constant, so:

$$K_{LO}G_L = \frac{1}{0.0305 \times 2} = 16.5 \text{ rad/sec.}$$
(insures stability)

and $$\epsilon_V = \frac{1600}{16.5} = 97 \text{ meters}$$

also $$b = \frac{K_{LO}G_L}{2\pi} = \frac{16.5}{2\pi} = 2.63 \text{ Hz}$$

and
$$X_{pL} = \sqrt{\frac{B}{b}} \quad X_{pi} \tag{83}$$

Assume $X_{pL} = 30$ dB (1000)

Since $$\sqrt{B/b} = \sqrt{\frac{3 \times 10^6}{2.63}} = 1070$$

then $X_{pi} \approx 1$

Recall $$N_i = K_B T B F_N \tag{84}$$

$$K_B T = -114 \text{ dBm/MHz}$$

$$B = 3 \text{ MHz}$$

$$F_N = 10 \text{ dB}$$

$$N_i = -99.2 \text{ dBm}$$

for $X_{pi} = 1$ (0 dB) $\rightarrow P_R = -99.2$ dBm

from
$$P_R = \frac{P_T G^2 \lambda^2 \delta \tan^2\theta}{64\pi^2 H^2} \tag{85}$$

H at 15.5 km = 83.8 dB

λ^2 at 9 GHz = −29.6 dB

δ = −20 dB

$\tan^2\theta$ at 12° = −13.4°

G^2 = 36.4 dB

$64\pi^2$ = 28 dB

P_R = −99.2 dBm = P_T −138.4 dB

so P_T = 39.2 dBm minimum = 8.3 W

$$\epsilon_o = 345\left(\frac{101}{1000}\right)^{1/2} + \epsilon_{HV}$$

$$= 109 + 97 = 206 \text{ meters}$$

All other things being equal, the error increases as the inverse square root of X_{pL}, which is proportional to peak transmitted power.

maximum ϵ_o = 0.02 × 15.5 km = 310 meters

so $\left(\epsilon_{HN} + \epsilon_{HB}\right)_{max}$ = 310 −97 = 233 meters

working backwards, the minimum P_T is 1.7 W.

Assuming each RFBB has a 0.7 W output,

then P_T = 11.2 W

ϵ_o is then 188 meters

Now, as the lander approaches the planet surface, H, V_V and t_r decrease; X_{pi}, X_{pL} and K_L increase. A full range AGC circuit is necessary, as it effectively reduces the noise in the servo loop, allowing V_T to decrease in magnitude (controlled by the analog output of the servo loop) thereby decreasing ϵ_{HB}.

Therefore, Equation (80) holds over the entire altitude range. At H = 2210 meters, t_r is limited by B. Above this altitude, the altitude error versus altitude can be found easily, since $t_r \sim H$

$$X_{pi} \sim H^{-2}$$

$$(\epsilon_o - \epsilon_{HV}) \sim X_{pi}^{-1/2} \quad t_r$$

so, $(\epsilon_o - \epsilon_{HV}) \sim H^2$

Using the above relationships and Figure 24, the errors shown in Table 2 were computed for altitudes above 2210 m. Figure 25 is partially plotted from this data.

Table 2. –Pulse System Errors at High Altitudes

H meters	V_V m/sec	ϵ_{HV} m	$(\epsilon_o - \epsilon_{HV})$ m	ϵ_o m
18,000	2000	120	123	243
15,500	1600	97	91	188
13,000	1160	70	64	134
10,000	800	61	38	99
7000	590	36	19	55
4000	420	25	6	31
2210	340	21	2	23

Below 2210 meters, t_r is limited by B and $(\epsilon_o - \epsilon_{HV}) \sim H$, but is less than 2 meters. ϵ_{HV} is still large as shown in Figure 25, but when the sector scan is considered, the maximum iteration time is reduced by one-half, because the "target" is in the four center scan positions simultaneously. This effect is apparent below about 3000 meters altitude. Therefore, below 2210 meters the errors were computed and are shown in Table 3.

Table 3. –Pulse System Errors at Low Altitudes

H meters	V_V m/sec	ϵ_{HV} m	$\epsilon_o - \epsilon_{HV}$ m	ϵ_o m
2210	340	10.5	2	12.5
1000	320	9.5	1	10.5
300	300	9.3	0.3	9.6

SCANNED VERSUS NON-SCANNED ANTENNA

Introduction

It is helpful to discuss a radar range measurement as it applies to an altimeter, where the radar target is extensive enough to be considered infinite. Consider Figure 26, which shows a radar being used as an air-to-ground ranger (measuring specifically the normal, or vertical air-to-ground range, which is altitude).

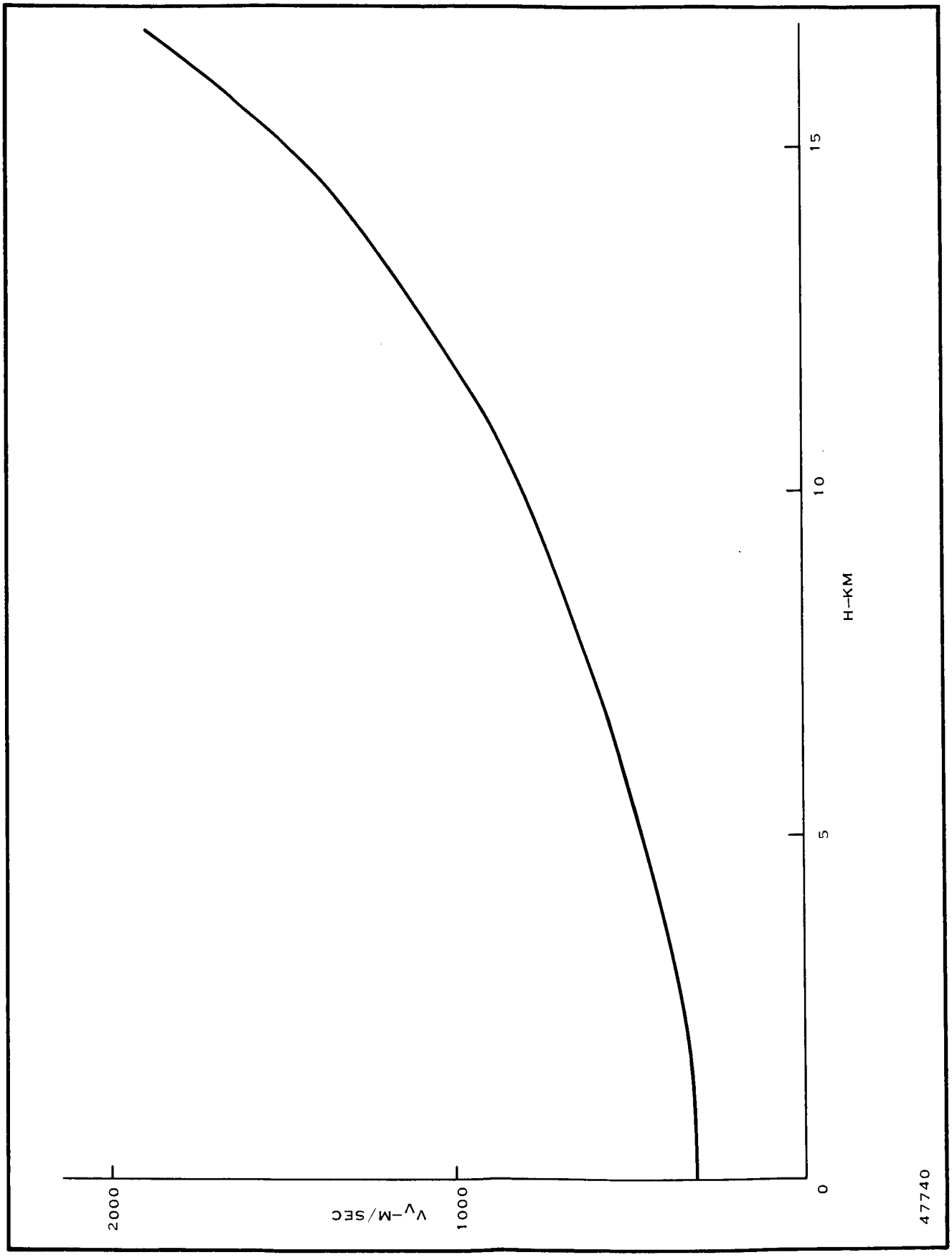

Figure 24. Vertical Velocity Component Versus Altitude

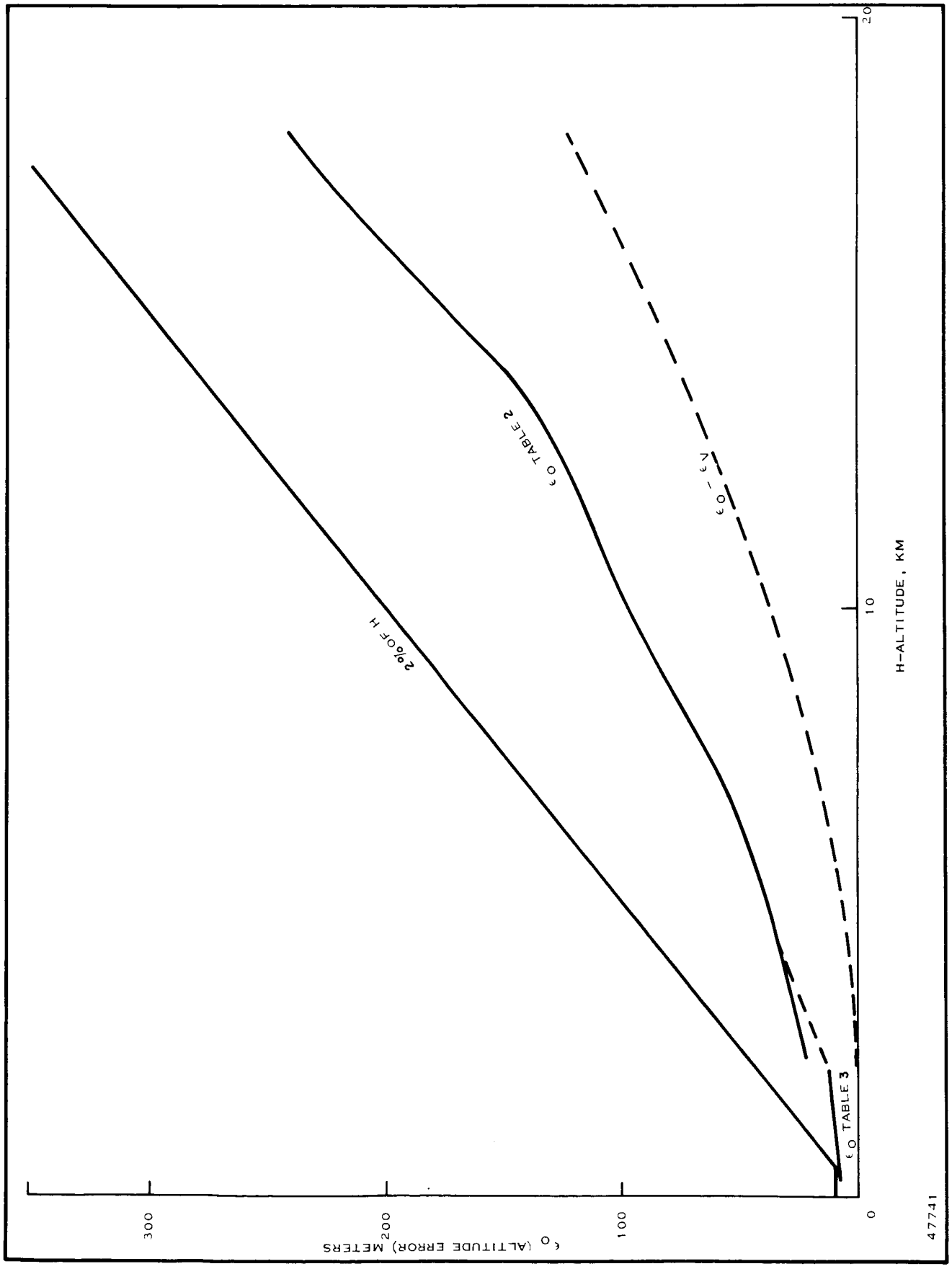

Figure 25. Pulse System Error Versus Altitude

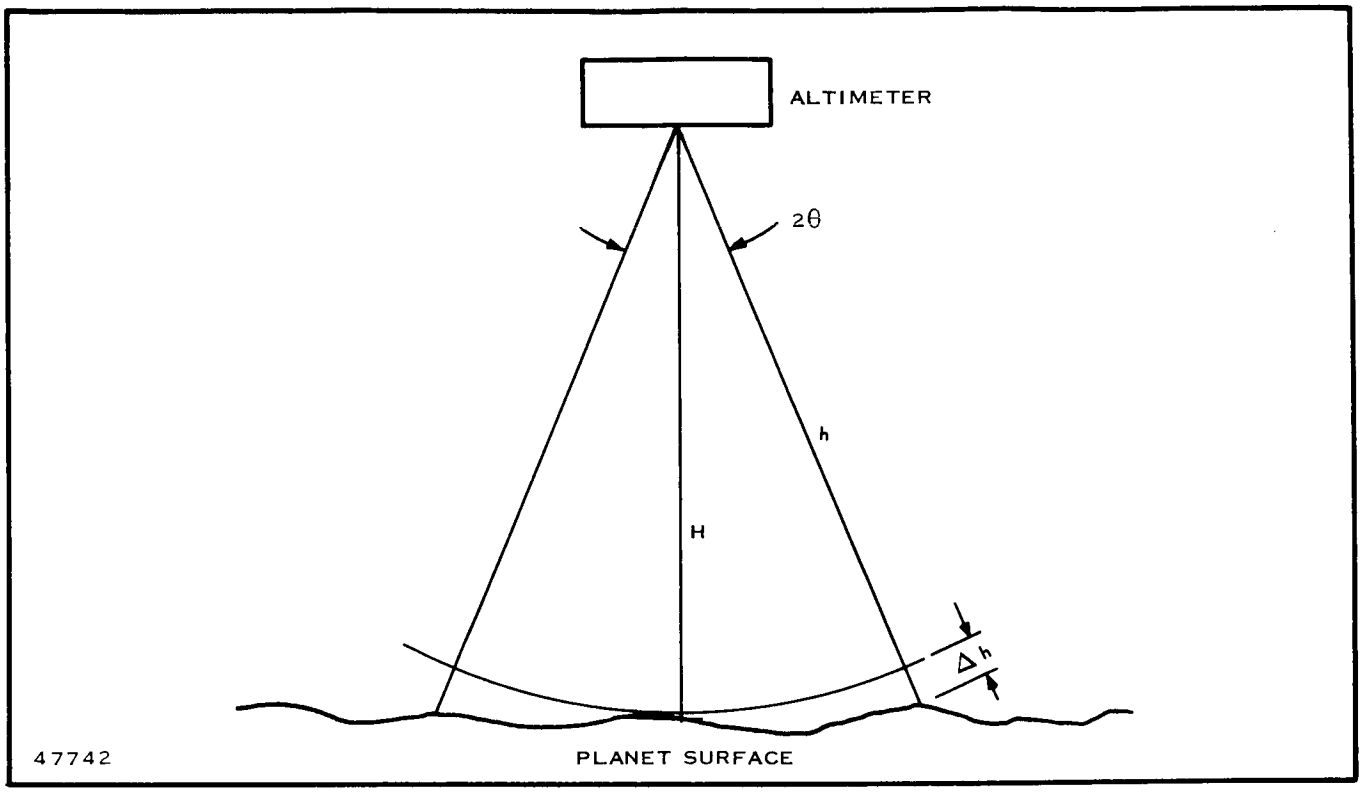

Figure 26. Basic Measurement Geometry of Radar Altimeter

The altitude H is the desired height measurement, but the total illuminated terrain will return energy to the receiver. Any height measurement will indicate an altitude H^1, which represents some threshold crossing of the returned energy. A zero error measurement is not possible as the target area is zero for $\theta = 0$. Δh represents a transit time delayed from the true transit time ($\tau = 2H/c$) first returned energy. In other words, as a wavefront illuminates the target, the terrain will first reflect energy directly below the altimeter, and as the wavefront spreads out on the terrain, the additional reflected energy will be delayed in transit time from that first returned energy.

In order to ensure measuring altitude within a specified error, only a certain portion of the reflected energy will be useful in that measurement. That portion of energy will be represented by a limited area of the terrain. If, for example, the altitude measurement is required to be within 2 percent of the true altitude:

Since $\Delta h = H \sec \theta$, and $\Delta h = h - H = 0.02\ H$,

then $0.02\ H = H \sec \theta - H$, or

$\sec \theta = 1.02$, and $\theta = 11.37$ deg.

Thus 2θ, the useful antenna beamwidth, that will ensure that the total energy returned will represent no greater than a 2-percent ranging error is 22.7 degrees. This does not include any other system errors, such as those due to noise, velocity, or equipment.

To guarantee a true, vertical range (not slant range) measurement, the illumination pattern must contain the vertical vector (normal to terrain). Therefore, any attitude variations greater than θ (boresight to vertical vector) could not produce information to the desired accuracy. Therefore, it is evident that an altimeter required to accurately measure height above terrain, where the expected attitude variations (rather than the required accuracy) dictate the minimum illumination coverage will not be the most efficient system, since much of the returned energy is not useful for the measurement.

A comparison of efficiency must now be made between a broad illumination system and a scanned beam system. Use of the following relationships will be made.

The area of a spherical segment (from Figure 27) is:

$$A_s = 2\pi h^2 (1 - \cos\xi) \quad . \tag{86}$$

The total area of the sphere is $4\pi h^2$. The ratio of the total sphere to the segment is:

$$\frac{A_o}{A_s} = \frac{4\pi h^2}{2\pi h^2 (1 - \cos\xi)} \quad .$$

Therefore, the directivity of an antenna with a beamwidth of 2ξ by 2ξ degrees is:

$$D = \frac{2}{1 - \cos\xi} \quad . \tag{87}$$

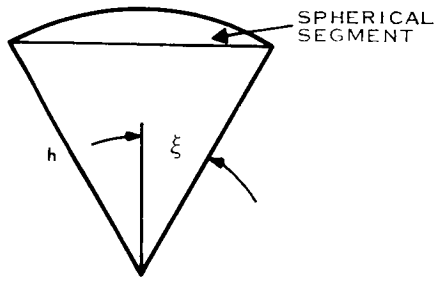

43509A

Figure 27. Beam Geometry for Directivity Definition

For a required antenna coverage of 2ξ by 2ξ degrees, and a maximum usable beamwidth of 2θ by 2θ degrees, N_A sectors must be scanned, considering a sector rather than continuous scan, where

$$N_A = \frac{2\xi \times 2\xi}{2\theta \times 2\theta} = \left(\frac{\xi}{\theta}\right)^2 \quad , \tag{88}$$

and the returned energy rate is reduced by N_A (assuming the target is "in" only one sector). For a broad beam system, the usable target area is (Figure 26):

$$A_u = \pi H^2 \tan^2 \theta \tag{89}$$

and the illuminated area is:

$$A_T = \pi H^2 \tan^2 \xi \quad . \tag{90}$$

A common radar range equation can be used to compare these systems. The received power is

$$P_R = \frac{P_T \delta A_T A_e G}{(4\pi H^2)(4\pi H^2)} \quad , \tag{91}$$

where δ = ground reflectivity (assumed to be independent of incident angle)

A_e = effective antenna aperture = $G\lambda^2/4\pi$

G = antenna gain = ρD

ρ = antenna efficiency ($\rho = 1$)

λ = wavelength

P_T = transmitted power

A_T = target area.

For the broad beam system

$$P_{RB} = \frac{P_{TB} G^2 \delta \pi H^2 \tan^2 \xi \, \lambda^2}{64\pi^3 H^4}$$

or

$$P_{RB} = \frac{P_{TB} G^2 \lambda^2 \delta \tan^2 \theta}{64 \pi^2 H^2}$$

and

$$G_B = \frac{2}{1 - \cos \xi_1}$$

so

$$P_{RB} = \frac{P_{TB} K_2}{(1 - \cos \xi_2)^2} \quad . \tag{92}$$

where

$$K_2 = \frac{\lambda^2 \delta \tan^2 \theta}{64 \pi^2 H^2}$$

For the scanned antenna

$$P_{RN} = \frac{P_{TN} G^2 \lambda^2 \delta \tan^2 \theta}{64 \pi^2 H^2}$$

and

$$G_N = \frac{2}{1 - \cos \theta}$$

so

$$P_{RN} = \frac{P_{TN} K_2}{(1 - \cos \theta)^2} \quad . \tag{93}$$

The ratio is:

$$\frac{P_{RN}}{P_{RB}} = \frac{(1 - \cos \theta)^2}{(1 - \cos \xi)^2} \quad . \tag{94}$$

Since the returned energy rate is continuous for the broad beam system, and reduced by a factor of N_A for the scanned system, the returned energy rate ratio is:

$$\frac{E_{RN}}{E_{RB}} = \frac{1}{N_A}\left(\frac{1 - \cos\theta}{1 - \cos\xi}\right)^2 = \left(\frac{\xi}{\theta}\right)^2\left(\frac{1 - \cos\xi}{1 - \cos\theta}\right)^2 \qquad (95)$$

for $\theta = 12$ deg

$\xi = 60$ deg (expected attitude variation)

$$\frac{E_{RN}}{E_{RB}} = \left(\frac{12}{60}\right)^2\left(\frac{1 - \cos 60°}{1 - \cos 12°}\right)^2 = 20.8 \ .$$

Therefore, a scanned system with a 2-percent specified error due to the antenna will return useful energy to measure altitude at 20.8 times the rate of a broadbeam system, using a required coverage of 120 × 120 degrees.

Peak Power Relationship

Looking again at the received power:

Scanned $$P_{RN} = \frac{P_{TN}K_2}{(1 - \cos\theta)^2}$$

Broadbeam $$P_{RB} = \frac{P_{TB}K_2}{(1 - \cos\xi)^2} \ .$$

For equal received power:

$$\frac{P_{RN}}{P_{RB}} = 1 = \frac{P_{TN}(1 - \cos\xi)^2}{P_{TB}(1 - \cos\theta)^2}$$

or

$$\frac{P_{TB}}{P_{TN}} = \frac{(1 - \cos \xi)^2}{(1 - \cos \theta)^2} \tag{96}$$

for $\theta = 12$ deg

$\xi = 60$ deg

$$\frac{P_{TB}}{P_{TN}} = 520 .$$

Therefore, for equal returned peak power (pulse system) the broadbeam system will require 520 times more transmitted peak power than the scanned beam system, but the data rate will be greater by a factor of $N_A = 5^2 = 25$.

CONCLUSIONS TO PART I

Selection of System Type

It has been shown that the basic FM-CW system would not be applicable to a Mars-probe altimeter because of the large doppler shift. Of the modifications analyzed, none were usable until the velocity decreased to the point where the doppler spectrum spread was less than the basic modulation frequency required for unambiguous altitude measurements.

It was also shown that an ICW altimeter would provide altitude measurements over the range of altitudes required and would provide doppler measurements below 17 500 to 15 000 ft. Two processing techniques were considered for the ICW altimeter. The early/late gate tracker would be simple to realize but would require precise gating at low altitudes where ±10 m accuracy is required. The second technique utilized phase measurements. Extreme accuracy was not required of the phase detector, but high-speed gating would be required at low altitudes. The circuitry for the phase system would be considerably more complex than the early/late gate technique. The RF power requirement was set by the acquisition requirements at 0.8 W net before any losses in the transmitter or receiver channels. Two IF bandwidths would be required during the mission. This power requirement could

be reduced by extending the acquisition time or by using a more complex receiver, which would use a frequency discriminator to control the LO as a function of doppler shift. This would permit the use of an IF bandwidth that is matched to the pulsewidth, thus reducing the noise bandwidth.

Further, it was shown that the pulsed altimeter would measure altitude over the entire range of interest and that there would be no range ambiguities or altitude "holes" because of the basic simplicity of the system. Also, since the short-pulse system inherently uses a broader spectrum of IF frequencies than the FM-CW or ICW systems, it is not affected by the large doppler frequencies encountered. The peak RF power requirement was shown to be 1.7 W for a marginal system, and that input power could be conserved by shutting off that portion of the receiver that is not being used, on a pulse-to-pulse basis. Also, the processing circuitry in the pulsed system is a type 1 (velocity sensitive) servo. In other words, the error signal on the average, in the servo is a velocity increment. Therefore, velocity information can be supplied by linearly amplifying the error signal.

All three of the systems are affected by the antenna beamwidth, where a narrower beamwidth will result in greater accuracy, less transmitted power, and simpler signal processing. However, the predicted attitude variations due to entry dynamics require that the altimeter cover about 120 deg by 120 deg. Since these two requirements are contradictory, a steerable beam is indicated.

Considering future altimeter requirements, which will involve higher velocities, greater altitudes, and greater accuracies, the pulsed system best meets this and future mission requirements. Also, to accompany large attitude variations, a steerable beam is required. A further advantage of a steerable beam is its adaptability to other radar functions, such as mapping.

A brief summary of various tradeoff parameters is shown in Table 4. In the tradeoff analyses, the FM-CW system was dropped early because even in more complex systems, the requirements of the Work Statement could not be met. A broad-beam ICW system was also dropped, because of the large errors involved, unless a very high transmitted power were used. The same argument is generally true for a broad-beam pulse system. Therefore, a scannable ICW or a scannable pulse system is indicated.

In the ICW system all the receiver circuitry must be on and operating at all times, whereas in the short pulse system, the receiver need be on only when a return is expected.

One processing technique of the ICW system uses the leading and trailing edges of the received pulses to measure altitude, and the rest of the spectrum is not used in the measurement.

Operating within the guidelines of the Work Statement, the pulse system with a steerable narrow beam is more attractive than any other system if other factors such as implementation, reliability, availability, maintainability, life and ability to withstand the environmental conditions, are equal.

Implementation

At this time, Texas Instruments is developing a completely integrated radar that uses a phase scanning array of radio frequency building blocks (RFBB). (Appendix) Each RFBB is an individually duplexed transmitter-receiver. This technique, if modified to implement a radar altimeter, will best fit the requirements of the Work statement. By taking advantage of this developmental program, a Molecular Electronics for Radar Application (MERA) altimeter for a space lander would provide maximum integration and reliability along with minimum weight, volume, and input power requirements (Table 5). An altimeter implemented with MERA technology would have:

a. A peak transmitted power of 16 W (design goal)
b. An antenna beamwidth of 24 deg by 24 deg
c. An antenna gain of 18 dB
d. A maximum scan angle of about 65 deg off center
e. A receiver noise figure of about 10 dB
f. An IF of 500 MHz.

From the earlier conclusions drawn, this system meets the requirements of the Martian lander.

Table 4. -Summary of System Types

System Type → / Parameter ↓	FM-CW	ICW Broad Beam	ICW Narrow Beam Scanned	Pulsed Broad Beam	Pulsed Narrow Beam Scanned
General Problems	Doppler frequency limits altitude to 5.5 km	Doppler frequency much larger than optimum receiver bandwidth	Data rate reduced	Requires 520 times more power than scanned	Data rate reduced
Processing	Phase comparison of modulation fundamental	Phase tracking of modulation fundamental or early/late gate		Leading edge tracking	Leading edge tracking
Growth Potential to 100 km	Problems more severe	Range ambiguity problems more severe		XMTR power increases as H^2	Expandable no concept change
$\frac{\text{Peak}}{\text{Average}}$ Power	———	———	$\frac{0.8}{0.4}$ (1)	$\frac{885}{4.4}$ (1)	$\frac{1.7}{0.0085}$ (1)
Acquisition Range	———	5 to 15.5 km no search	5 to 15.5 km no search	0.3 to 15.5 km in search mode	0.3 to 15.5 km in search mode
Optimum Receiver Bandwidth at Maximum Altitude	5 kHz (2)	5 kHz (2)	20 kHz (2)	0.5 MHz	0.5 MHz
XMTR RFI to Other Payloads % of Time	100%	50%	50%	0.5%	0.5%
Range Ambiguities	None if modulation frequency is low	Possible at low altitudes	Possible at low altitudes	None	None

(1) For 2% accuracy

(2) Doppler is 100 kHz

Table 5. –Size, Weight and Input Power for Selected System Types

System	Size (volume) & Percentage of Specified Maximum	Weight & Percentage of Specified Maximum	Input Power & Percentage of Specified Maximum
ICW-scanned	256 in^3 85%	6.6 lb 110%	27.5 W 250%
Pulsed-nonscanned (Magnetron as RF source)	450 in^3 150%	16 lb 270%	35 W for Magnetron only 300%
Pulsed-scanned (MERA) all-solid-state	256 in^3 85%	6.6 lb 110%	14.86 W 99%
Specified maximum	300 in^3	6 lb	15 W

PART II

DETAILED DESIGN OF PULSED RADAR ALTIMETER

INTRODUCTION

After concurrence by NASA of the pulsed type of radar altimeter, a thorough study of that type was undertaken. This part of the report contains descriptive details of the suggested pulsed altimeter design.

Figure 28 is a basic block diagram of the suggested system. The heart of the altimeter is the phased array of RFBB, which comprise the front end of the altimeter. This array performs the functions of transmitter, antenna, duplexer, and receiver. RF power for the array is developed in the RF source and a corporate feed structure divides this power to the individual RFBB inputs, as well as sums the output. The rest of the system is more conventional. Details of the various functional blocks are contained in the following text. Antenna patterns and sector scanning techniques are discussed, as well as power conditioning, system interfaces, and a post sterilization operational test is outlined. A physical description of the proposed system is shown. Also given are the thermal considerations and radar terrain analysis.

An advanced design analysis concludes the main body of Part II, and results of the complete study are given in the conclusion. The appendix material describes the MERA program.

DETAILED ALTIMETER DESIGN

Figure 29 is a detailed block diagram of the altimeter circuitry. The heart of the altimeter is the array of 16 individually duplexed transmitter-receiver radio frequency "building blocks" (RFBB's). The building blocks are described in the section on RFBB's, and a brief description of the altimeter system follows. In the transmit mode, the TR switch selects a low power RF signal at 2250 MHz which is distributed in the manifold to the RFBB's where it is phase shifted, amplified, and multiplied to provide a nominal 1 W output at 9 GHz per RFBB. The amount of phase shift for each individual RFBB is selected by the scan programmer. The transmitted signal is reflected by the terrain and received in the same array, now switched to the

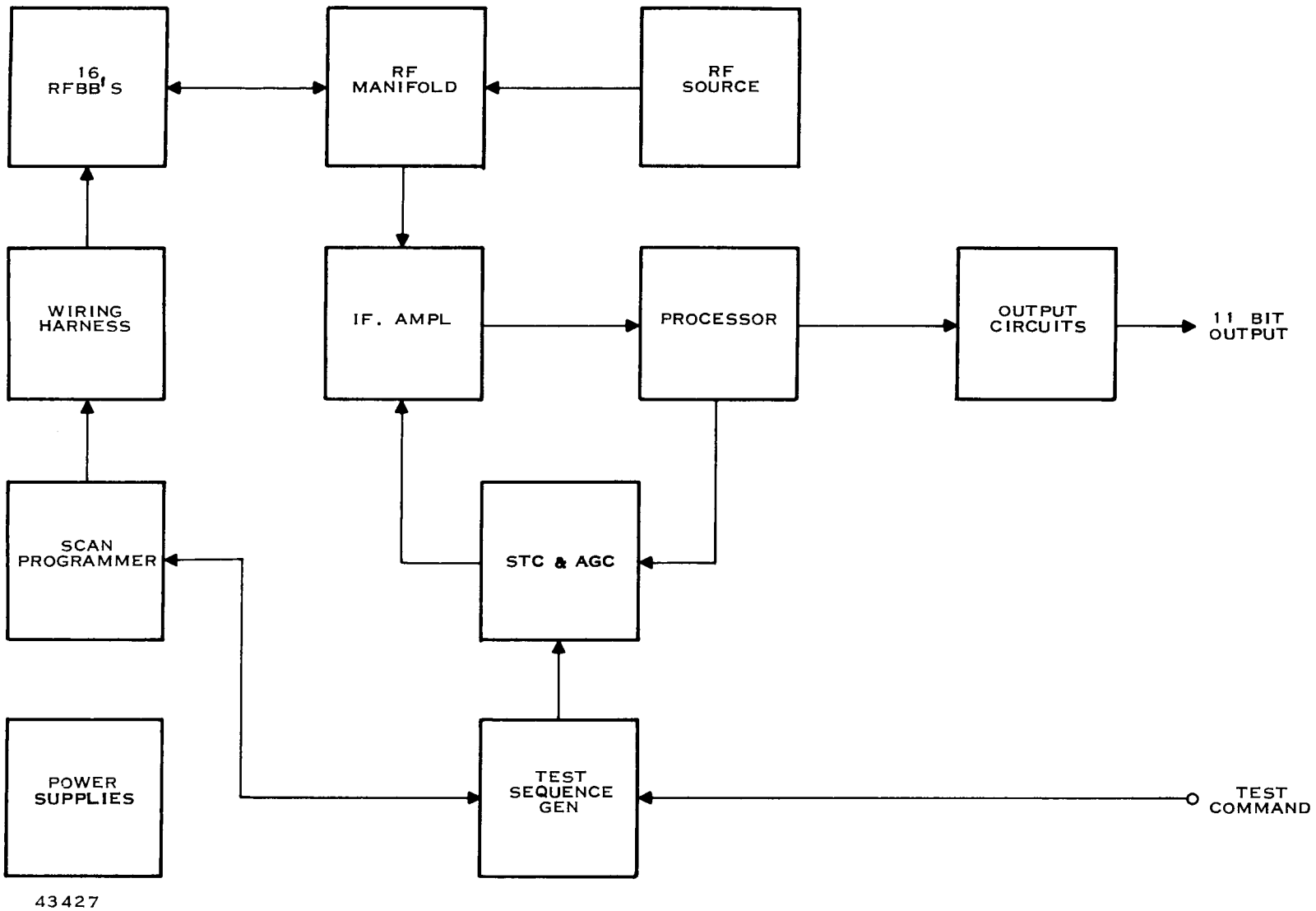

Figure 28. Radar Altimeter, Basic Block Diagram

receiver mode. It is mixed with a 8.5-GHz local oscillator signal (generated similarly to the transmitted signal). The 500-MHz IF outputs are preamplified, summed in the manifold, and fed into the post IF amplifier. The signal is then amplified, video detected, and amplified, where it is ready for processing.

The narrow beam of the antenna is switched to cover 16 distinct sectors in a cone. While in each sector position, four pulses are transmitted and received. The antenna beam is held in each fixed position for 2 msec.

The system output altitude data is updated every 0.5 msec.

The theory of operation of the circuitry will now be broken down into the following headings:

a. RF Power Generation
b. Manifold
c. RFBB's
d. Antenna Patterns and Sector Scan
e. Altitude Tracking Loop
f. AGC Loop
g. PRF Selection
h. Power Conditioning

RF Power Generation

Thirty-two milliwatts of power at 2250 MHz required (on a pulse basis for transmit) and 32 mW of power at 2125 MHz (on a CW basis for the local oscillator) are developed in the RF source. The outputs of two crystal controlled oscillators (93.7500 MHz and 88.5417 MHz) are amplified and the two outputs are fed to an externally controlled single-pole double-throw diode switch. The output of the switch is amplified and frequency multiplied through amplifiers and varactor multipliers that have a bandwidth wide enough to pass either frequency. A 32 mW output at either frequency will be supplied to the manifold to drive the local oscillator and transmitter circuits. A nominal output power of 20 mW is supplied by each oscillator. Low power oscillators are used because they will be left on continuously (to increase stability and expected life). Buffer amplifiers with 4-dB gain can be gated off when not needed. A power amplifier (12.4-dB gain) provides 700 mW to drive the frequency multipliers. A times 4 (-3-dB eff.) and a times 6 (-7.4-dB eff.) frequency multiplier chain develop the 32 mW at 2250 MHz or 2125 MHz.

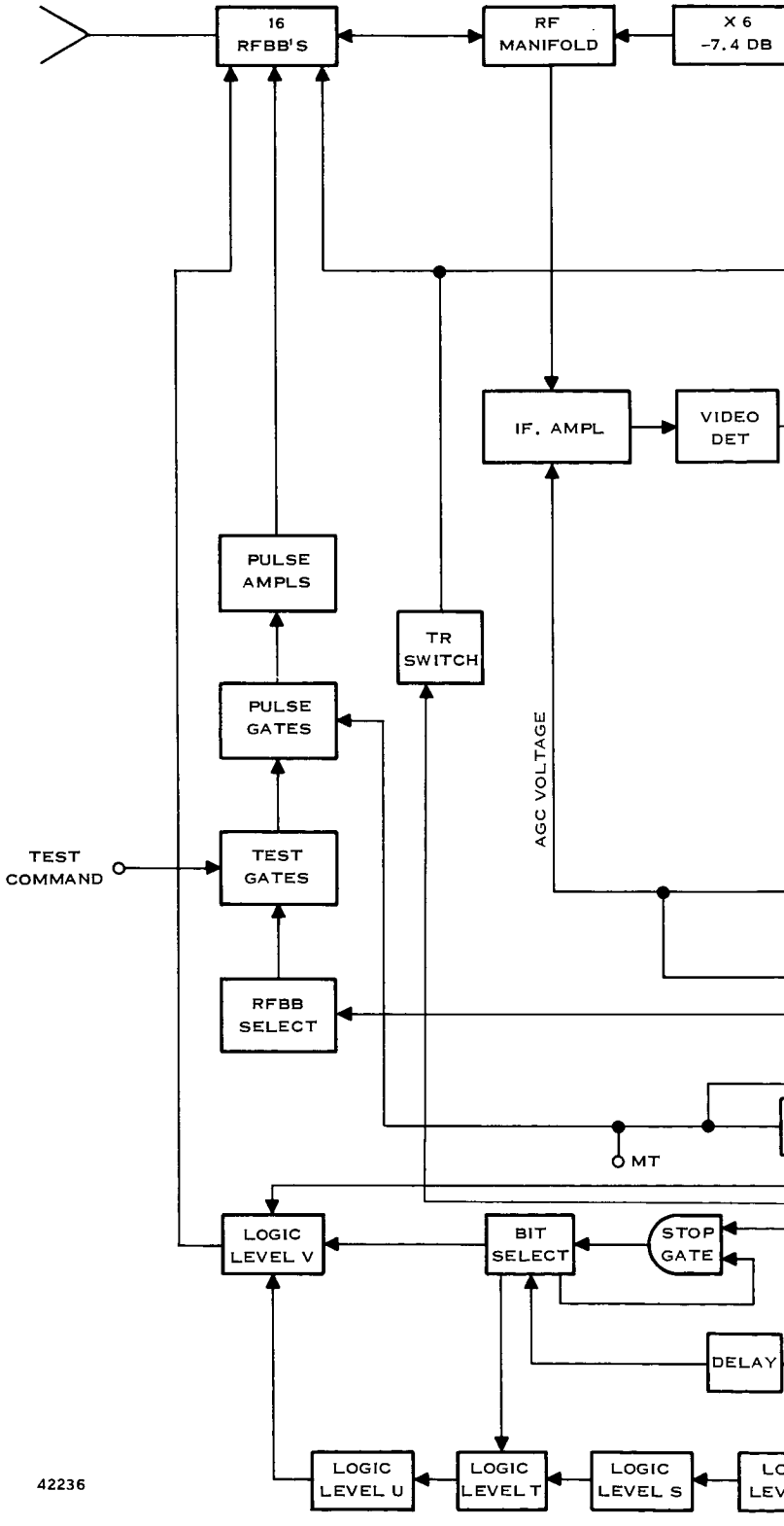
16
RFBB'S
RF
MANIFOLD
X 6
-7.4 DB
IF. AMPL
VIDEO
DET
PULSE
AMPLS
TR
SWITCH
PULSE
GATES
AGC VOLTAGE
TEST
COMMAND
TEST
GATES
RFBB
SELECT
MT
LOGIC
LEVEL V
BIT
SELECT
STOP
GATE
DELAY
LOGIC
LEVEL U
LOGIC
LEVEL T
LOGIC
LEVEL S
42236

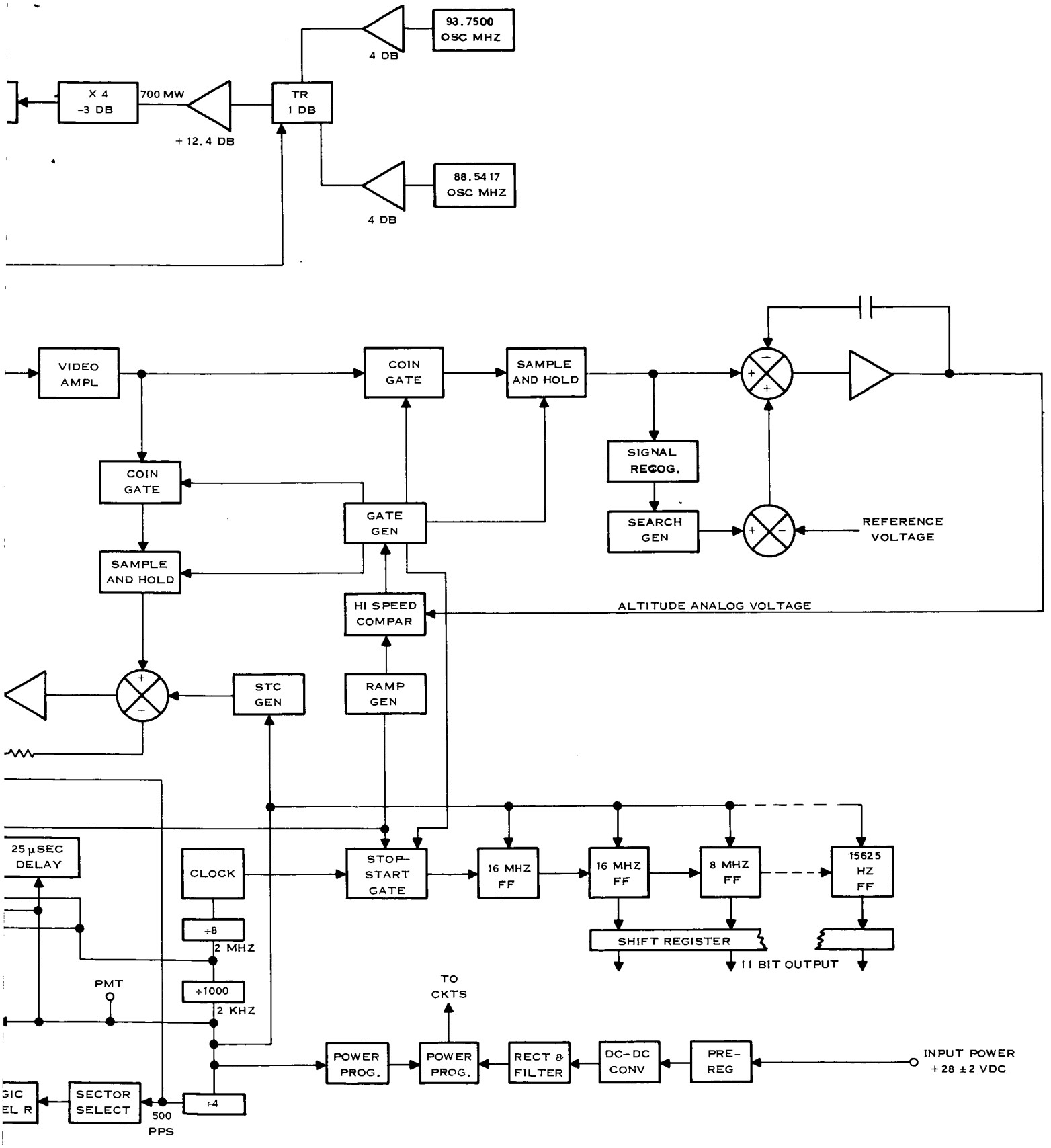

Figure 29. Pulse Altimeter, Detailed Block Diagram

RF Manifold

The basic function of the manifold is to take the input S-band power from the RF source and divide it equally in amplitude and phase to the inputs of the 16 RFBB's. Also, it must take the IF output signals from the 16 RFBB's and sum them to a single output for processing. The RF manifold is basically of stripline construction. There are three layers of board containing circuitry and connections, plus any stiffening layers required. Looking at Figure 30, which is the first layer of the manifold (the layer immediately adjacent to the RF building blocks), it is seen that there are 16 connections (labeled S1) where

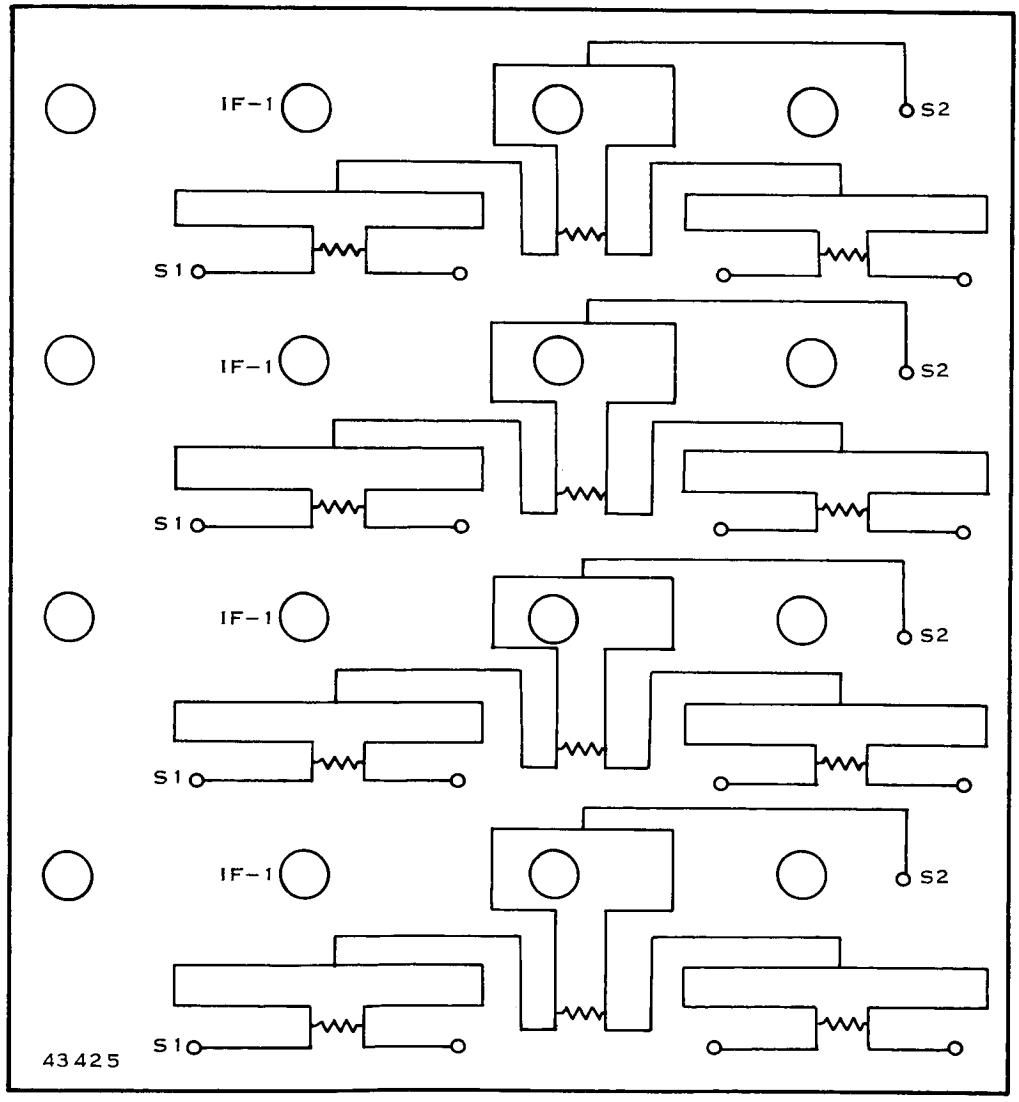

Figure 30. RF Manifold Front Layer, Functional Diagram

the RFBB S-band inputs connect to the manifold. These 16 connections, or outputs, come from eight two-way power dividers which, in turn, come from four two-way power dividers. Therefore, there are four inputs to this board at S-band; these four inputs are labeled S-2. These four inputs are fed through the center layer (Figure 31) to the back layer (Figure 32). In Figure 32 the four terminals (S-2) are developed from two two-way power dividers which, in turn, are fed by a single two-way power divider from the S-band input labeled S-3. Therefore, the 16 equal amplitude and equal phase outputs of the manifold to the building blocks are developed through 15 two-way power dividers from a single S-band input. The total power loss through these power

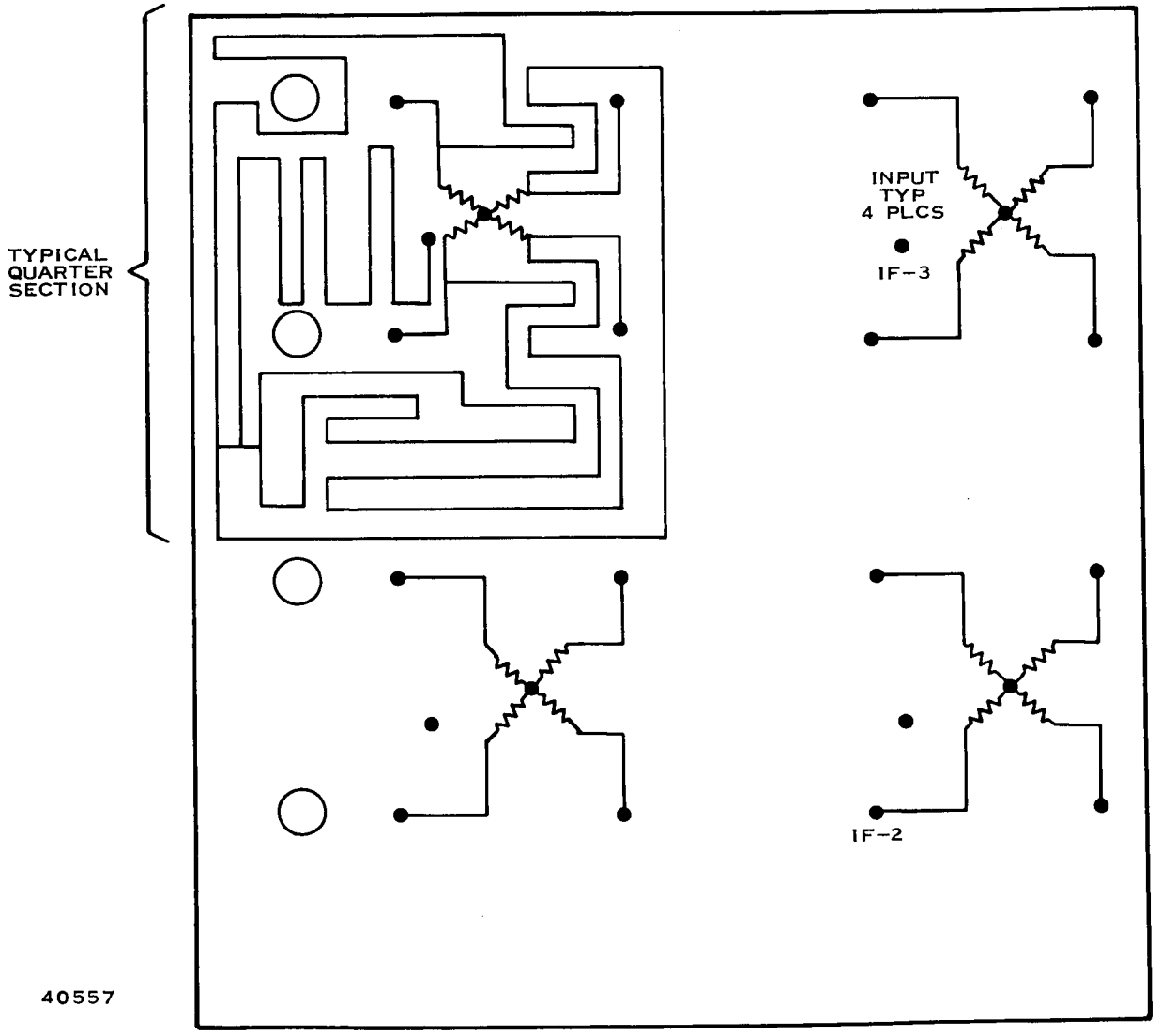

Figure 31. RF Manifold Middle Layer, Functional Diagram

dividers will be 3 dB maximum. Looking again at Figure 30, there are 16 feed-through holes labeled IF-1, where the 500-MHz outputs of the building blocks are fed to the second board (Figure 31). The center board contains four four-way power adders to sum up the 500-MHz IF output to four outputs, to be fed through to the back board (Figure 32). The back board contains a single 500-MHz four-way power adder which gives a single output of 500 MHz. There is a quarter wave matching section on the output of the power adder to match the IF amplifier to the manifold. The loss in this circuit is expected to be somewhat less than 3 dB.

Figure 33 shows a tentative outline of the manifold construction. The solid dots show the 500-MHz connections to the RFBB and the circles show the S-band connections. The side view shows the construction of the manifold. There are two aluminum stiffening layers which form a compact, rugged sandwich construction for the manifold. The output can be taken from the side of the back layer or from the back surface, which gives great flexibility to the packaging engineer.

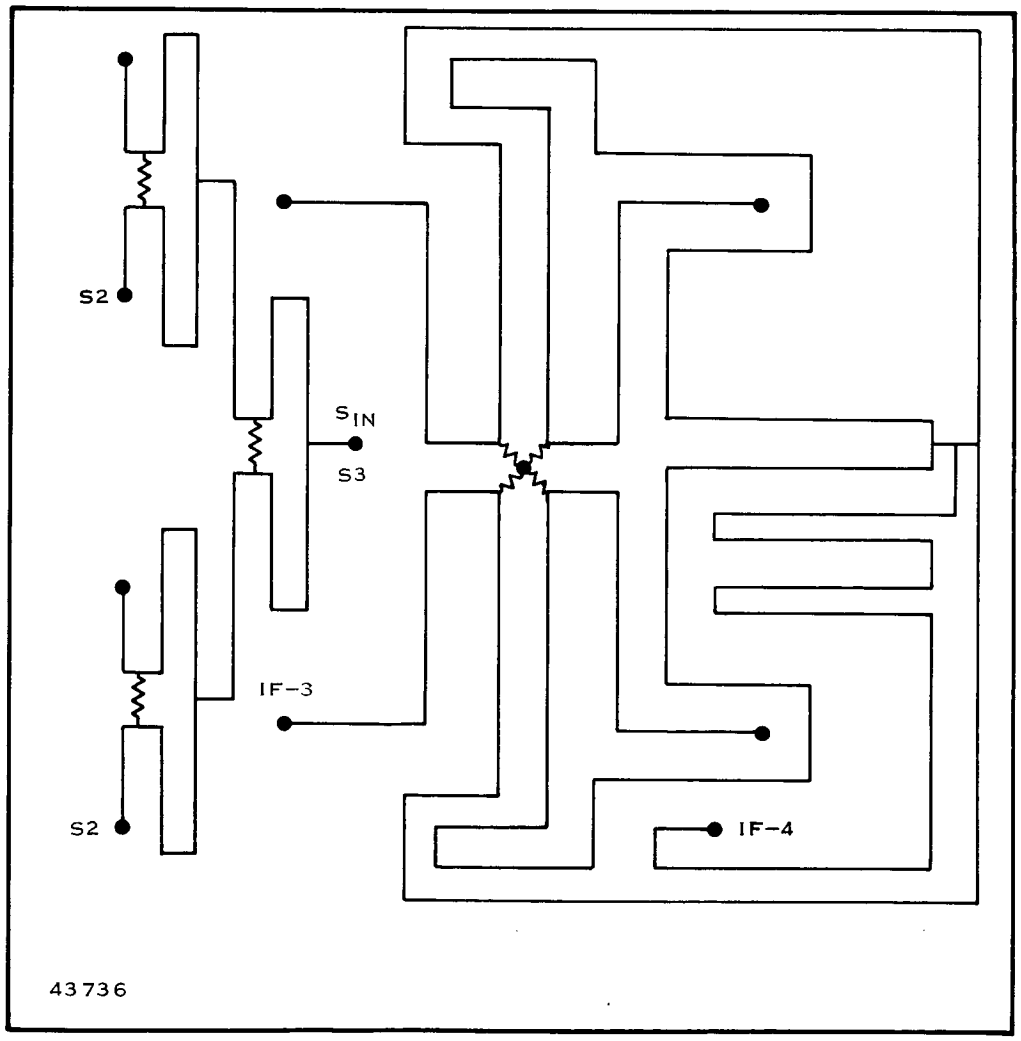

Figure 32. RF Manifold Back Layer, Functional Diagram

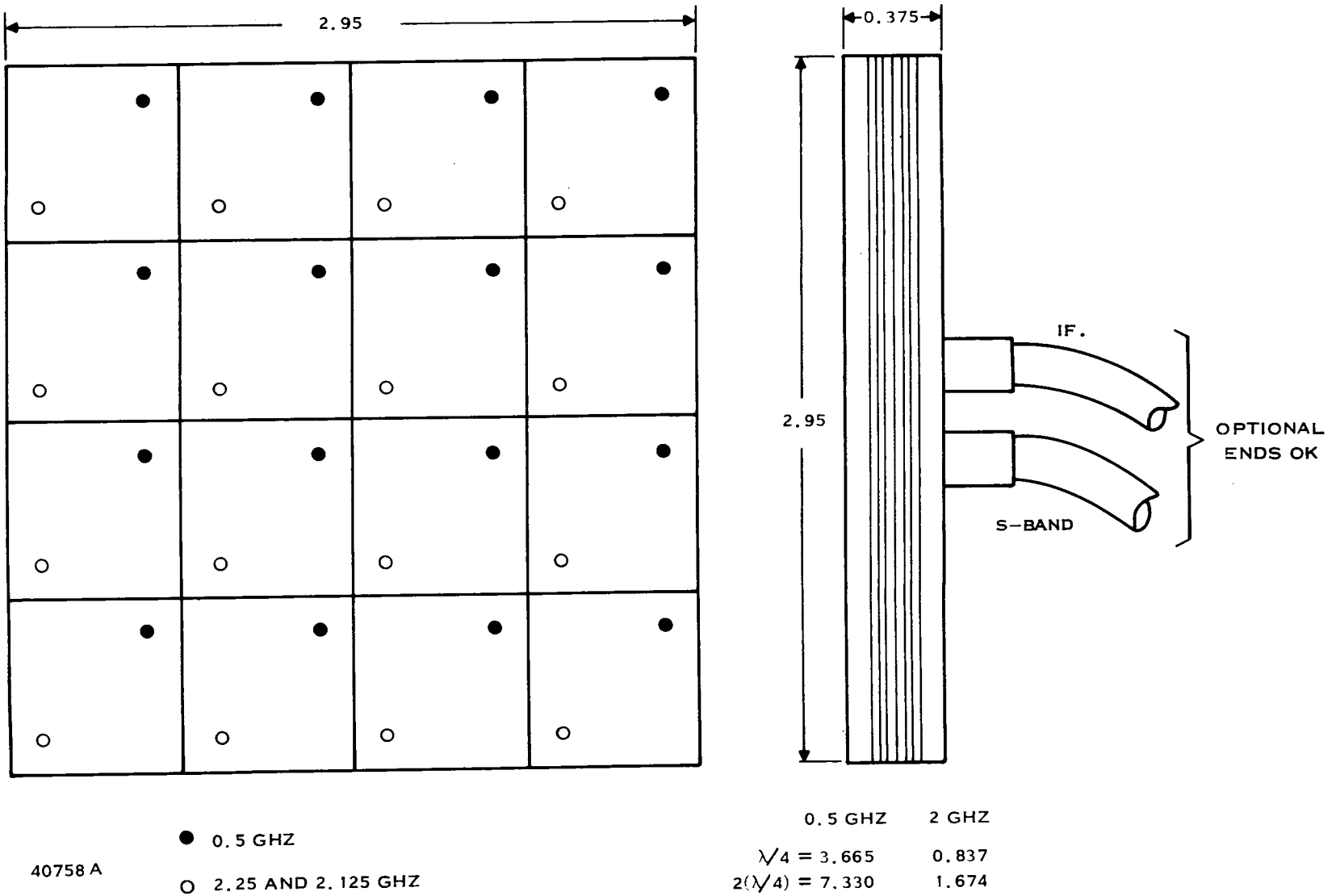

Figure 33. RF Manifold Outline

Radio Frequency Building Blocks

Refer to Figure 34 for a block diagram of the RFBB's.

The input S-band power (2 mW) is amplified 10 dB to 20 mW in a power preamplifier. In the transmit mode, the amplified input is switched in an externally controlled TR switch to the transmit phase shift network, which is a set of line lengths selected by diode switches. The diode switches, in turn are controlled from the outputs of a 4-bit phase shift counter. Therefore, after presetting the counter, it is possible to program phase shift increments by providing the correct number of input bits, or phase "counts" to this counter. A 3-dB loss is expected in the phase shift network. Therefore, 10 mW of power drives the power amplifier, which is pulsed into operation with a 30-volt positive pulse applied to the collector circuits. Since there is a small but finite time required for the amplifier to stabilize, the 30-volt pulse must be applied shortly before the input RF power is applied. This timing is accomplished in other circuits in the altimeter. The 2-W peak output power of the amplifier is quadrupled to the 9-GHz transmitting frequency at a power level of 1.0 W maximum. Finally, an externally controlled antenna TR switch feeds this power to the radiator.

In the receive mode, the input S-band power is again preamplified and phase shifted, this time by the complementary logic outputs of the counter, since the reflected wave will be shifted by 180 degrees. This power is then quadrupled to 8.5 GHz at a power level of 2 mW, and is used as the local oscillator.

The received signal is mixed with the local oscillator to provide a 500-MHz IF frequency, which is preamplified 19 dB in the IF preamplifier.

Antenna Patterns and Development of Sector Scan

It was determined that a four by four array of 16 RF building blocks would be an adequate system for this mission. To estimate the expected antenna coverage for this array, use will be made of Figure 35 for angle definition. Point P_A is the point above the xy plane with coordinates x1, y1, and z1. Vector OP_A will represent some look angle of the antenna above the xy plane. Angle θ_A is measured from the z axis to vector OP_A, and will be a function of both α_A and ψ_A. O_{y1} is the component of vector OP_A on the y axis, and O_{x1} is the component of OP_A on the x axis. The angle θ_A will represent the amount of scan angle from zero boresight, which will be considered as the z axis, normal to the xy plane with the array in the xy plane. Angle Φ_A

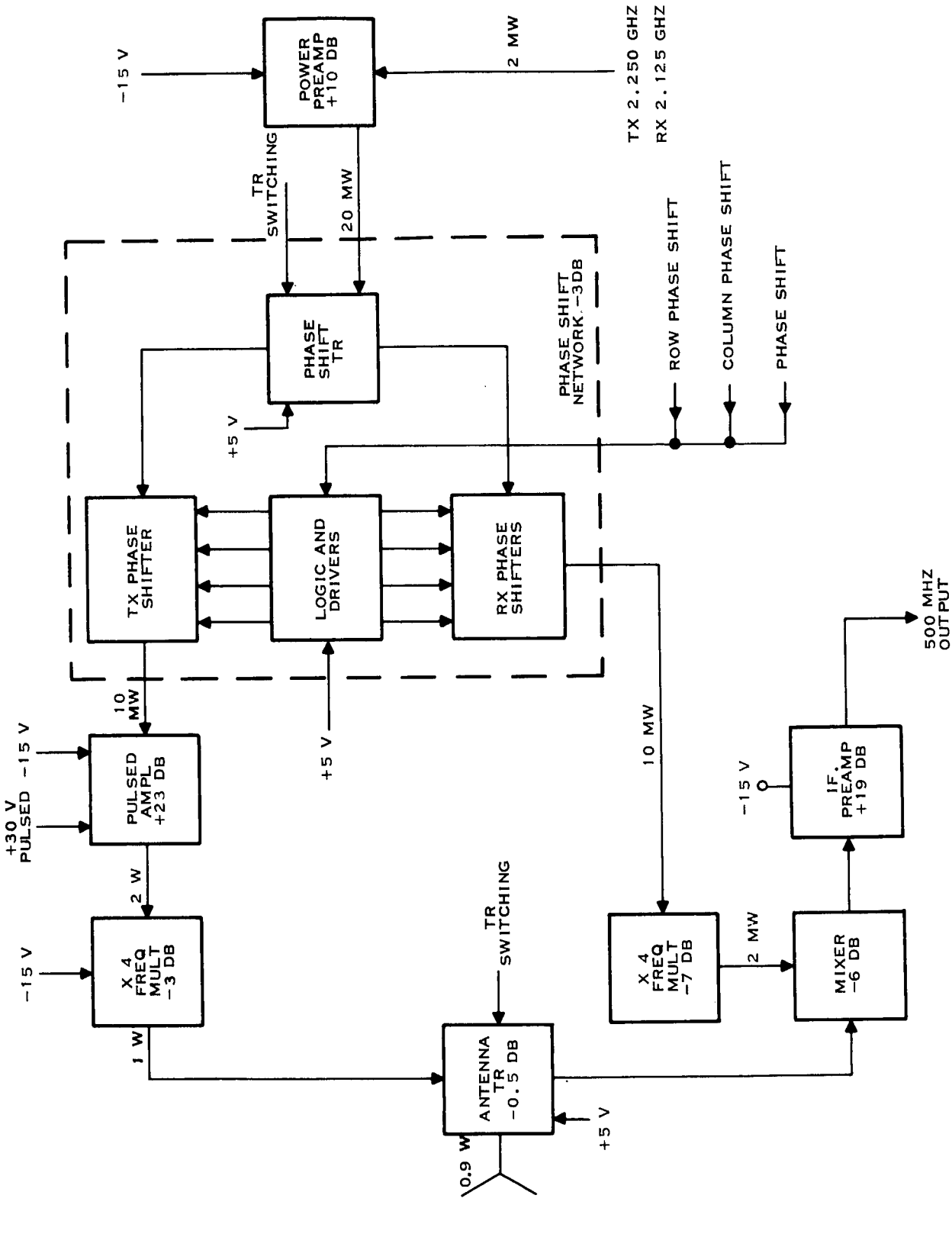

Figure 34. RF Module Block Diagram

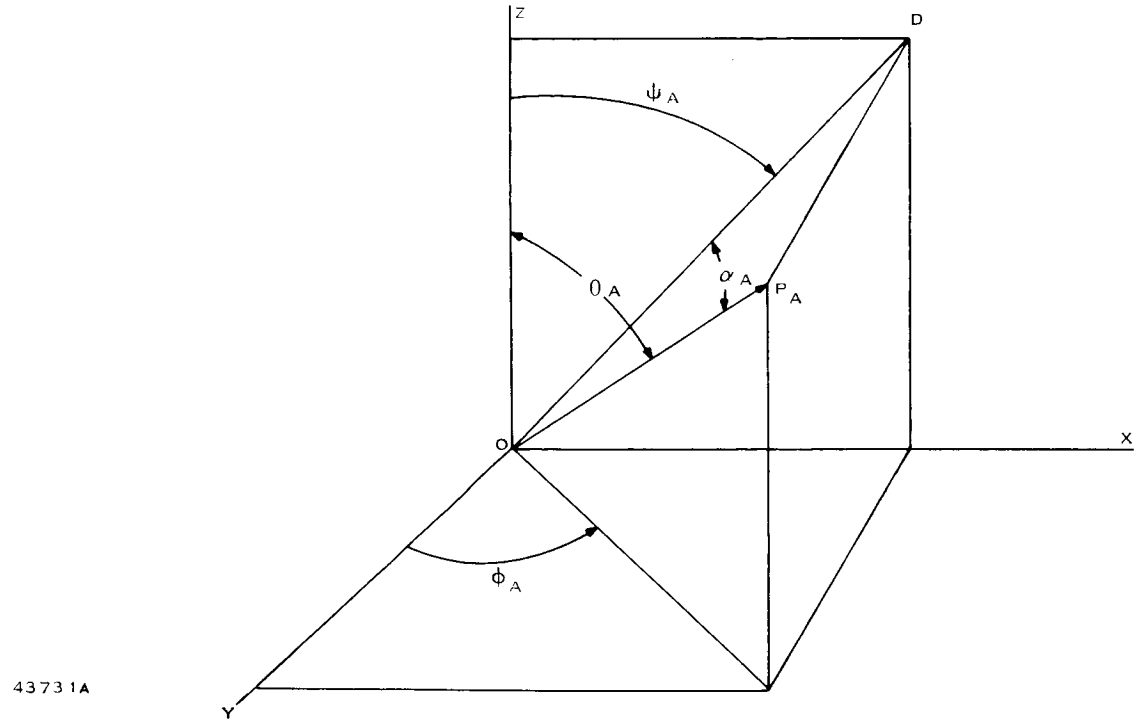

Figure 35. Antenna Variables Definition

is a reference in this plane from the y axis. To plot the antenna pattern on a plane, polar coordinate paper can be used where ϕ_A will be plotted counter-clockwise and θ_A will be plotted radially.

Figure 36 is a plan view of the array in the xy plane with the origin at the center of the array, and Figure 37 is a side view of this array. This is a common means of computing the necessary phase shift for phase scanning. The angle θ_A is shown and the solid line P_F in Figure 37 represents an equal phase front.

To develop this equal phase front, each of the four radiators R1, R2, R3, and R4 are phase shifted in a certain manner. The electrical length is equal to the separation between the radiators times the sine of the scan angle. Therefore, it is easy to determine the required amount of phase shift for any particular scan angle. To scan in two planes or, in other words, to determine the angle ψ_A and α_A, this technique can be expanded to provide the amount of H_S, or horizontal, and V_S, or vertical, phase shift required for that scan angle.

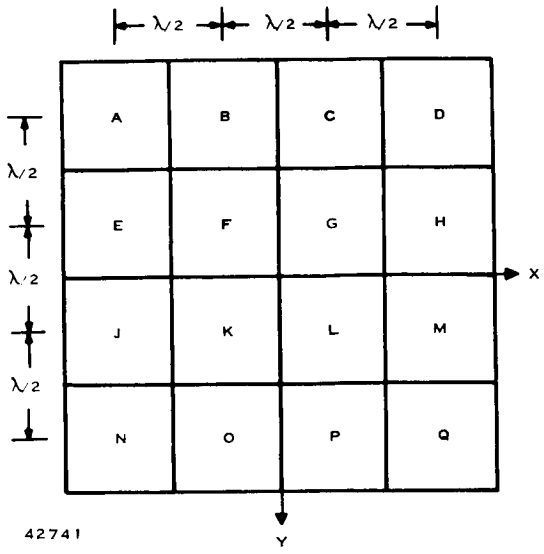

Figure 36. RFBB Array, Plan View

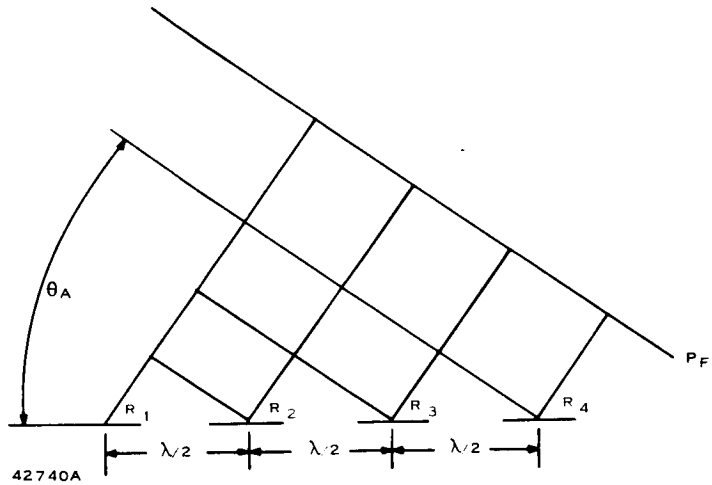

Figure 37. RFBB Array, Side View, Idealized

Since the horizontal phase shift bits for each vertical row of radiators is the same, and the vertical phase shift bits are the same for each horizontal row, only eight outputs from the scan programmer are required for a four-by-four array. For instance, to scan the beam to the left (Figure 36), RFBB's O, H, M, and Q will have the same program. Therefore, knowing the beam steerage required, the correct amount of phase shift for each RFBB can be determined. However, since the phase shift network in the building block is digital, and not continuous, only a certain multiple of a basic phase shift can be used. In this case, with 4 bit phase shift networks, there are available 22.5-degree phase shift bits in each RF building block. This phase shift amount is determined in turn by the number of counting bits supplied to the input of each building block. Therefore, it is only necessary to determine the number of H_S bits and V_S bits for each building block for each sector to develop the scan program.

Figure 38 is the result of a computer program used to find the expected coverage for this altimeter antenna. Each radiator is essentially a dipole, or the equivalent of a dipole, and will, therefore, have a cosine squared (power) pattern. The lines are loci of the 3-dB down power contours of each pattern. It is seen that there is adequate coverage over the space segment of interest.

There is no amplitude weighting of the radiators, only phase weighting to develop these patterns.

After this program was set up and computed, it was an easy matter to rerun the program with certain failure modes. Figure 39 is the result of some of these runs which show that with two failures in amplitude or two failures in phase, chosen arbitrarily, there is very little degradation in the total overall coverage for the altimeter antenna. Therefore, it is assumed for practical purposes that the RF building blocks contribute very little to the failure rate of the entire system and the failure of the building blocks will not jeopardize the missions success unless it affects other elements of the altimeter. The RF manifold has been designed to effectively isolate each RFBB from the others so a failure will not affect the others. The individual pulse amplifiers have been designed so that a short circuit load on one of them will not affect the others; therefore, it is considered very unlikely that failure in any mode of any one building block will affect the operation of any other part of the system, including any other building blocks.

Scan Programmer. – Since the scan, or sector switching, is continuous, the scan program is not interrupted when a signal is received. This method ensures that the beam will search all sectors should the tracking loop ever unlock. It is possible to stop the scan when a returned signal is being tracked, thereby increasing the PRF in that sector. However, vehicle attitude changes during entry are expected which would necessitate another sector search. The measurements lost during these searches may be critical, and since the required performance can be met with a continuous scan, this method was employed. The sector search should not be confused with the normal search mode of the altimeter; the former is a search in position, while the latter is in time. Additions could be made to the circuitry to read out vehicle attitude (accurate to one-half antenna beamwidth) by using logic circuits to determine which sector respresented the closest return, since the various returns, if there are more than one, will be time-separated. The method recommended (i.e., continuous sector scan) works well with the attitude tracker suggested, since it will track the leading edge of the sum of all received signals. The relatively long time constant of the tracking servo loop ensures that the track point will not "jump" from pulse to pulse, if the pulses are not time (range) coincident.

To select the correct number of counter bits for each building block for each scan position (sector), a digital scan programmer, shown in Figure 40, will be used. Four flip-flops connected as a ripple-through counter, along with 16 four-input gates (logic level "R") select the sector to be used. Each sector will be "looked at" for four transmitted pulses, so the sector selector is changed 500 times per second. Therefore, the clock input to the sector select counter is at 500 Hz, which is generated by counting down the 2-kHz PMT. The premaster trigger (PMT) is, in turn, generated by counting down the 2-MHz input to the programmer.

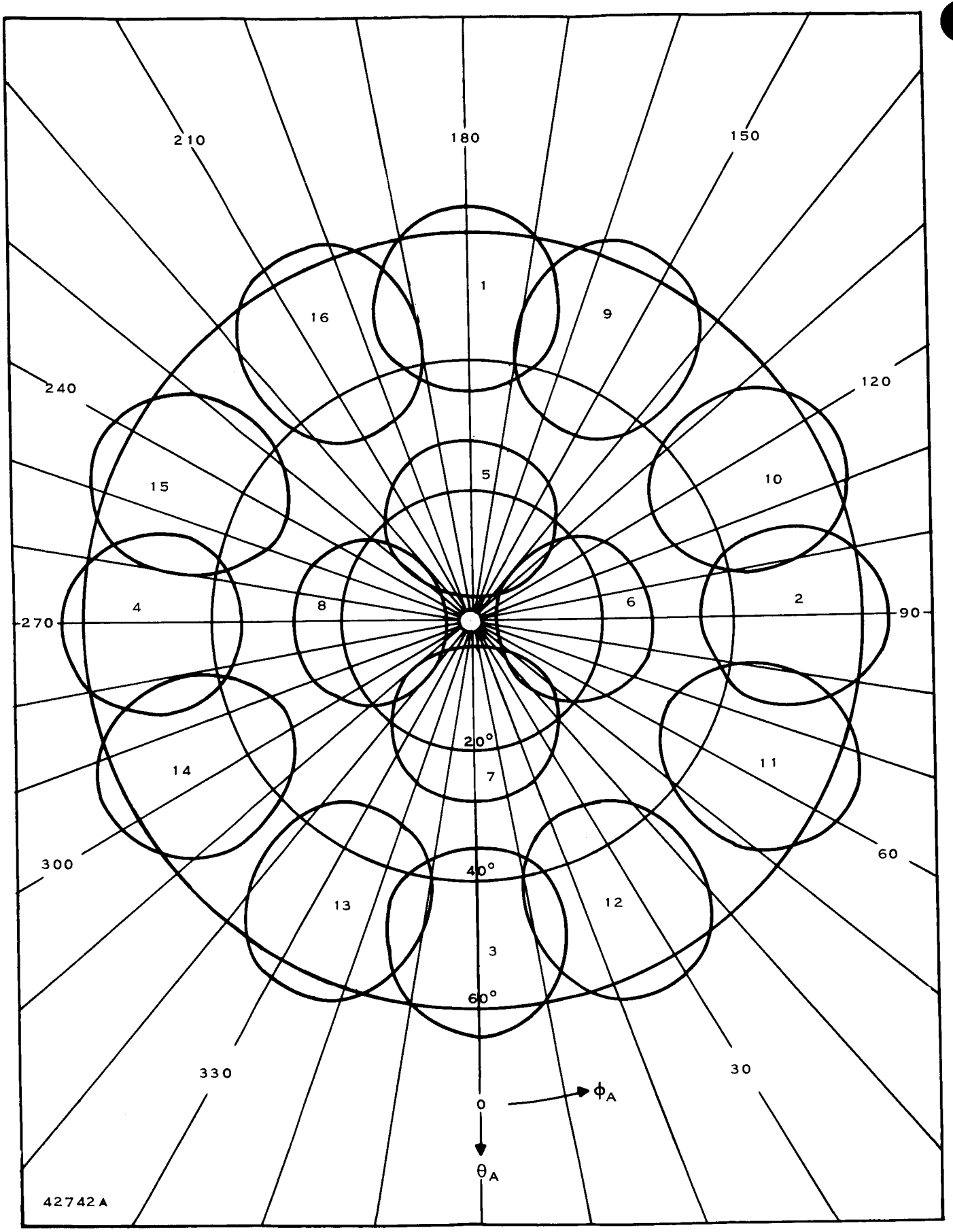

Figure 38. RFBB 4 X 4 Array, Radiation Pattern

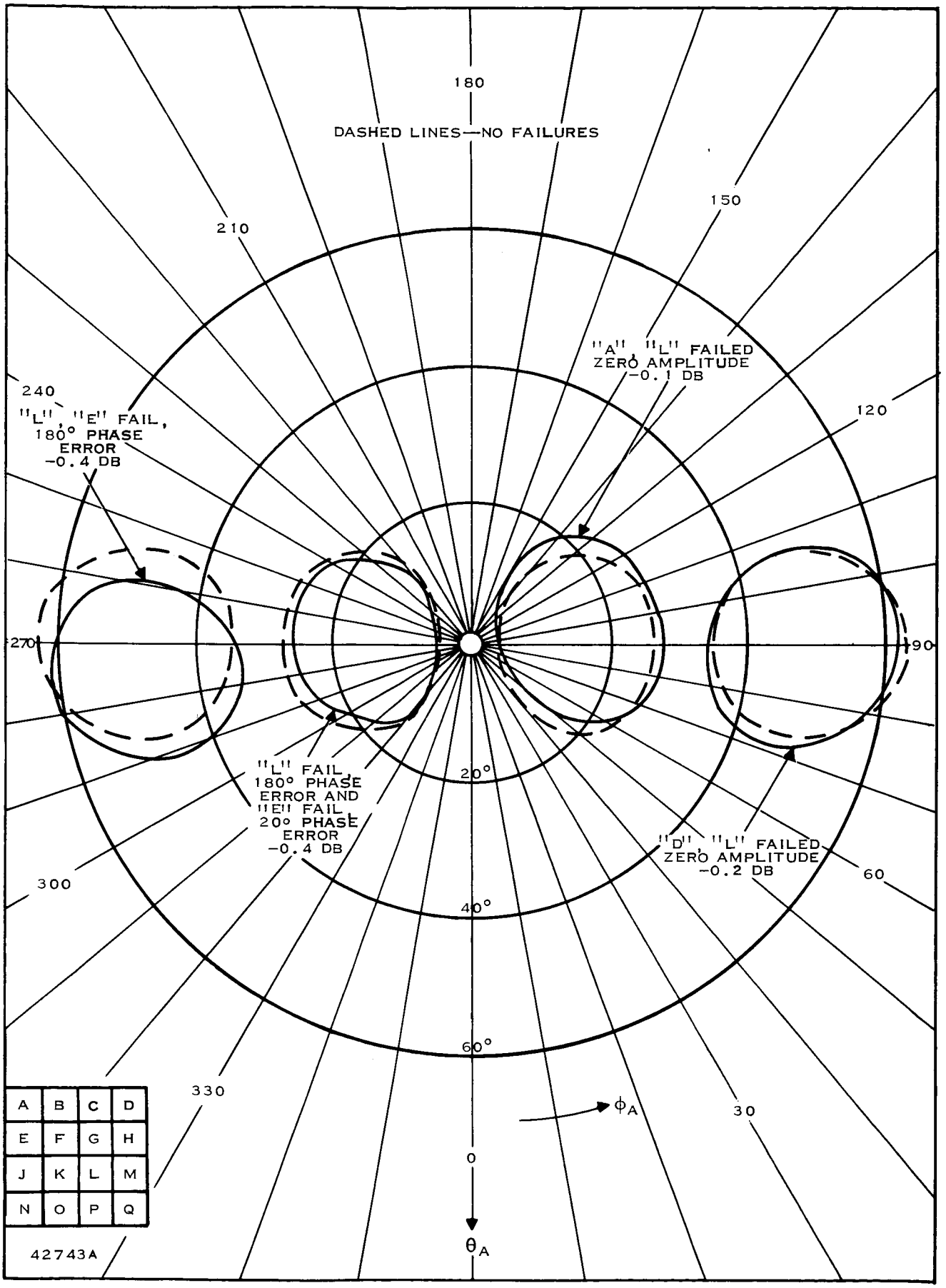

Figure 39. RFBB 4 X 4 Array, Radiation Pattern with Random Failures

A six-stage ripple counter is used for the bit selection. Since the output stage will disable the input clock through the stop gate, this counter will count 32 pulses and stop. Thirty-two pulses represents full 360-degree phase-shift bits for both the horizontal and vertical components of the scan angle. This method has been selected as most economical considering complexity, power dissipation, and reliability.

This counter is preset through a 1 μsec delay, to ensure against false programming due to propagation delays in the counting circuits. The fifth flip-flop stage of this counter determines whether the horizontal or vertical bits are fed to the RFBB's.

Logic level S is the actual program stage, as it selects the counts (bits) needed for each sector. Logic level T combines the bits required (from S) with the pulse lengths needed to limit the counts. Logic level U steers these programs to the correct RFBB groups, and logic level V selects either the vertical or horizontal bits, as well as supplying the actual clock pulses (2 MHz) to drive the RFBB's.

Mechanical Scan

A simpler means of scanning the antenna beam would be desireable. For instance, a mechanical conical scan would offer most of the advantages of the phased array; however, it was felt that the environimental extremes that the lander would be subjected to would limit the growth potential of this approach. Lubrication problems, as well as electrical interference problems appear to be the primary technical problem areas of this limitation – not to mention the added size, weight, and power consumption of a mechanically steered antenna beam.

Altitude Tracking Loop

An analysis of this radar application showed that the optimum filter receiver contained a type 1 servo loop. This loop tracks the leading edge of the envelope of the received pulse. To maintain the fast response necessary, and also reduce the effective noise bandwidth of the system, a sampling circuit is employed. Figure 29 shows the servo loop and its associated circuitry. The IF input is envelope detected and amplified in a video amplifier. A linear AND-gate, or coincidence gate, supplies the common output of the leading edge of the received pulse and the trailing edge of a tracking pulse to a sample and hold (boxcar) detector. The tracking pulse and boxcar trigger are generated as time gates dependent on the output of a high-speed comparator, and the comparator output is triggered when the ramp voltage exceeds the output of a pure integrating amplifier. Since this amplifier amplifies only a change in the input, it is velocity sensitive, or type 1. Therefore, any change in the time between the last received pulse and the pulse in the loop is detected and the loop reacts to track it.

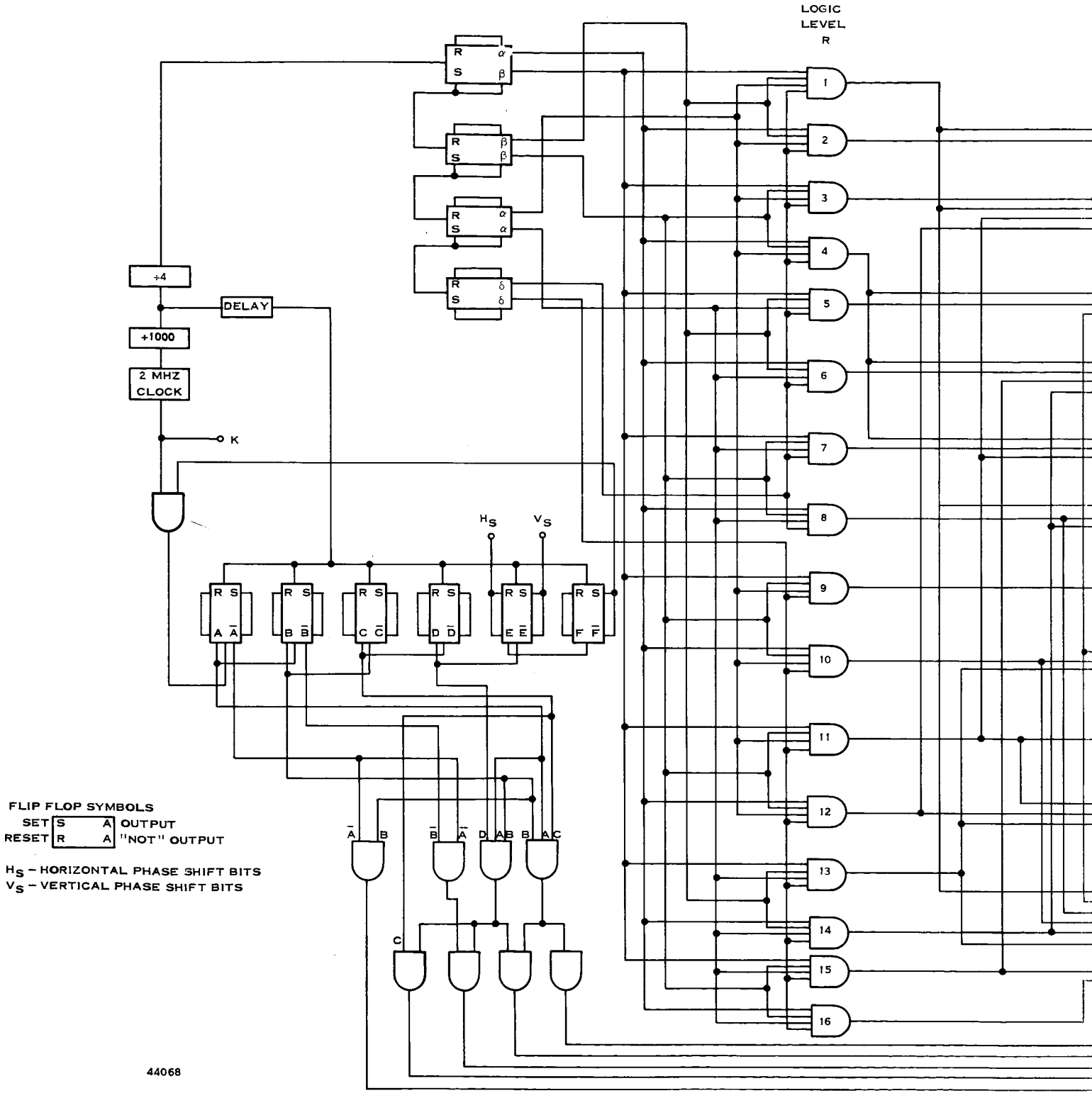
LOGIC
LEVEL
R
+4
DELAY
+1000
2 MHZ
CLOCK
K
H_S
V_S
1
2
3
4
5
6
7
8
9
10
11
12
13
14
15
16
FLIP FLOP SYMBOLS
SET S A OUTPUT
RESET R A "NOT" OUTPUT
H_S – HORIZONTAL PHASE SHIFT BITS
V_S – VERTICAL PHASE SHIFT BITS
44068

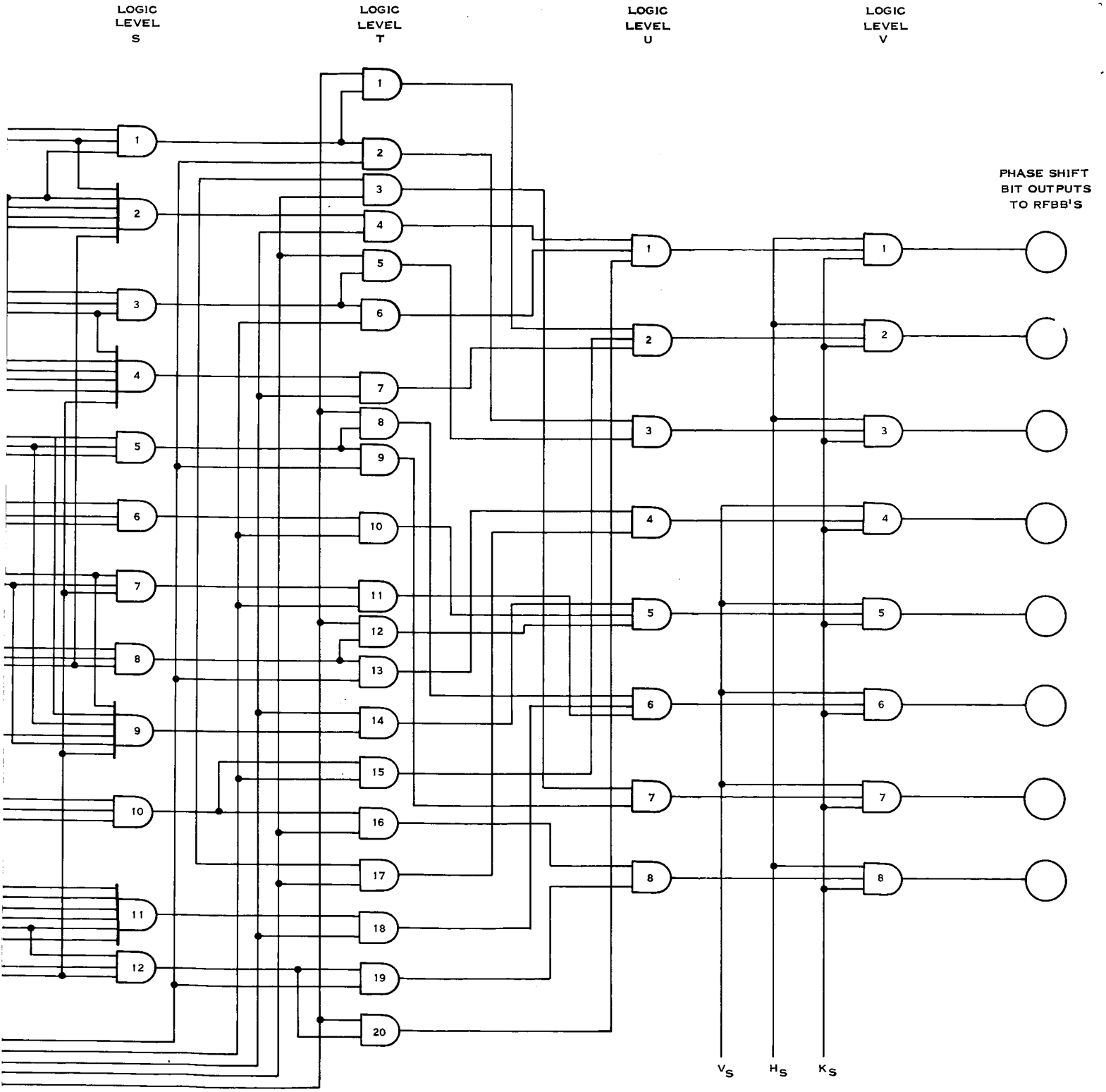

Figure 40. Scan Programmer Logic Diagram

If no signal is present, the signal recognition circuit will sense a zero output of the hold circuit, and activate a search generator which drives the integrating amplifier slowly from zero time to maximum time, or zero altitude to maximum altitude. Thus, the search generator is automatically activated whenever the received signal is "lost" outside the tracking loop.

AGC Loop

An accurate measurement of the threshold crossing of the leading edge of the received pulse envelope, and hence system accuracy, depends on the received signal having a relatively constant amplitude over the altitude range. Therefore, a good AGC circuit is required. The coincidence gate is similar to the gate in the altitude tracking loop, except that the gate pulse is longer to ensure measuring the peak amplitude of the video signal and not the leading edge. A boxcar detector (sample and hold) is used for the same reasons as in the altitude tracking loop. A low-pass amplifier allows the loop to respond to average signal strength changes, and not to pulse fading or sampling rates. The STC (sensitivity time control) circuit increases the loop gain with time (altitude), thereby decreasing the required dynamic range of the AGC loop.

Power Conditioning

There are several supply voltages required to power the altimeter circuitry, and it is assumed that the lander will have a single voltage source. Therefore, a power conditioning circuit is required to efficiently transform this single voltage into the several required voltages, and also to take advantage of certain "dead times" in the altimeter circuitry. For example, the maximum required altitude of altimeter operation is 15.5 km, which represents 103 μsec of signal travel time; the system PRF is 2000 PPS for a system time between pulses of 500 μsec. Therefore, portions of the altimeter are not needed for about 400 μs, or 80 percent of the time.

In order to minimize the power drawn from the lander, and also decrease the heat production of the altimeter, the power programmer will shut off supply voltages to the unused circuits during these "dead times." By utilizing this approach, the altimeter power requirements are reduced more than 40 percent, as can be derived from the data in Table 6.

Table 6. –Altimeter Circuitry Power Requirements

Voltage (volts)	Current (ma. peak)	On Time (percentage)	Average Power (watts)
+5	354	100	1.770
+5	2059	28	2.880
+10	55	100	0.550
−10	18	100	0.180
−15	326	28	2.590
+30	68	28	0.574
+30	68	4	0.082
+30	7200	0.6	1.296
		Total	9.922 W

The circuits which must run continuously are the altitude tracking loop, the output circuits, the two crystal controlled oscillators in the RF source circuit, the power programming circuits, and a portion of the scan programmer. The altitude tracking loop circuits include the coincidence gate, gate generator, sample and hold circuit, high-speed comparator, signal recognition circuit, search generator, reference voltage supply, and integrating amplifier. The output circuits consist of the 16-MHz precision clock, its stop-start gate, the eleven flip-flops used as a counter, and the eleven flip-flops in the shift register. The scan programmer circuits mentioned previously are the divide by eight circuit (three flip-flops), and the sector selection counter (four flip-flops) as they must retain memory.

PRF Selection

The selection of system pulse repetition frequency was controlled primarily by two factors. A large PRF, consistent with unambiguous range measurements, results in a smaller velocity error. However, a smaller PRF allows a simple input "power saver" to be utilized. This "power saver" is described in the following text. A 2000 PPS pulse rate is close to optimum for the above two conditions, and calculations of error and input power, using this pulse rate, shows that the system is within specifications.

Much of the circuitry is only needed for approximately 28 percent of the time. These circuits include the AGC tracking loop, which is the IF amplifier, video detector, video amplifier, the coincidence gate, sample and hold network, STC generator, and the integrating amplifier in the AGC loop. Other parts are

the phase-selecting flip-flops in the RF building blocks, the major portion of the scan programmer, and the local oscillator circuitry, which includes the power amplifier driven from the mixer in the RF source, the various TR switches, the IF preamplifier and the pre-power amplifier in the building blocks.

A small part of the circuitry only has to be run for about 4 percent of the time, that is the power amplifier which supplies the 9-GHz input to the building blocks (the one driven from the 93.75-MHz precision oscillator). The power amplifiers in the RF building block need only to run for about 0.6 percent of the time (the pulsewidth divided by the time between pulses).

Figure 41 shows the circuitry required to generate these voltage-time functions. The lander power is assumed to be +28 volts ±2 volts. An input preregulator Q1, CR1, and CR2 regulates the input voltages to 25 volts ±0.1 volt. A simple regulator is sufficient because of the constant load. CR1, CR2, and Q1 will be chosen so that the temperature variation in the zener voltages will compensate for the temperature change in the base-emitter voltage drop of Q1.

Q2, Q3, and T1, along with the associated bias circuitry, form a square-wave oscillator. The secondary of T1 is tapped to provide the input voltages to five full-wave rectifiers which supply, after filtering, +5, +10, −10, −15, and +30 volts. With proper design, a 90-percent efficiency is easily realizable in this type of DC to DC converter.

The system trigger (PMT-premaster trigger) starts timing circuits (MSMV's) in the power programmer, and the MSMV's, in turn, drive transistor switches to provide the required duty factor for each switched voltage. A 95-percent efficiency can be achieved in the programmer.

SYSTEM INTERFACES

Input Power

The input power has not been defined for this mission; therefore, for the purposes of this study, it will be assumed that the input power is supplied at 28 ±2 volts dc. If there are any noise pulses or high frequency components of ripple expected on the supply, they must be specified and reviewed to see what effect they might have on the altimeter.

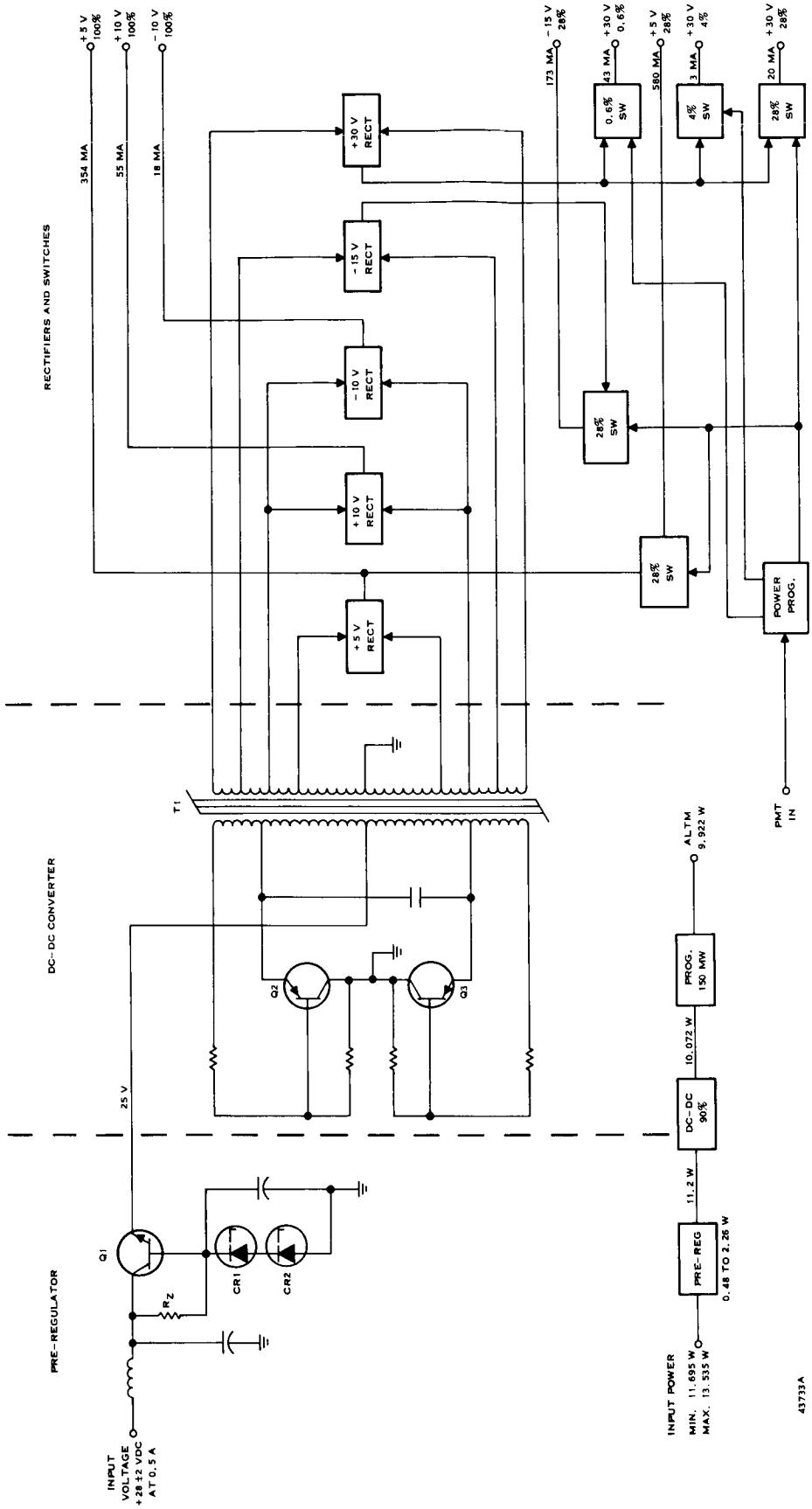

Figure 41. Power Conditioning Circuits Functional Diagram

Output Circuitry

The output of the altimeter is an 11-bit digital code. The 11 bits are supplied from logic gates with an approximate 100-ohm output impedance in the high voltage or logical one condition and an approximate 12-ohm output impedance in the zero voltage or logical zero condition. The zero volt output is not exactly zero volts, but is 0.4 volt or lower. The high voltage will be approximately 2.4 volts to 5 volts for a noise margin of 2.0 volts. The output data will be updated every PRF, or 2000 times per second.

Ground

The power and signal ground to the altimeter is assumed to be common and connected to the frame of chassis of the lander and altimeter.

Test Input

The test input voltage will be approximately 4 volts dc, which will disable the pulsed voltage supply to the RF power amplifiers in all the RF building blocks, and will turn them on one at a time in a particular sequence. Since they are now time separated, the output of each building block can be monitored separately. The input voltage must be between 2.8 and 5.0 volts dc for proper operation.

There is a possible problem with this test voltage being incorrectly disconnected when the sterilization shell is ejected after the spacecraft leaves the earth's atmosphere. It is presumed that this test line will be connected to the altimeter through a bulk head connector on the sterilization cannister. When the sterilization cannister is ejected, this line must be grounded at the altimeter to ensure that the altimeter will operate properly when needed and not remain in the test mode. At the input to the altimeter, this test voltage will be grounded through a resistor. Now, as this line is left floating after the sterilization cannister is ejected, the inputs will be grounded through the resistor, which will be enough of a zero logic input to disable the test function and allow the altimeter to operate properly. A safer condition would be a break-away connector, at the altimeter, on this umbilical cord that will automatically disconnect this line from the altimeter to allow the grounding through the resistor.

POST STERILIZATION OPERATIONAL TEST

After the final sterilization heat soaks, with the altimeter mounted on the lander which is enclosed inside a metal sterilization cannister, it is important to know if the altimeter is still operable. The operating parameters that would be desirable to test are:

a. Transmitter Power Level
b. Transmitted Pulse Shape
c. Antenna Scan
d. Receiver Sensitivity
e. Signal Acquisition
f. Signal Tracking
g. Output Circuits.

Since the altimeter must be tested while inside the sterilization cannister, there appears to be no practical way to check the antenna pattern because of multiple reflections and questionable near-field antenna parameters. A major problem is the extremely difficult task of maintaining dimensional stability of the cannister. It is considered unlikely that a practical method of post-sterilization testing of the altimeter antenna parameters will be developed. Confidence gained in the qualification testing phase would in all probability be the only method of ensuring post-sterilization operation of the altimeter to a satisfactory confidence level. Other on-board subsystems may also be extremely difficult to check out, so an Earth run of the mission could be used for the entire lander, that is: (1) Sterilize the lander, (2) Simulate launch and Earth to Mars trip environments, and (3) Test all subsystems.

The transmitted power level, pulse shape, and the receiver sensitivity can be tested for each individual MERA module if a built-in test function allows time discrimination between modules. This feature has been designed in the altimeter, and its operation is described in the sections on the Altimeter Operational Test Set and Test Sequence Generator.

After the terminal sterilization heat soak, a test sequence, where each RFBB is used by itself as a transmitter-receiver, is activated by a single wire command (Figure 42) which gates on this circuit. Four flip-flops, connected as a ripple-through counter, and 16 four-input gates select the RFBB to be tested. Therefore, the outputs of the RFBB's are time separated and can be monitored individually. The pulse amplifiers supply the power to the RF amplifiers in the RFBB's.

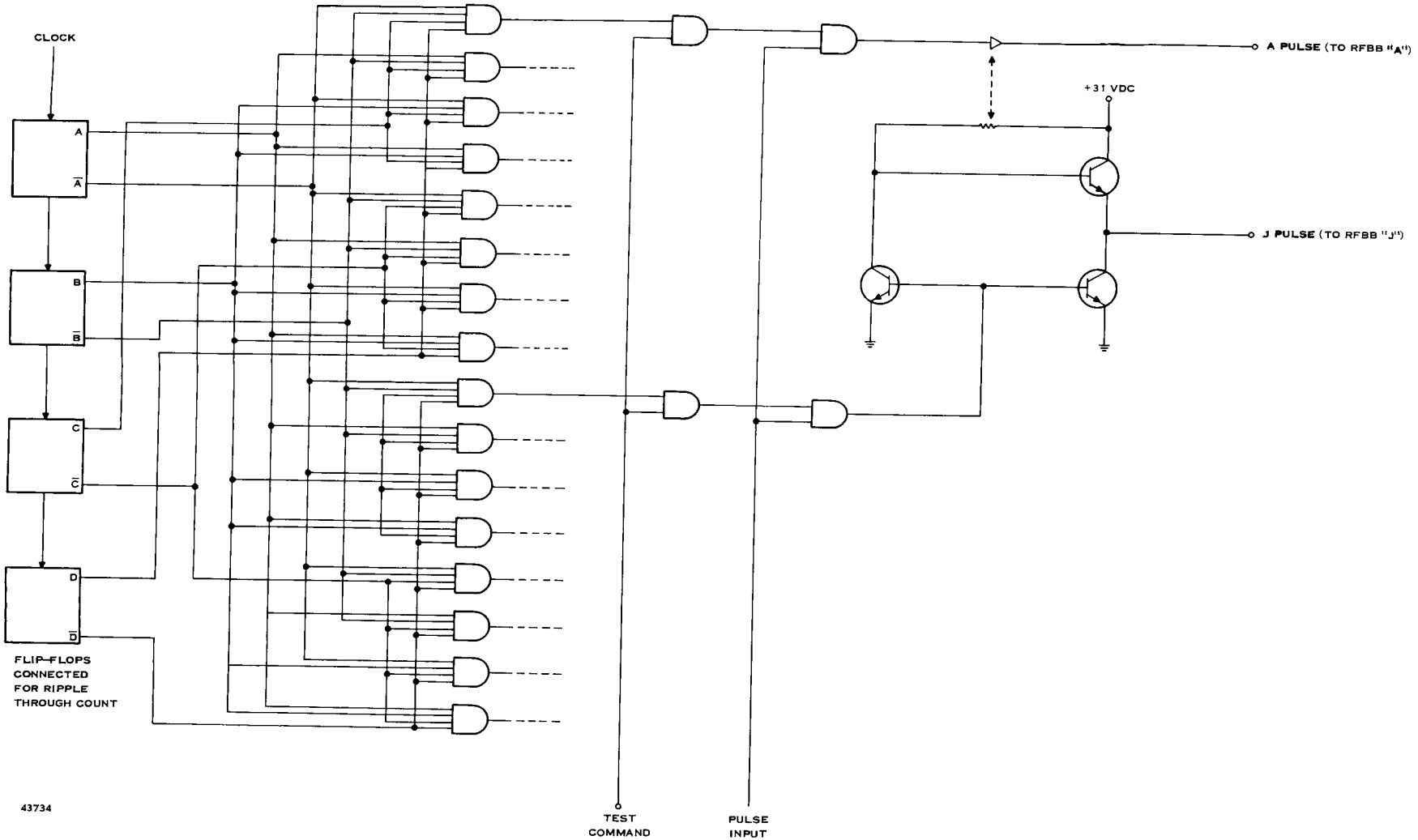

Figure 42. Test Sequence Generator Functional Diagram

ALTIMETER OPERATIONAL TEST SET

Introduction

An operational test set is desirable for these reasons:

a. It is possible to check the operations of the altimeter during the breadboard and prototype build phases of development by simulating actual operating conditions.
b. Each production unit can be tested to give a greater degree of confidence in its operational integrity.
c. The operation of the altimeter can be monitored during environmental tests.
d. The altimeter can be checked during pre-launch operations.

Figure 43 is a block diagram of an altimeter test set that will:

a. Check the radar altimeter for measurement accuracy during a simulated Martian landing.
b. Check the radar altimeter for measurement stability by static tests (constant altitude).
c. Check the altimeter for measurement accuracy under varying doppler frequencies, altitudes, received pulse rise time degradation and gross surface reflectivity (attenuation).

Description of Circuits

The test set is basically a microwave repeater. An antenna coupler is either attached directly to the altimeter radiative section, or placed at an optimum distance from the altimeter in an anechoic chamber. With the altimeter operating and the test set antenna coupler tightly attached to the altimeter radiative section, it is possible to monitor the peak transmitted power of the altimeter. A portion of the received energy is coupled to a calibrated detector to make this power measurement.

The modulation characteristics of the transmitted signal can also be monitored by displaying the detected signal on the oscilloscope. The received signal is also detected, amplified and used as a timing reference for the rest of the test set. Part of this detection process is a frequency conversion to a suitable IF frequency, making use of a stabilized local oscillator.

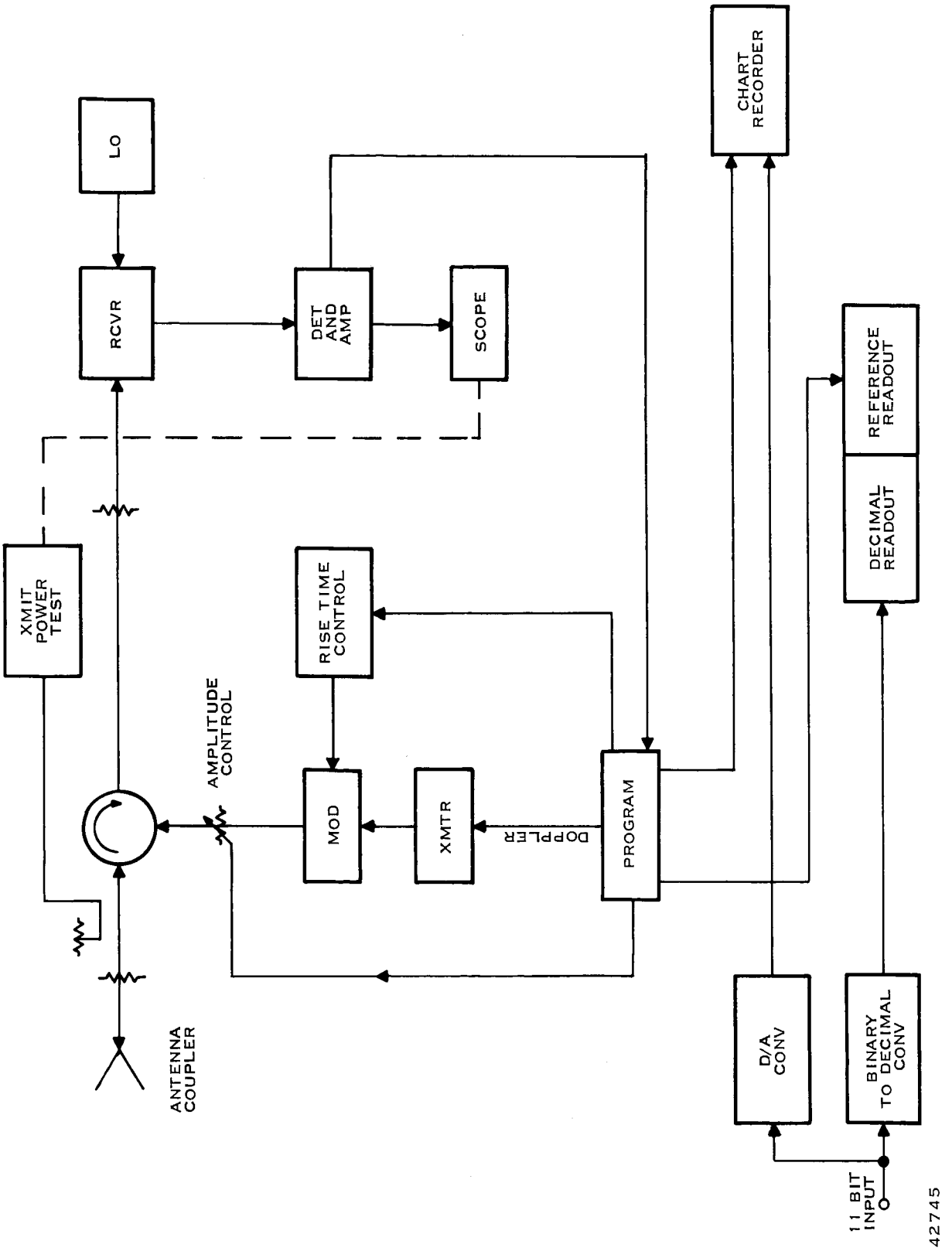

Figure 43. Block Diagram, Altimeter Operational Test Set

The transmitter need be only a low power RF source electronically tunable over the range of doppler frequencies expected. An amplitude modulator will be connected to the output of the transmitter which will allow electronic control of the signal amplitude. These two features along with suitable time delay programs to simulate changes in altitude, will allow the re-transmitted pulse back to the altimeter to simulate the received pulse from an actual landing flight profile. The program will be basically a linear sweep generator which will have an output signal modified through operational amplifiers with appropriate transfer functions to approximate the actual changes in signal strength, pulse rise time degradation and doppler frequency shift versus time, or altitude.

A chart recorder can be used to compare programmed versus measured altitude for real-time comparison. An essential part of this monitoring is an accurate digital-to-analog converter.

Static stability tests are better made by comparing two digital readouts, one from the altimeter output, the other generated within the test set.

It is desirable to interrupt the transmitted signal from the test set independently from any program, to test the altimeter in the search mode. All of these features are contained in the proposed test set.

PHYSICAL DESCRIPTION OF PROPOSED SYSTEM

During the course of this study, a model of the proposed altimeter was constructed, and photographs of this model are shown as Figures 44, 45, 46, 47, and 48. The radar "front end" (Figure 45) is composed of a square array of 16 MERA RF modules. Each module has a cavity fed slot radiator. Interconnections to the modules and the rest of the altimeter are made through a corporate feed structure, or printed circuit manifold, and wiring harness represented by the large flanged block in Figure 44. A description of the RF modules is contained in the Theory of Operations section. This array is mounted in a cast frame to form the assembly shown in Figure 46. All associated circuitry can be mounted in recesses in the housing, or in the back structure (Figure 48). The back structure is mounted to the housing to form the complete altimeter, with a single connector protruding from the back cover. With the back cover and side covers removed, all circuitry is exposed for final assembly, testing and maintenance. A more detailed description of the altimeter, including thermal paths, mounting interfaces, etc., is contained in sections which follow.

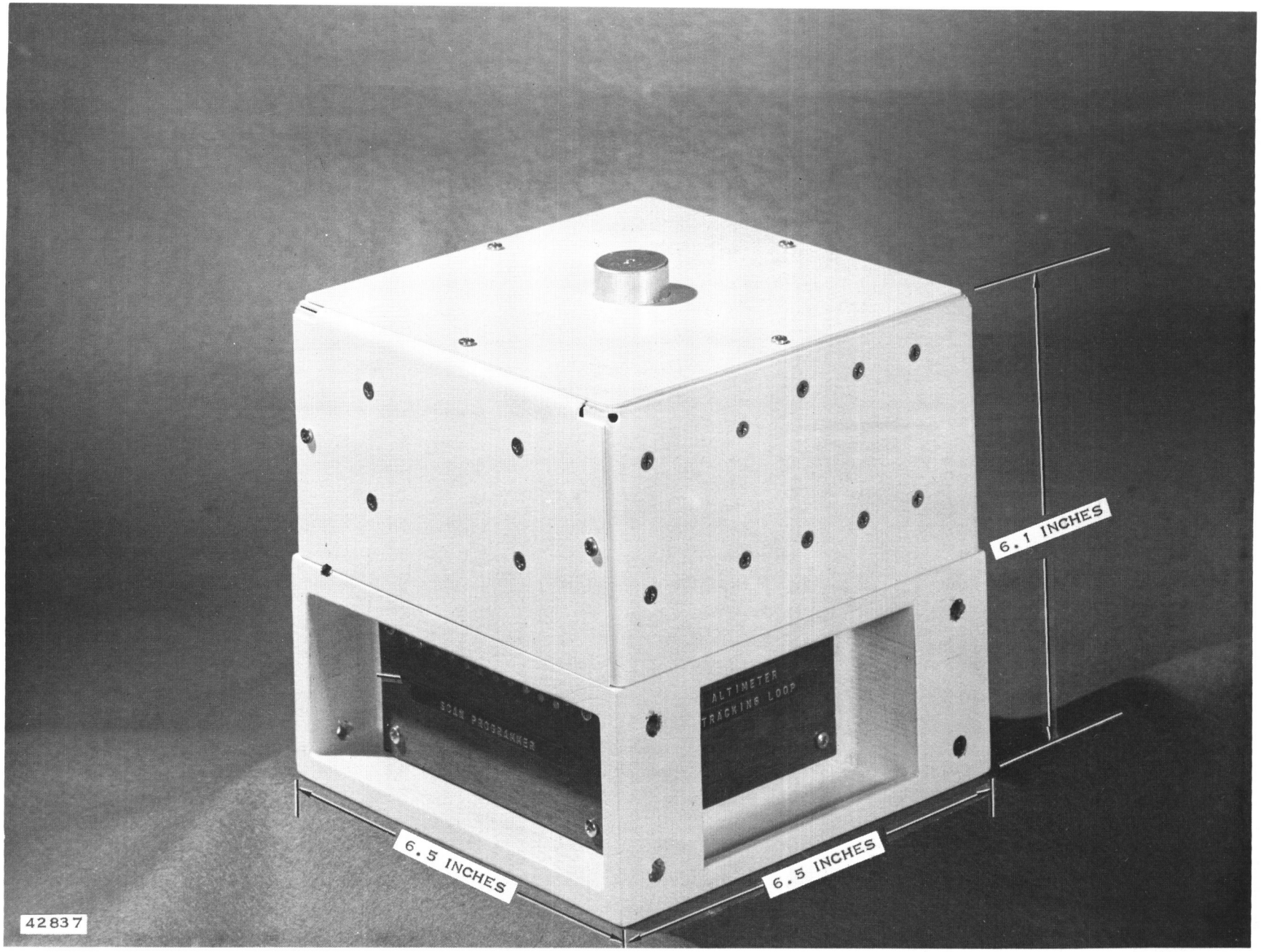

Figure 44. Proposed MERA Altimeter

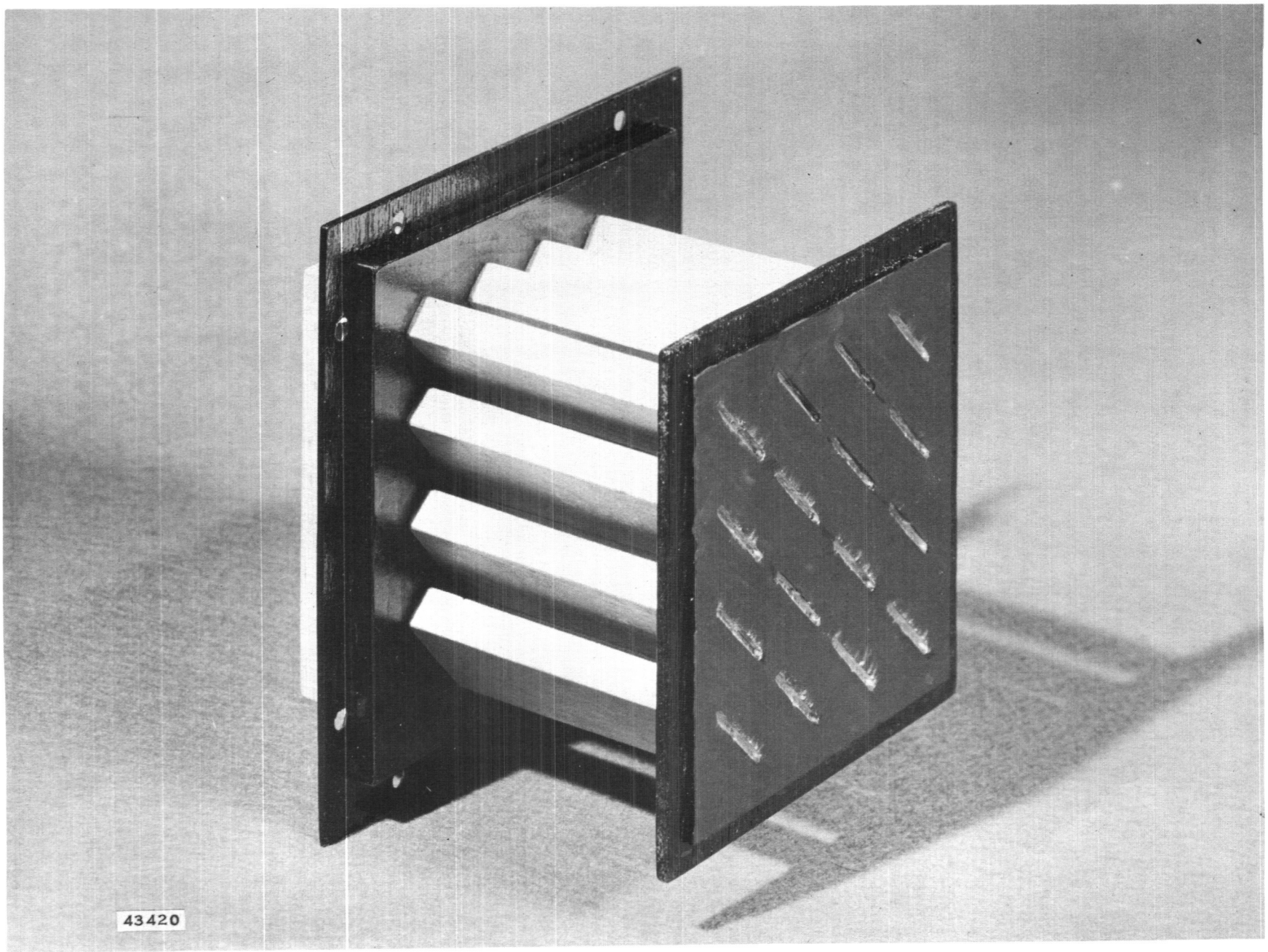

Figure 45. Photograph, Altimeter MERA Array Mockup

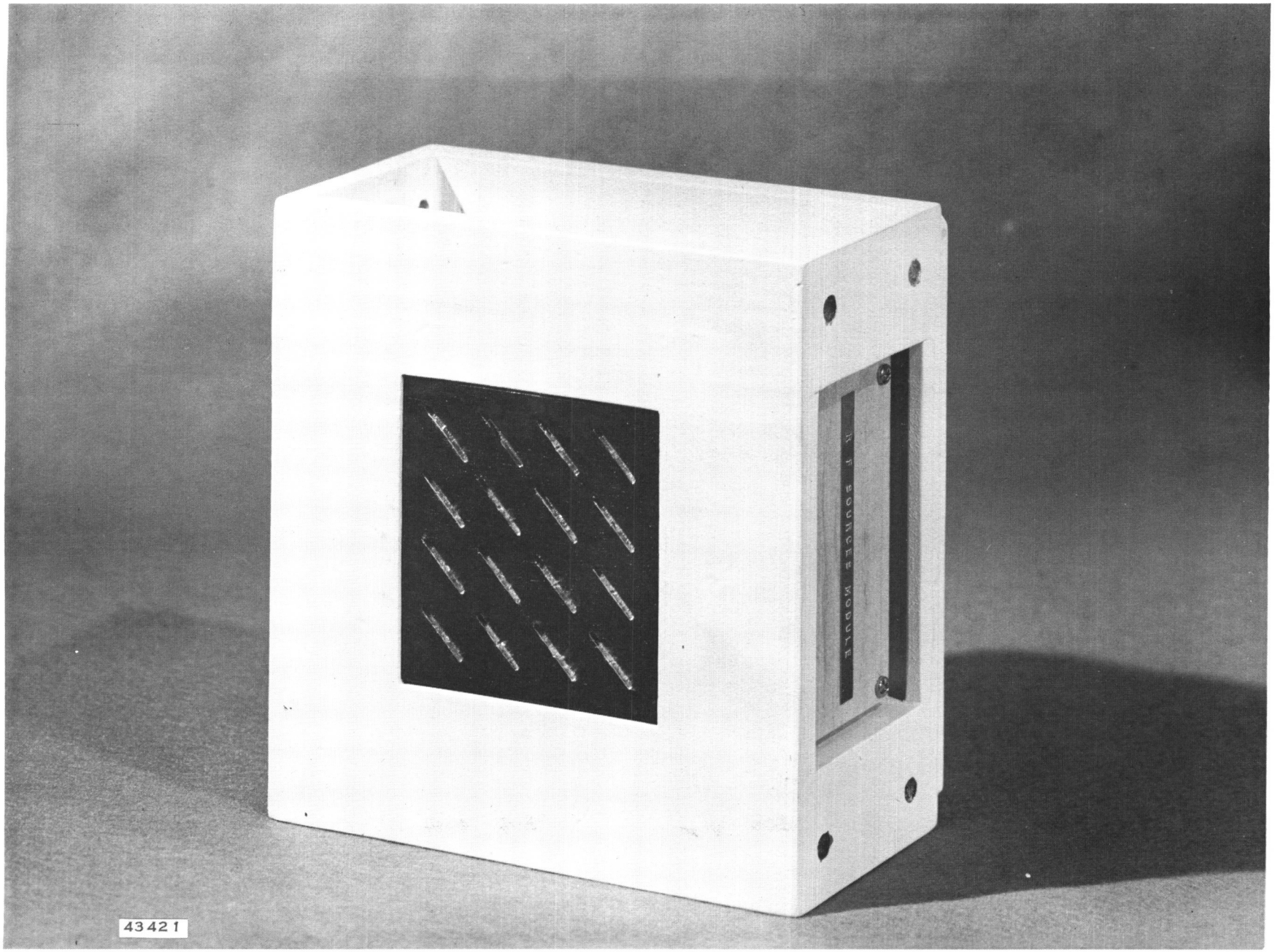

Figure 46. Photograph, Altimeter MERA Array Mockup Assembly

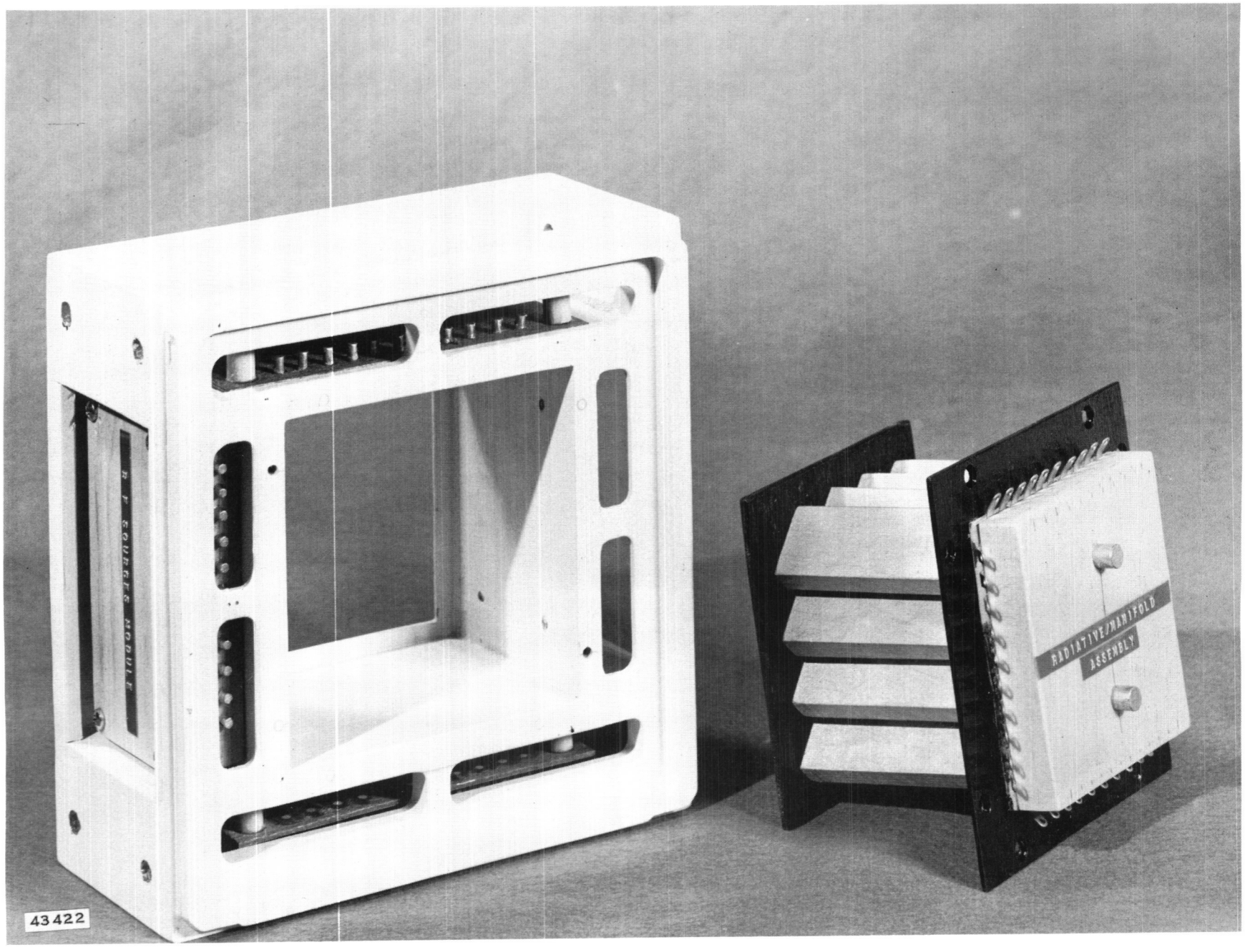

Figure 47. Photograph, Altimeter MERA Array Mockup, Disassembled

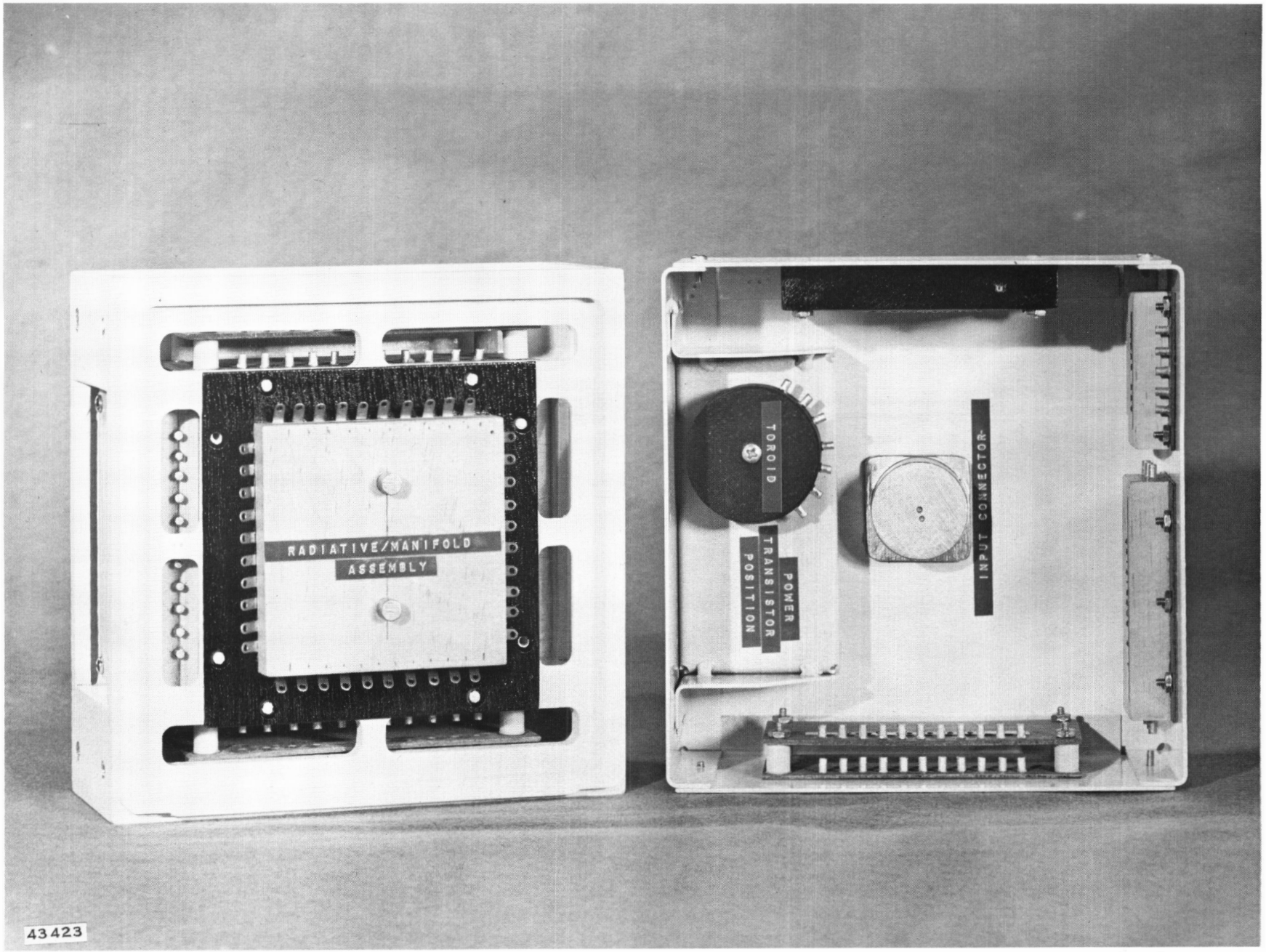

Figure 48. Photograph, Altimeter Mockup, Disassembled

Subsequent to the submission of the preliminary study report covering Phase I changes in the form factor of the MERA radiative elements has required a corresponding change in the basic packaging approach. This new approach has resulted in the unit as shown in Figure 44 and as described herein.

For purposes of the description below the following distinct sections of the system are identified on Figure 49, namely:

a. Radiative/Manifold Section
b. Base Structure Section
c. Back Structure Section.

Table 7 lists the major elements of the system, their basic sizes, weight, heat dissipation values, as well as their location within the above named section. Figure 49 shows an exploded view of the complete system.

MERA Module Configuration

The MERA module configuration around which the proposed altimeter design is based is as shown in Figure 50. This is identical with the standard MERA element as developed at Texas Instruments with the following exceptions:

a. A slotted cavity has replaced the dipole antenna.
b. The connection pins will be designed for soldered or welded connections to the manifold circuitry to eliminate any connector type failures.

The circuitry and interconnection concept for the module is shown by Figure 34. The structural concept is shown by Figure 51.

Radiative/Manifold Assembly

In order to gain structural integrity to fulfill the rigid environmental conditions, the MERA radiative elements and the manifolds, both dc and RF, are assembled into a single assembly element. Figure 52 shows the overall assembly form factor and other details necessary to understand its construction. As can be seen, when the unit is assembled it becomes an unseparable assembly which can be installed within the base structure as a single unit and subsequently interconnected to the other circuitry assemblies in the base and/or back structure.

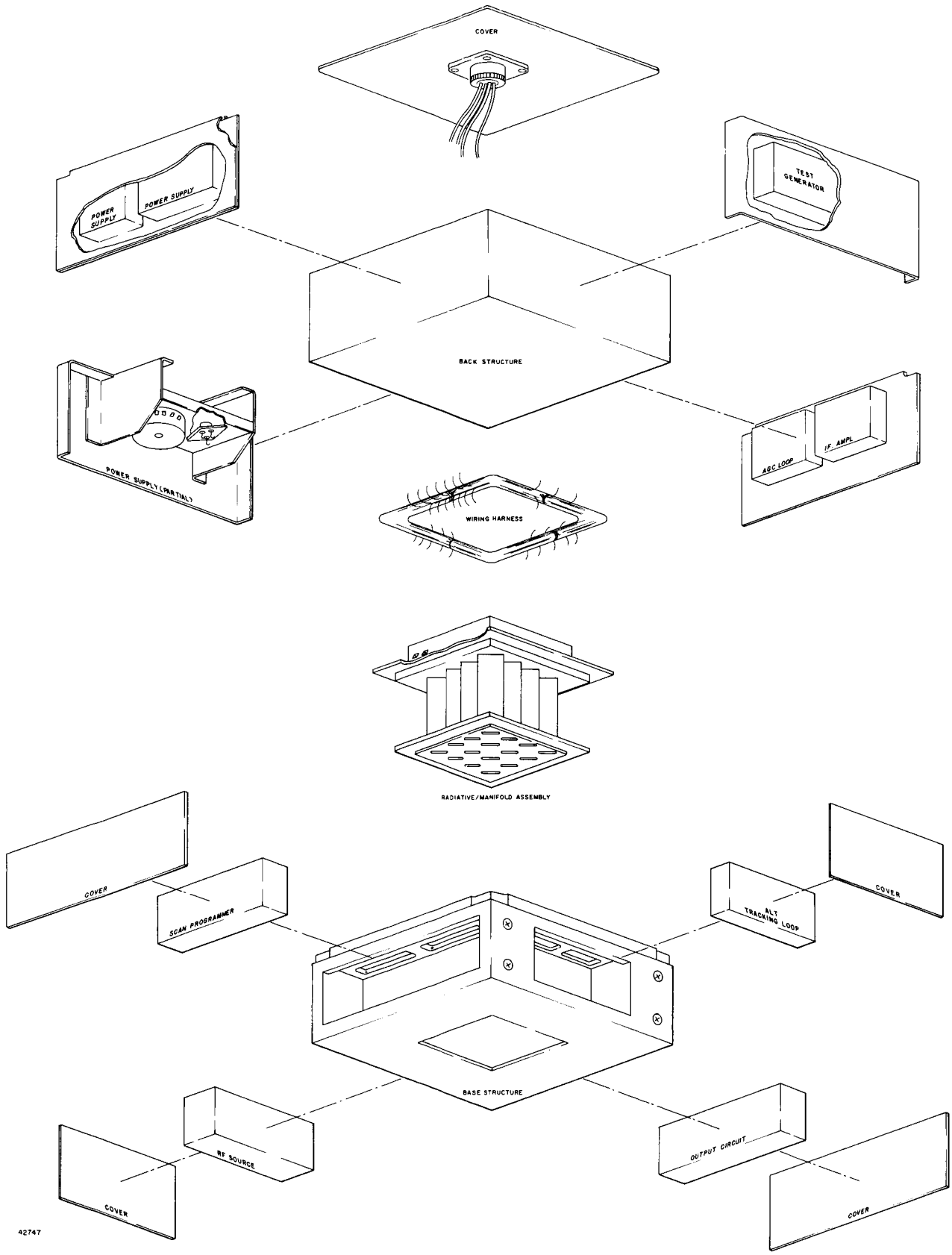

Figure 49. Altimeter Exploded View, Major

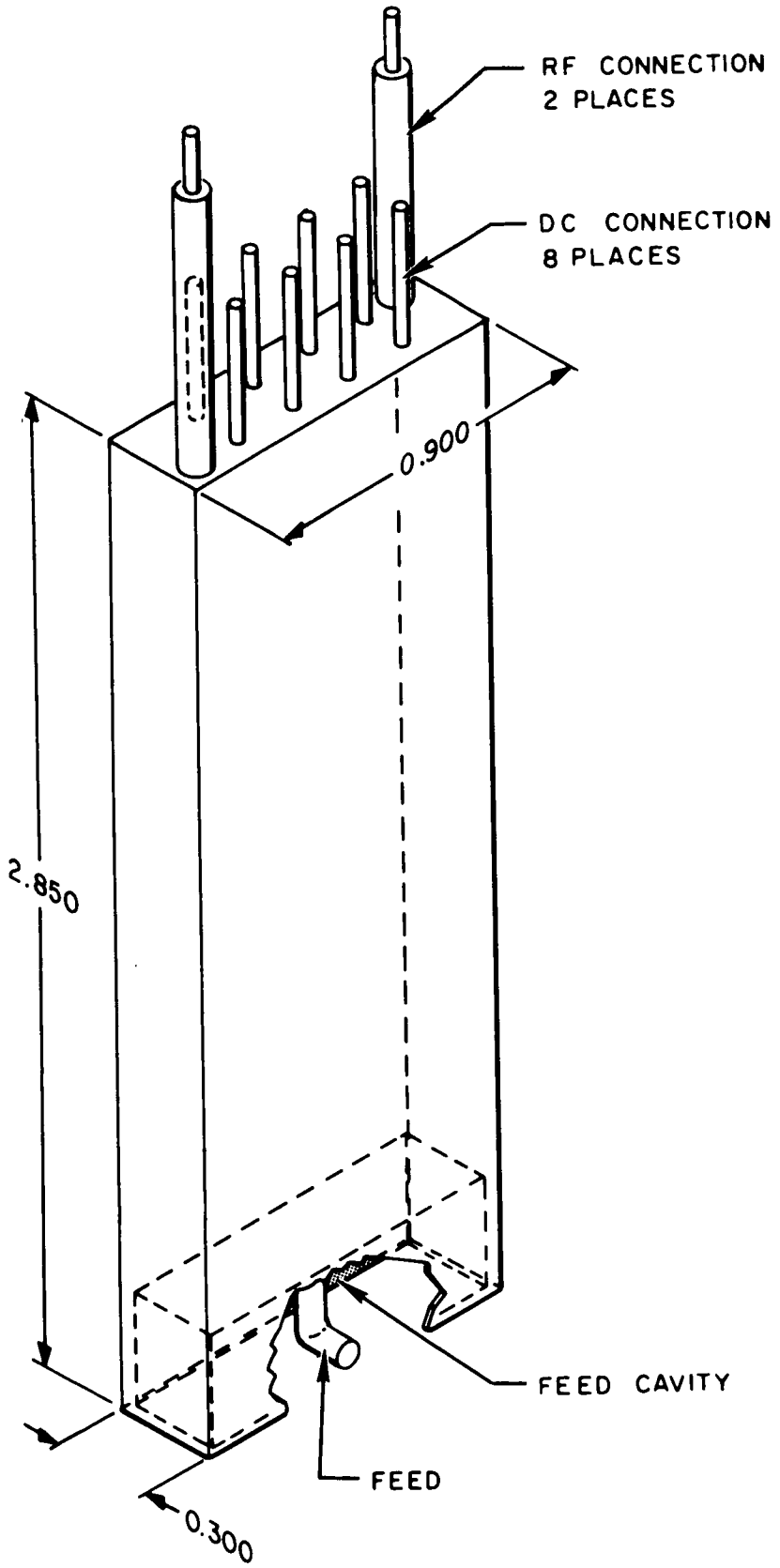

Figure 50. MERA Module Configuration

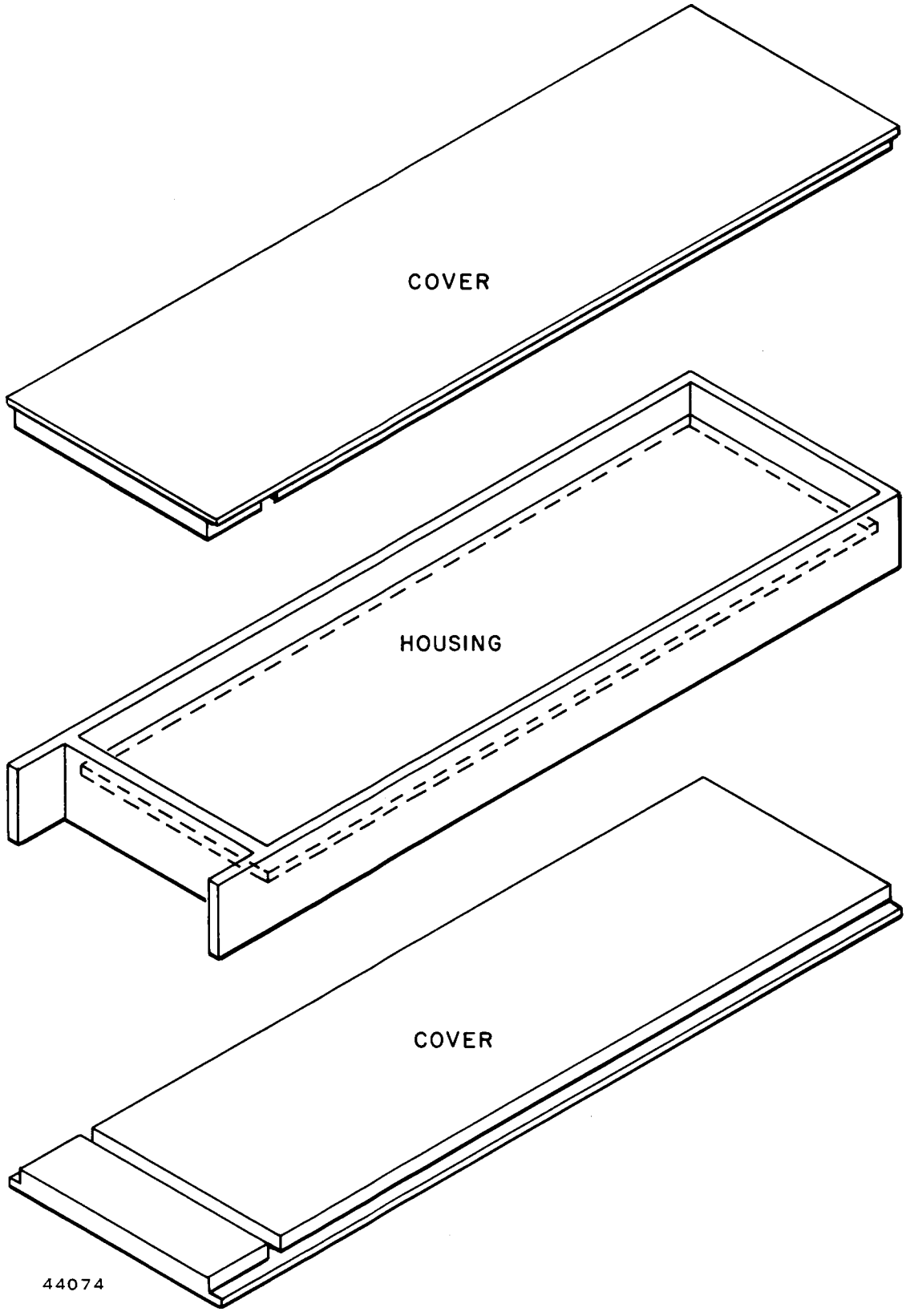

Figure 51. MERA Module Structural Configuration

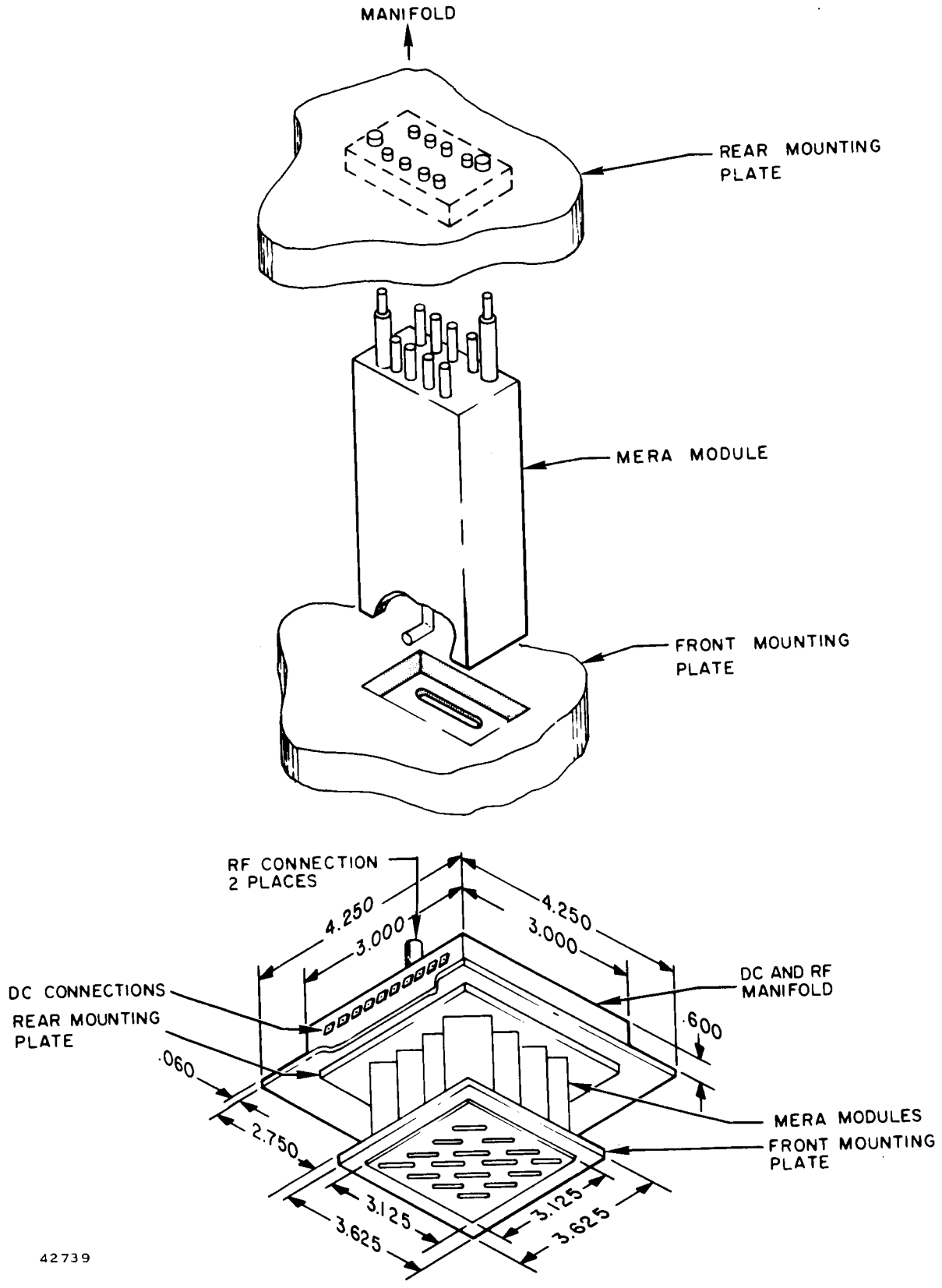

Figure 52. Altimeter Array Module Mounting

It is to be emphasized that all MERA element to manifold connections will be soldered or welded to ensure reliability. In addition, the modular design allows the complete transmit-receive function to be thoroughly tested before assembly into the altimeter itself. It is realized that this concept requires extremely rigid controls over all fabrication and assembly processes to ensure 100-percent yield, not only as far as the MERA elements are concerned, but particularly as the manifolds are built up and the connections from the radiative elements to the manifold are accomplished.

Base Structure Section

The base structure section consists of a cast structural element which provides the mounting interfaces with the lander as well as attachment points for the distinct circuitry elements or modules and the individual sides of the back structure. The design of this base provides cavities in each of the sides into which these circuitry modules are located and also allows wiring access to the back structure section and the manifolds. Each of the subject cavities will be covered as shown in Figure 49. The casting has been designed to allow sufficient heat flow paths from the major heat dissipating elements to the mounting interfaces. This packaging arrangement has allowed the location of all the major heat load elements, with the exception of the power supply circuitry, to be within the base structural casting immediately adjacent to the mounting interfaces. The effect of this is shown in the thermal analysis given herein.

As now envisioned, the base will be cast of aluminum but could be a dip-brazed assembly using wrought material dependent upon the quantities to be made. Certainly the dip-brazed method would be used for the initial development models.

Back Structure Section

The back structure will be made up of sheet metal sides which provide mounting positions for the individual circuitry subassemblies as shown in Figure 49, as well as a back cover to which the input/output connector is attached. Inspection of Figure 49, indicates that a part of the power supply circuitry is mounted on a shelf structure in such a way that the heat produced by the power transistor and the transformer is conducted to the base structure and, hence, to the mounting interface through a minimum length path. The arrangement of components on each of the side walls of the back structure allows access to the wiring bundle and all connections on that panel by removal

of individual sides and pivoting the side about the lower edge. Although many other component arrangements were investigated, the design shown is felt to provide maximum access and offers the maximum capability for structural integrity for all expected environments.

Weight

As shown in Table 7, the maximum weight expected for the altimeter is 6.959 pounds, which is 0.959 pounds over the maximum allowed by the Work Statement. Although the calculations made were detailed in nature based upon all known factors, it must be recognized that it is but an estimate at this point in time. It is felt that the individual weights shown are realistic and that consistent effort will be required throughout the actual development of the system to reduce this figure to a minimum.

THERMAL CONSIDERATIONS

In the Phase I report, it was stated that the lander mounting interfaces must be capable of absorbing the total heat dissipated within the altimeter and that the interfaces must be held below 100°C as a limit. This statement was based upon the design of the MERA elements, the altimeter circuitry, and the altimeter structure as envisioned and presented at that time. As a result of the changes in system configuration, outlined herein, resulting from the changes in the MERA element package, a re-examination of the thermal effects has been necessary.

The approach has been to determine temperature drops throughout the system, based upon a maximum semiconductor device junction temperature of 125°C. In each case, a rough calculation was made for all such critical devices throughout the system but, again, it was found that the devices within the MERA blocks are the most critical. Based upon the assumption of the worst possible condition, that of 0.344 W, dissipated within the module concentrated at the center of the "H" frame structure rather than distributed on the circuit substrates as indicated in Figure 53, the temperature of the mounting plates would be 111°C which compares with 115°C specified as the temperature at the top and/or bottom base of the module for the Phase I configuration. The temperature at the mounting interfaces, considering a one-dimensional heat path from the radiative/manifold assembly, would be 108°C. When the other heat sources are considered, the 100°C temperature, as previously specified, will allow adequate protection.

Table 7. –Radar Altimeter—Estimated Volume, Weight, and Heat Load

	Item	Quantity	Volume (cu in)	Weight (lbs)	Heat Load (mW)	Basic Dimensions
1.	RF Building Blocks— Includes Mounting Plates	1	35.70	1.308	5506	2.75 × 3.60 × 3.60
2.	Manifold	1	7.78	0.690	32	0.60 × 3.60 × 3.60
3.	Scan Programmer	1	4.80	0.115	788	0.60 × 2.00 × 4.00
4.	RF Sources	1	6.84	0.398	744	0.95 × 2.00 × 3.60
5.	IF Amplifier	1	2.25	0.158	168	0.50 × 1.50 × 3.00
6.	Altimeter Tracking Loop	1	3.00	0.043	450	0.50 × 2.00 × 3.00
7.	Output Circuit	1	6.75	0.140	1650	0.75 × 2.00 × 4.50
8.	Test Generator	1	6.75	0.200	213	0.75 × 2.00 × 4.50
9.	Power Supply					
	Pre-Reg	1	2.00	0.200	5000[1] max.	0.50 × 2.00 × 2.00
	Toroid-XFMR	1	2.30	0.750		0.75 × 1.75 × 1.75
	Rectifiers and Switch Circuits	1	4.20	0.076		0.60 × 2.00 × 3.50
10.	AGC Loop	1	2.40	0.029	93	0.60 × 2.00 × 2.00
11.	Wiring, Hardware, Connector	Set	See Below	0.500	----	
12.	Material—Base	1		1.500	----	
13.	Material—Covers, Back Structure	Set		0.852	----	
			84.77*	6.959	14 644	

*Volume of basic components only
Total Volume = 6.50 × 6.50 × 6.10 = 257 cu in

[1]Varies with input voltage

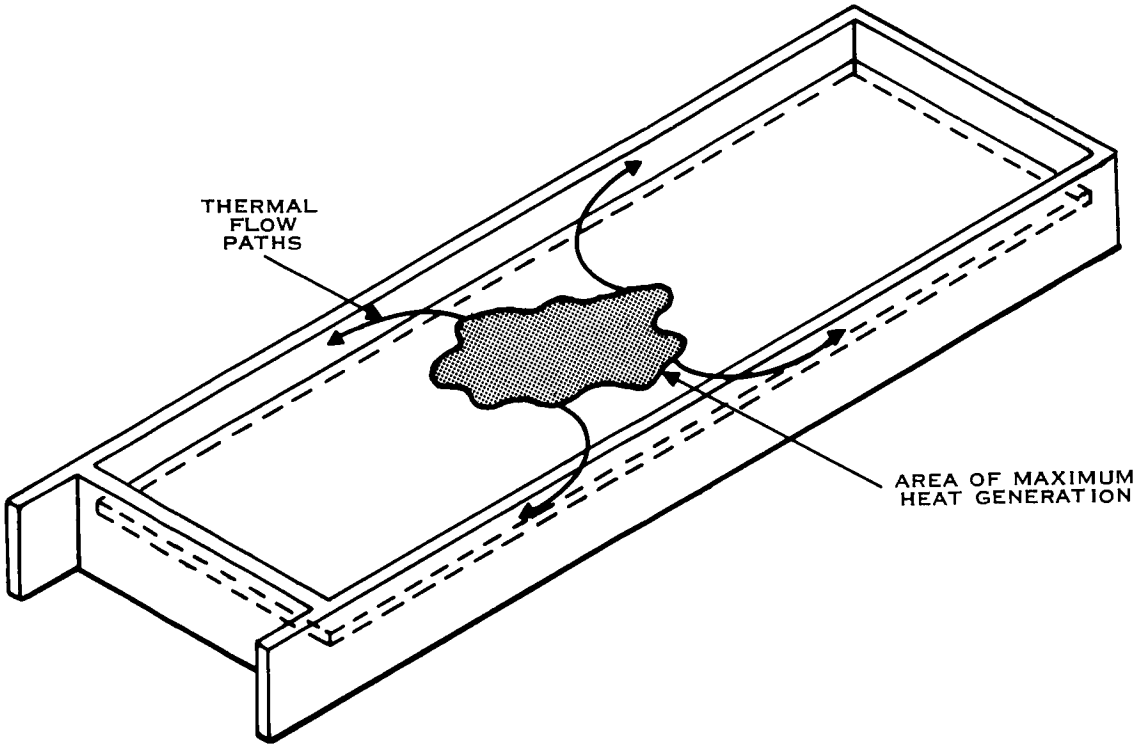

Figure 53. MERA Module Thermal Map

The analysis indicates that the specific design of the base structure, as well as the back structure and the circuit elements, has a critical effect on the heat distribution and conduction paths, but it is evident that the final structural design will be controlled by the vibration and shock requirements rather than by thermal considerations.

It will be noted that the mounting interfaces have been changed to four separate areas rather than the two larger surfaces shown for the Phase I configuration. The present surfaces are adequate, but if during the development of the system, additional surface area is required due to lander structural requirements, it can be realized in several ways, namely:

a. The cover for the circuitry cavity on the interface sides can be removed entirely or recessed to present a smooth surface for a larger lander mounting plate.
b. The back structure sides adjacent to the interfaces can be made an integral part of the base structure itself, such that the complete side surfaces, 6.500 inches wide by approximately 6.10 inches high, can be made the mounting and heat dissipating surfaces.

The design, as presented herein, allows a great amount of latitude for variations such as those noted above, should such be necessary to solve thermal, structural, or other such problems during actual development.

RADAR TERRAIN ANALYSIS

As mentioned in the introduction, a desirable feature of the altimeter would be a capability to do some terrain analysis, specifically roughness measurements. Present methods of terrain analysis in aircraft make use of an observer (either immediately, observing a display, or later, observing a film record of the display) to select prominent features of the landscape. Obviously, a Mars lander will not have the advantage of a "human" scanner and threshold detector; therefore, some means of automatically discriminating among various possible terrain configurations must be devised.

A brief discussion of three possible methods of radar terrain analysis is contained in this section. These three methods are:

a. Comparative ranging
b. Pulse fading
c. Polarization reversal ratio.

The only two outstanding features of terrain that are sensitive to radar measurements are the mean reflectivity and roughness. In this case, roughness means whether or not the terrain is above or below an RMS roughness defined by the Rahleigh criterion. Since the Rahleigh criterion is represented by surface deviations less than a wavelength, this characteristic is more or less meaningless for this mission. The reflectivity is a function of surface composition (water content, etc.) and can be assumed to be independent of incidence angle for this discussion. A reflectivity on Earth which is dependent on the angle of incidence would be a smooth water surface, a flat road or runway, etc., where the majority of incident energy is reflected as from a mirror.

Therefore, the only means left to determine in some way the roughness, or major terrain features, is to time separate the ranging measurements; in other words, scan the antenna beam smoothly and compare differences in received power as a function of time.

As mentioned in Part I of this report, a pulsed altimeter system has, as an inherent ranging error, a degradation in the rise time of the leading edge of the pulse. If the transmitted pulse were made to approximate a Dirac delta function, an approximation of the impulse response of the surface may be obtained, since the wavefront "scans" the terrain in an increasing diameter annular ring. However, the high speed processing required, along with the averaging effect around the circumference of the scanning annulus, leaves considerable doubt as to the value of such a measurement.

Another possibility lies in the fact that there is a component of lander velocity in the horizontal direction. If the lander were over a valley and near the center of a circle which roughly described the outline of the valley, there would be no rise time degradation, and the first time derivative of the received pulse would be at a maximum. Conversely, if the lander were over a large mound (convex shape) the rise time would be degraded to a maximum extent, and the first time derivative would have a minimum value. Consider the geometric representations in Figure 54, which assume idealized conditions of average reflectivity.

Assuming a very short transmitted pulse at position A, the rise time would be degraded as shown, and at position B degradation would be minimal. With good AGC control, this "pulse fading" may yield some crude roughness information. This is a greatly simplified discussion, since the altitudes where the horizontal velocity component is large is in all probability too high for the expected terrain features to effect the rise time to any reasonable extent.

A third possibility is to measure the ratio of the polarization reversal of the surface. A much more complicated transmitter, and two receivers are required for this test, so this method was not considered further.

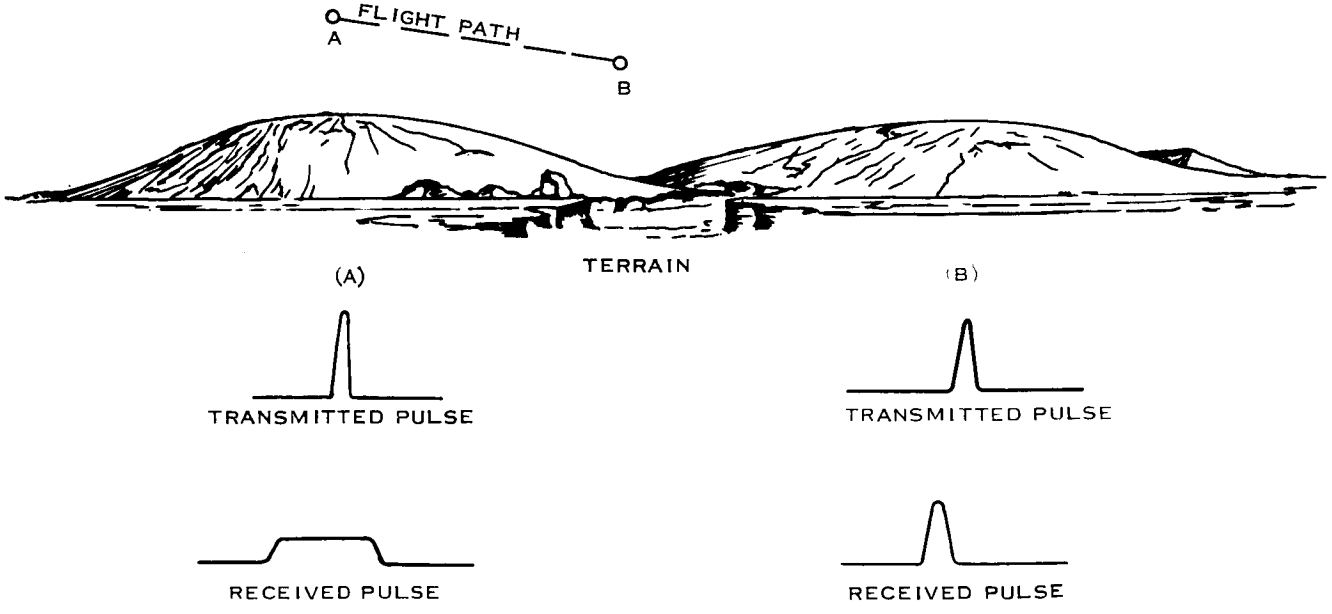

Figure 54. Positional Influence on Received Pulse

It is concluded that a much more sophisticated radar system is required to make meaningful measurements of the surface characteristics, and that the size, weight, power consumption, etc., outlined in the Work Statement are too severe restrictions to allow surface measurements along with the basic altitude measurements of the altimeter.

ADVANCED DESIGN ANALYSIS

A computer program has been used to demonstrate the most obvious growth potential item, that of changing the array size for different applications. Figure 55 shows the gain of various size square arrays. Other growth potential items are discussed as follows:

Greater Accuracy

In the discussion of the pulsed system in Part I, several attempts at system simplification resulted in an acceptable, but not optimum, processing technique. If the various system parameters were programmed and optimized to altitude, less measurement error would result. Also, since a large part of the error is due to the degraded pulse-rise-time, some of the error could be processed out of the measurement.

Low Altitude Capability

The FM/CW system, as shown in Part I, is the best system to use at low altitudes. The pulse system is limited in low altitude operation by duplexing time and the difficulty in measuring very short delay times. The MERA RFBB's can be designed to operate in a dual mode (Pulse and Low Power CW) and will therefore, lend themselves to this type of dual mode operation.

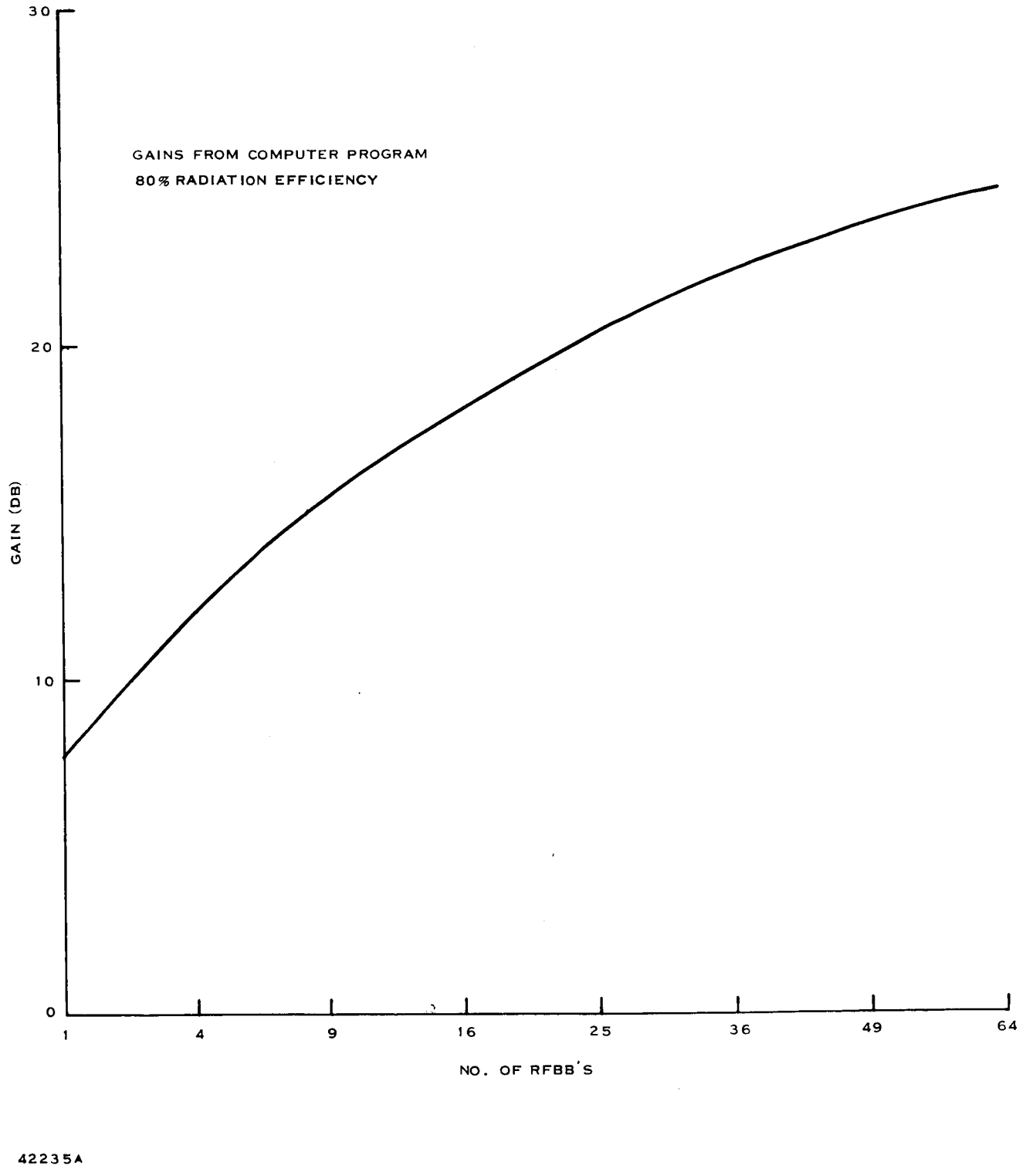

Figure 55. Gain of Square MERA Arrays

Pulse Compression

The MERA radar system is being designed to utilize pulse compression. This is shown in the Appendix of this report. A 20-dB gain in transmitter power will extend the maximum range capability and, with proper signal processing, decrease the measurement errors at lower altitudes.

Input Power Reduction

A more elaborate power conditioner programmer could be devised where the circuits not needed are de-energized, except just before and just after a received signal is expected. Of course, this type of programmer consumes power itself and a detailed analysis would have to be made to determine the real usefullness of such a scheme; particularly, when reliability, size, cost, and other parameters are considered.

FUTURE DESIGN

Using the same techniques described in this report for the basic altimeter, the advanced (future design) altimeter requirements, as specified in the Work Statement, can be met with a unit of approximately as follows:

Weight	12.5 pounds
Size	450 cubic inches
Input Power	20 watts continuous (30 watts intermittent, for an estimated 2 to 3 seconds, five times during descent. However, this requirement perhaps can be eliminated).

This unit would include an 8×8 array of RFBB's, and the processing would require bandwidth and pulsewidth switching. A means of determining surface roughness was not included in the design, but logic circuits to identify the attitude of the lander are included. A digital word having a length consistent with the number of sectors will be provided to indicate (within one-half antenna beamwidth) vehicle roll and pitch attitude.

CONCLUSIONS TO PART II

During the detailed design effort in this part of the program, it was concluded that an array of 16 MERA RF building blocks is applicable for the Martian lander. Further analysis showed that an acceptable IF bandwidth is 3 MHz. The 3-MHz bandwidth is narrow enough to limit the high-altitude error below that specified and also broad enough not to severely limit the

pulse information at the low altitudes, so it will also keep these errors below specified. Any other bandwidth would be optimized to particular altitudes and would, therefore, not work as well over the entire altitude range.

A PRF of 2000 PPS was chosen as a near optimum tradeoff between input power requirements and unambiguous range requirements. The total input power is shown to be about 13.5 W. This low power level was achieved by turning off portions of the altimeter circuitry that are not used, on a pulse-to-pulse basis.

A test mode was built into the altimeter circuitry for checking out each RF building block individually by time separating them during a prelaunch checkout period.

Several methods of measuring terrain roughness were analyzed, and none of them appear to be feasible for this altimeter. The spectrum signature of the returned signal does not appear to contain enough information to be worth the greatly increased complexity of an altimeter to analyze this information.

From information obtained from NASA personnel during the presentation of results from the first part of this program (that is, connectors of any kind are high-failure items in space equipment) the implementation has been changed to eliminate all connectors except the input power connector to the lander. Modular construction has been incorporated where the front-end section (the array of RF building blocks and the associated manifold) is assembled into a frame, and all the circuit interconnections are either welded or soldered.

Other results of this study, such as reliability and manufacturing plans, are contained in other documents as listed in the Foreword.

The calculations in this report assume a power output of 1 W from each RF module. This power level is a design goal of the MERA program. Actually, there is little effect on system operation for a decreased power output, since the system design has been conservative. For instance, a surface reflectivity of −20 dB was assumed when computations of received signal strength were made. A more realistic value (Figure 2) would be −13 dB. Another factor is the minimum required power for a marginal system design. This value was 1.7 W. Therefore, a total design margin of 16.7 dB exists in the calculations. If the design goal of 1 W per RF module is not met and the minimum expected value of 0.6 W output per RF module cannot be increased, the design margin will still be 14.5 dB.

Tables A1 and A2 show tentative module parameters and circuit specifications for the MERA RF module. At this time it appears that the peak output power will be 0.9 W, with a design goal of 1.0 W and an absolute minimum of 0.6 W.

APPENDIX

DISCUSSION OF MERA SYSTEM AND CONCEPTS

APPENDIX

MERA

SYSTEM AND CONCEPTS

MERA is an acronym for Molecular Electronics for Radar Applications, a program at Texas Instruments Incorporated with the United States Air Force, Air Force Systems Command, Systems Engineering Group (RTD), Wright-Patterson Air Force Base, Dayton, Ohio, under Contract Number AF33(615)-1993.

This program involves the development of integrated circuits and the demonstration of compatibility of these circuits in a terrain-avoidance, phased-array radar research vehicle which will be developed as part of the program.

The MERA system is being developed to operate in terrain-following/terrain-avoidance (TF/TA), ground mapping (GM), and air-to-ground ranging (AGR) modes. It will use pulse compression and a phased-array antenna design to produce an equivalent peak pulse radiated power of 60 kW at X-band. The system is composed of 604 RF modules arranged in an octagonally shaped structure measuring approximately 20 inches across. The modules are interconnected by a manifold. The system's low frequency circuitry is behind the RF manifold. A photograph of a mockup of this system is shown in Figure A-1, and a simplified block diagram is shown in Figure A-2.

The heart of this system is the front-end assembly of RF modules. Figures A-3, A-4, A-5, and A-6 show features of these modules. (See Theory of Operation section on RFBB's for a detailed discussion of these modules.) Basically, this system employs a pseudomonopulse processing technique for angular resolution improvement. The monopulse antenna beams are developed in the RF distribution manifold, which is in itself arrays of stripline power dividers and adders. A single RF source supplies the input drive to all the RF modules, ensuring a constant phase reference for the antenna beam development. The rest of the low-frequency circuitry is more conventional, except that a large portion of that circuitry will be integrated.

The major milestones in the RF module development programs are:

a. Complete engineering prototype, 29 March 1967
b. Complete preproduction prototype, 1 June 1967
c. Supply 604 modules for MERA system, 31 December 1967.

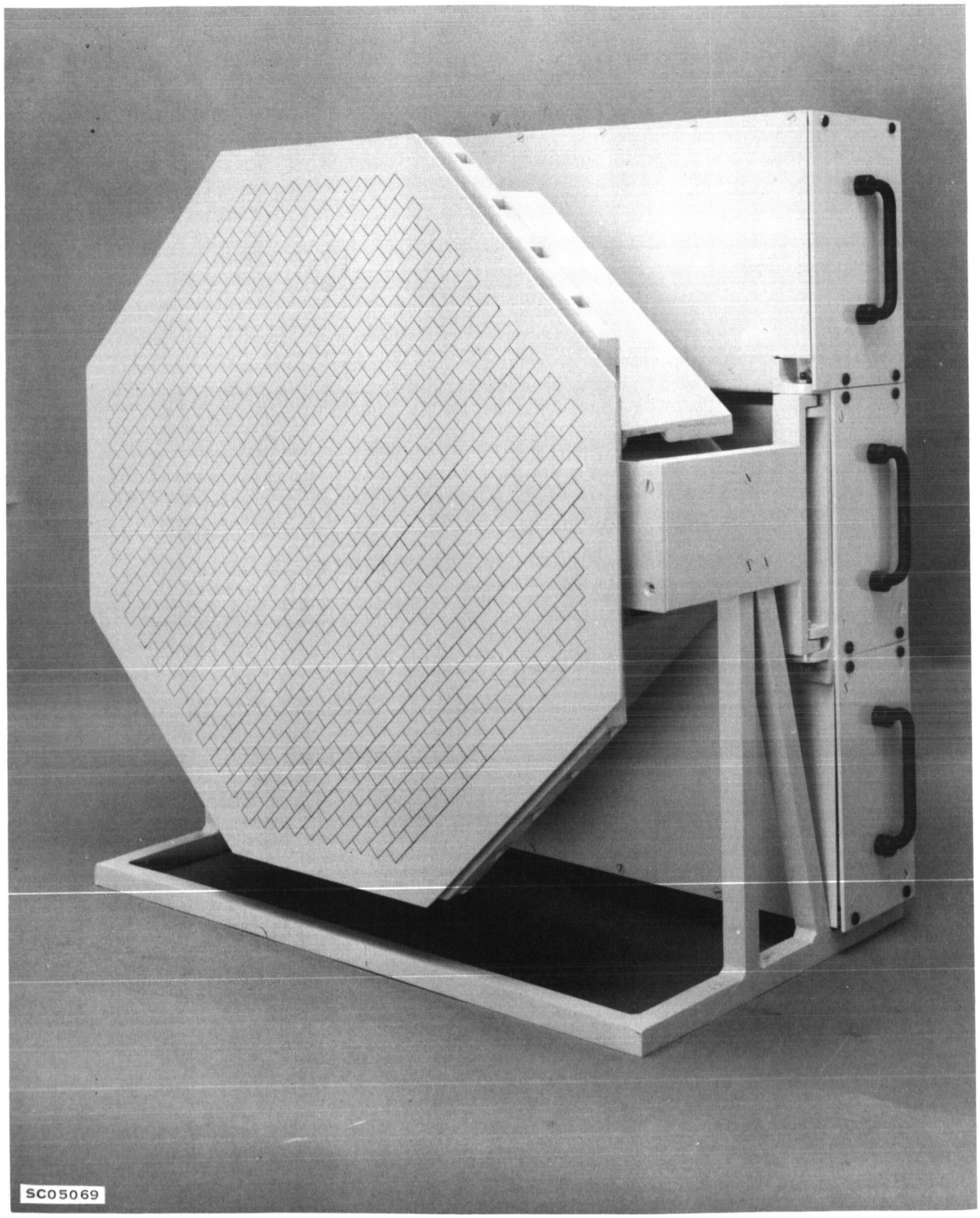

Figure A-1. Photograph, MERA Mockup, Front Oblique View

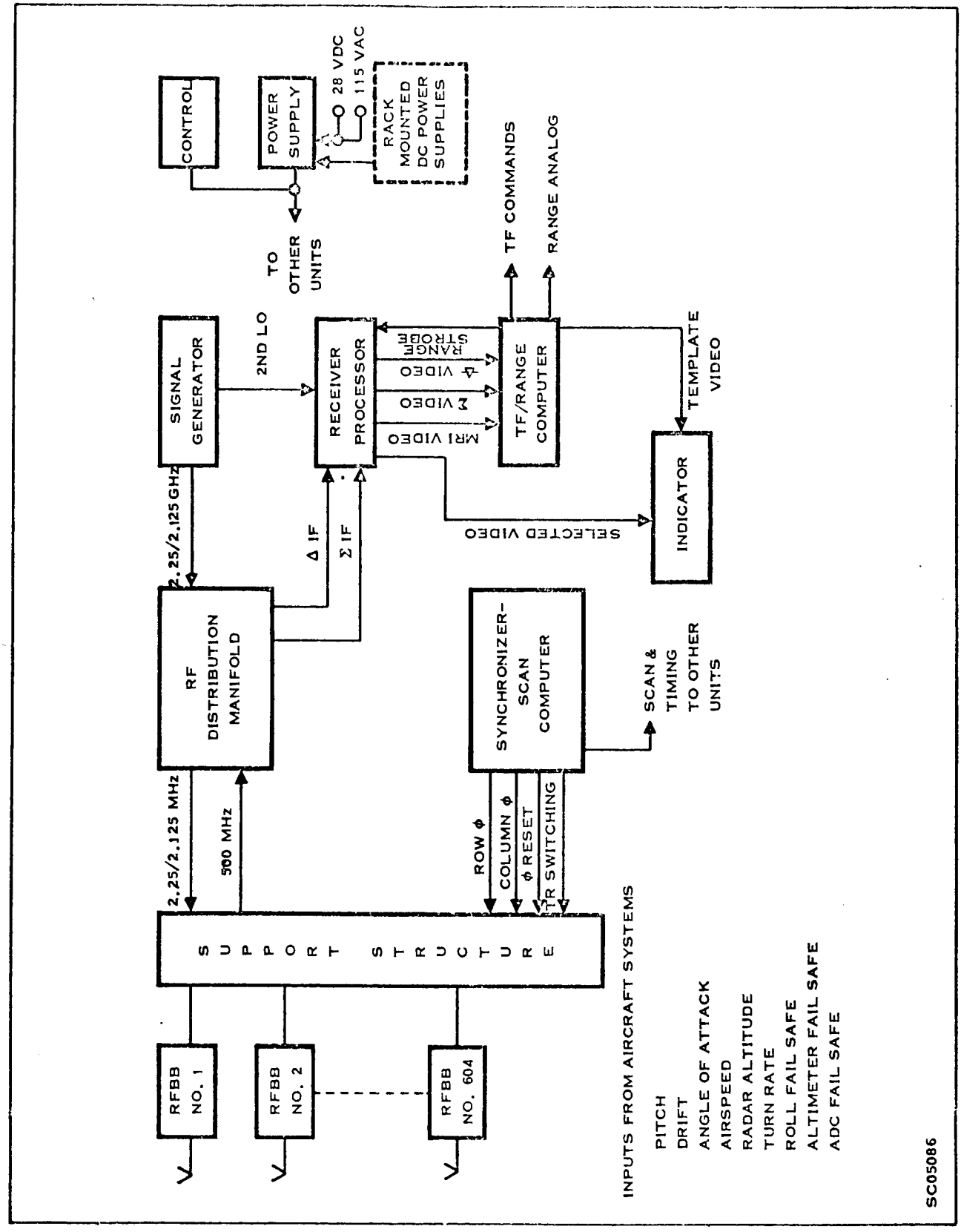

Figure A-2. Simplified Block Diagram, MERA System

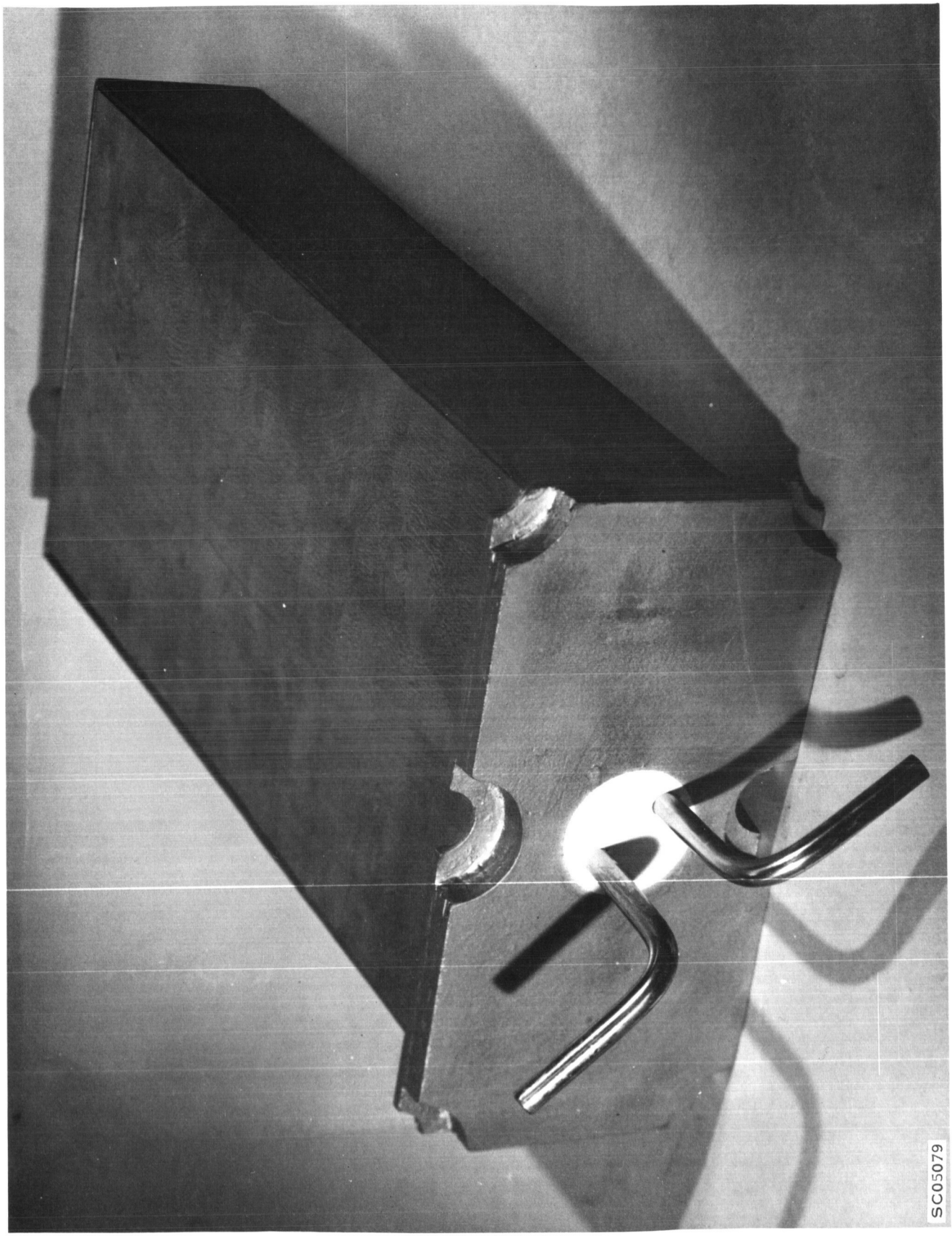

Figure A-3. Photograph, RF Module 10:1 Mockup, Front View

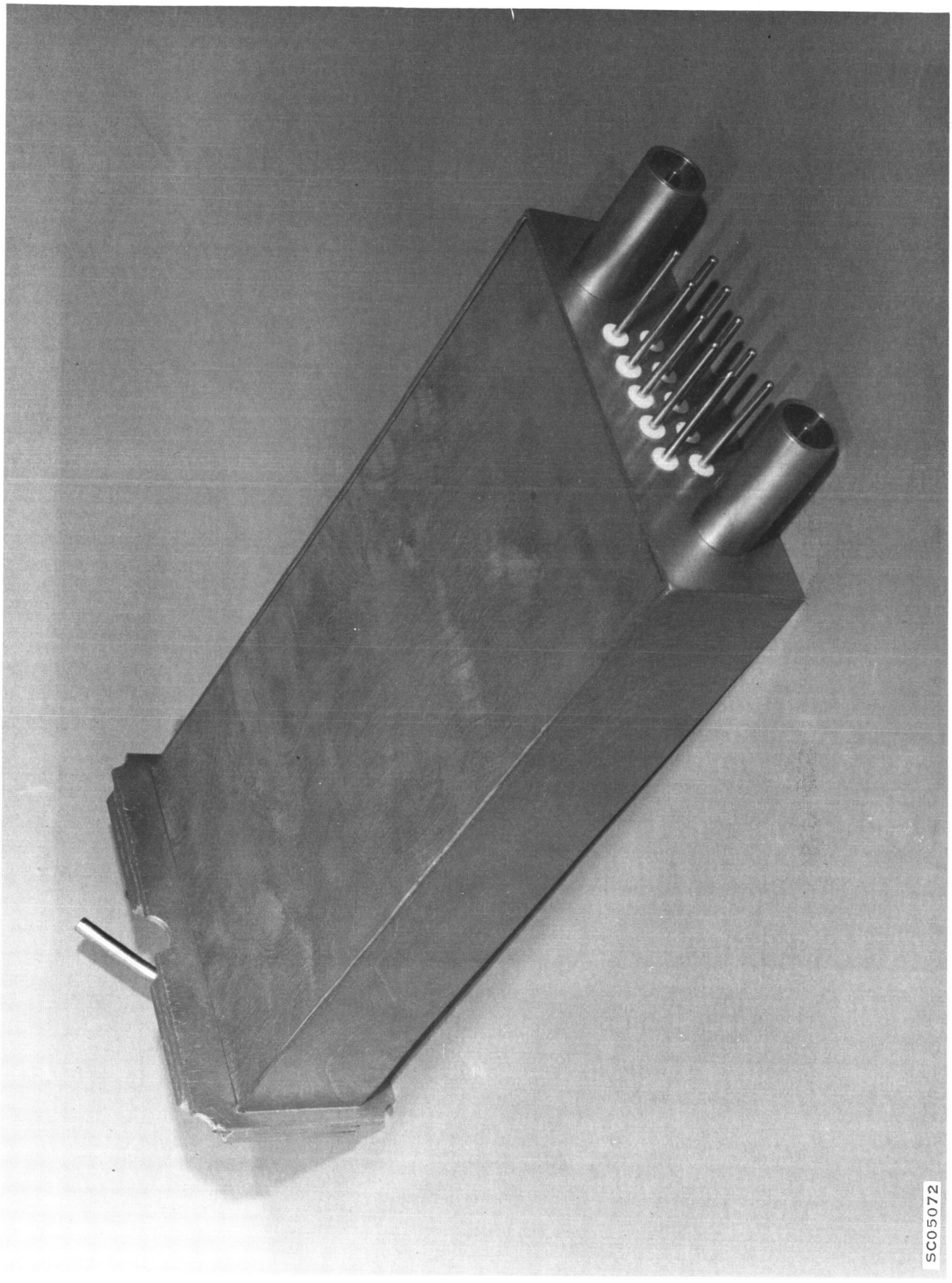

Figure A-4. Photograph, RF Module 10:1 Mockup, Rear View

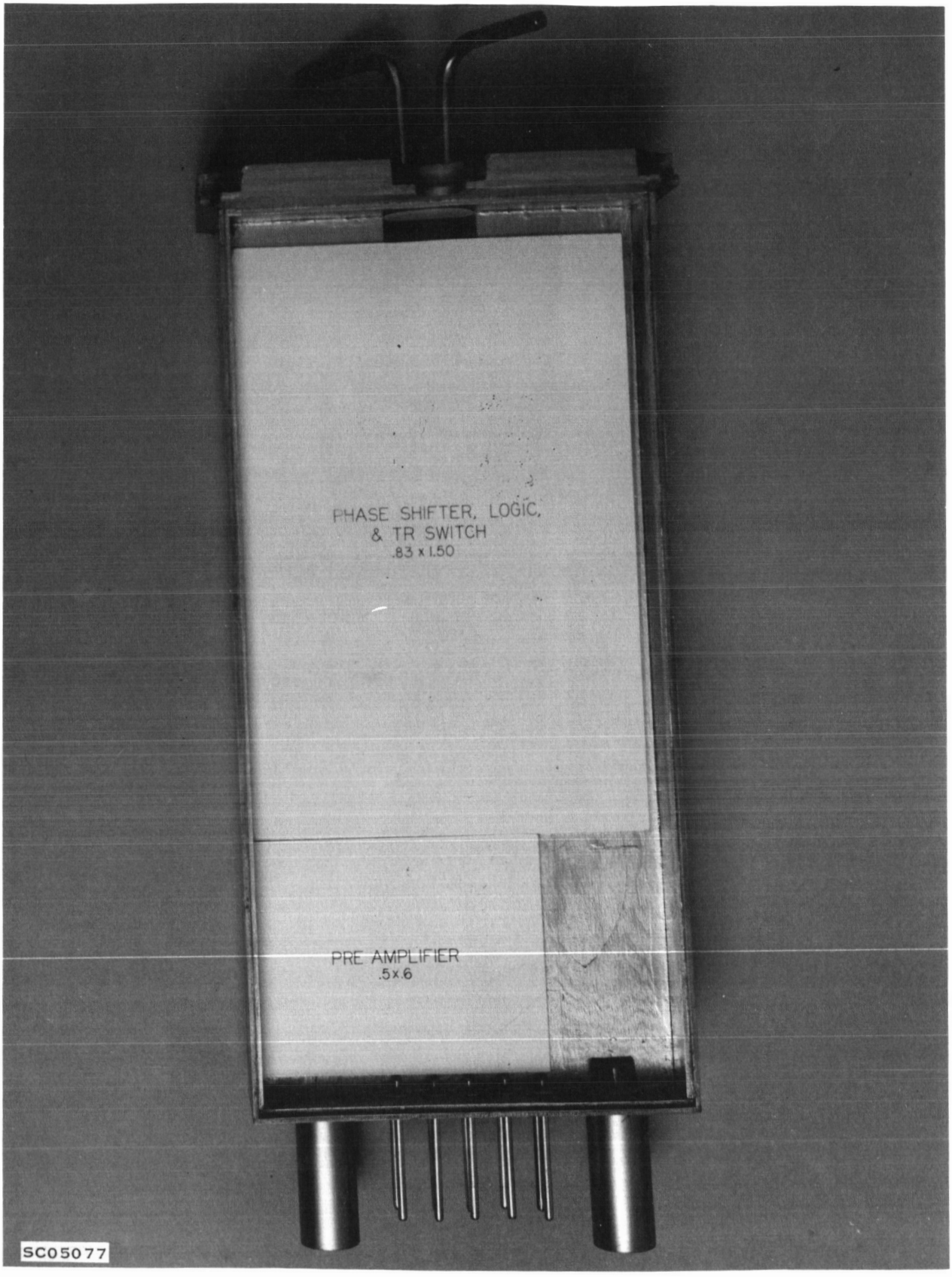

Figure A-5. Photograph, Top View RF Module 10:1 Mockup, Cover Off

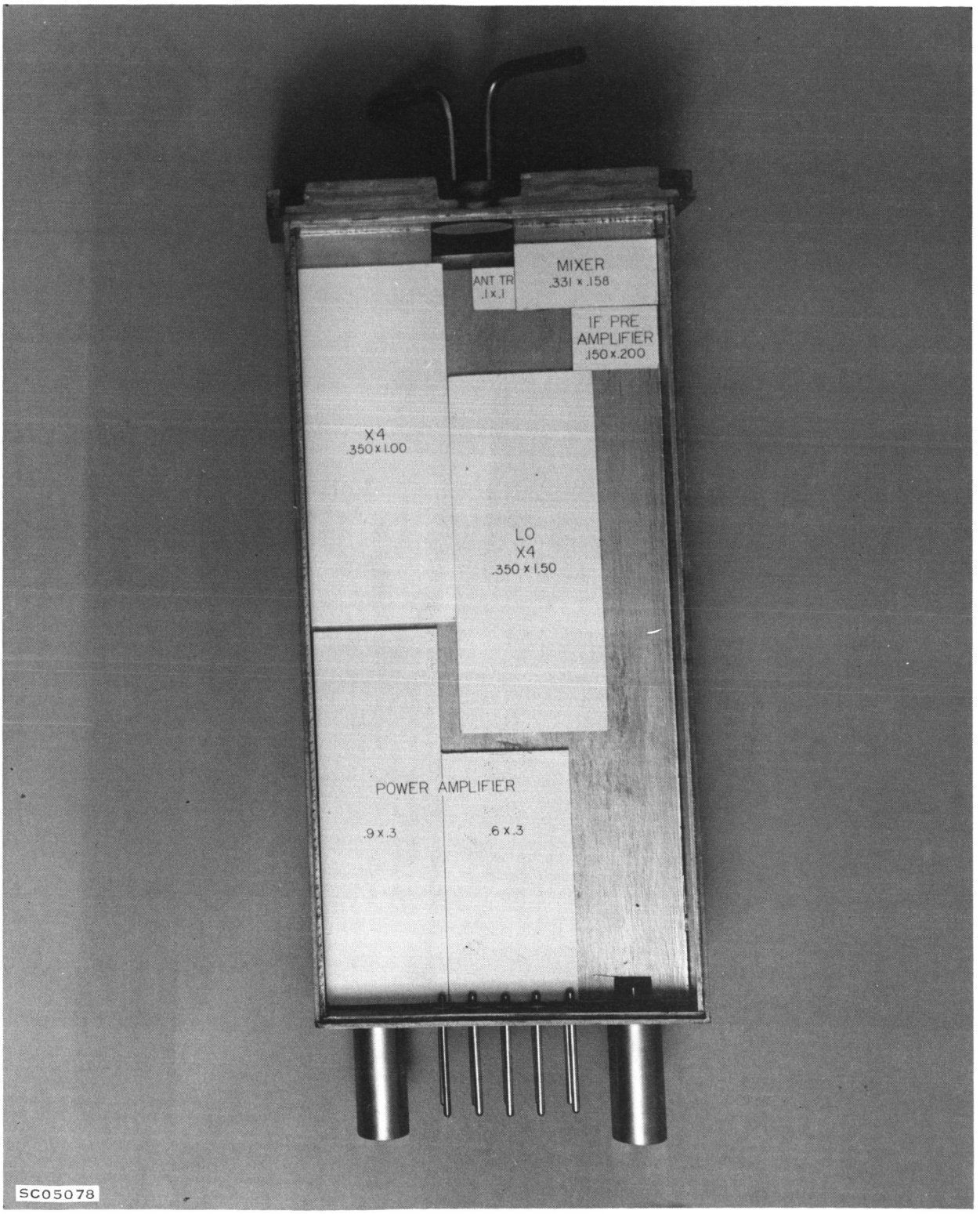

Figure A-6. Photograph, Bottom View RF Module 10:1 Mockup, Cover Off

APPENDIX

More detailed descriptions of the RF module construction and circuitry are contained in the Theory of Operation section. Tentative RF Module parameters are shown in Table A-1 and circuit specifications are given in Table A-2.

Table A-1. – Tentative RF Module Parameters

Parameter	Specification
Output frequency	9.0 GHz
Peak output power	0.9 W nominal
Spurious radiation	−30 dB maximum
Instantaneous bandwidth (3 dB)	100 MHz minimum at S-band and IF
	400 MHz minimum at X-band
Noise figure	10.5 dB nominal
Gain compression	1 dB at −30 dBm input
TR switching	1 μs maximum
Transmitter excitation	2.250 GHz ±0.75 MHz FM
	2 mW maximum
Local-oscillator excitation	2.125 GHz
	2 mW maximum
Receiver channel gain	12.5 dB ±1.5 dB
Phase uniformity* (TX and RX)	±20 deg (at any input level)
Power output uniformity*	1.0 dB
Receiver channel gain uniformity*	1.0 dB
Module size	2 × 1 × 0.5 in.

*Between RF modules.

Table A-2. – Tentative RF Module Circuit Specifications

Parameter	Specification
Power preamplifier	10 dB gain, 300 MHz bandwidth, minimum 20 mW output CW or pulsed
Phase-shift network (includes phase-shift TR, logic, and TX and RX phase shifters)	4-bit phase shifter, 0 deg to 90 deg in 5.62 deg steps, 3 dB maximum loss
Power pulsed amplifier	23-dB gain, 100-MHz bandwidth minimum 2 W output, pulsed 10% duty cycle
Power X4 frequency multiplier	2.25 GHz to 9.0 GHz, 2% minimum BW, 10% or greater desired, 3.0-dB design goal, 4.5 dB maximum conversion loss; 2 W input, 10% duty cycle maximum
Antenna TR	0.5 dB maximum insertion loss, 20 dB minimum isolation in transmit and receive states, 2% minimum bandwidth, 10% or greater desired
Antenna and Balun	Required radiation pattern in free space with 1.3 VSWR maximum for antenna and balun over 5% minimum bandwidth, 10% or greater desired
LO X4 frequency multiplier	2.125 GHz to 8.5 GHz LO, 10% minimum bandwidth, 10% design goal, 6 dB maximum conversion loss, 10 mW input CW
Mixer	9.0 GHz signal, 8.5 GHz LO, 10% minimum bandwidth, 8 dB maximum noise figure with 1.5 dB IF at 500 MHz
IF preamplifier	500 MHz center frequency, 100 MHz bandwidth, minimum, 19 dB gain, 4 dB noise figure, maximum

REFERENCES

1. J. V. Evans and G.H. Pettengill, "The Radar Cross Section of the Moon," Journal of Geophysical Research, Vol. 68, No. 17 (September 1963).

2. Walter R. Fried, "An FM/CW Radar for Simultaneous Three-Dimensional Velocity and Altitude Measurement," IEEE Transactions ANE, March 1964, pp. 45-67.

3. Merrill Ivan Skolnik, Introduction to Radar Systems (New York: McGraw-Hill, 1962), Eq. (10.35), p. 468.

4. David Knox Barton, Radar Systems Analysis (Englewood Cliffs, New Jersey: Prentice-Hall, Inc., 1964), p. 364.

5. Skolnik, op. cit., Eq. (10.13), p. 463.

6. Ibid., pp. 36-37, (Reference 3)

7. Ibid., pp. 37, 64, (Reference 3)

8. Ibid., p. 464, (Reference 3)